University of the Pacific Theses and Dissertations

University Libraries

2020

midazole-based pH-sensitive Convertible Liposomes for Anticancer Drug Delivery

Ruiqi Huang
University of the Pacific

IMIDAZOLE-BASED PH-SENSITIVE CONVERTIBLE LIPOSOMES
FOR ANTICANCER DRUG DELIVERY

By

Ruiqi Huang

A Thesis Submitted to the

Graduate School

In Partial Fulfillment of the

Requirements for the Degree of

MASTER OF SCIENCE

Thomas J. Long School of Pharmacy and Health Sciences
Pharmaceutical and Chemical Sciences

University of the Pacific
Stockton, California

2020

IMIDAZOLE-BASED PH-SENSITIVE CONVERTIBLE LIPOSOMES
FOR ANTICANCER DRUG DELIVERY

By

Ruiqi Huang

APPROVED BY:

Thesis Advisor: Xin Guo, Ph.D.

Committee Member: Xiaoling Li, Ph.D.

Committee Member: Joseph Harrison, Ph.D.

Department Chair: William K. Chan, PharmD, Ph.D.

IMIDAZOLE-BASED PH-SENSITIVE CONVERTIBLE LIPOSOMES
FOR ANTICANCER DRUG DELIVERY

Copyright 2020

By

Ruiqi Huang

DEDICATION

This thesis is dedicated to my father and grandmother for encouraging me to major in pharmaceutical sciences seven years ago.

ACKNOWLEDGEMENTS

My sincere gratitude goes to Dr. Xin Guo for his continuous mentorship and support throughout my graduate studies. The work presented here could not have been accomplished without his insightful inputs. He provided constant guidance and encouragement to me, from which I have learned how to become not only a good graduate student but also an independent researcher. I believe the professional research experience, the verbal and written communication skills, and the scientific thinking that I have obtained from his guidance will be extremely helpful for me future studies and career in pharmaceutical sciences.

I would like to thank my thesis committee members Dr. Xiaoling Li and Dr. Joseph Harrison for their time, advice, and invaluable contribution to my thesis. I also thank Dr. Li, Dr. Harrison, and Dr. Guo for kindly providing the recommendation for my application to Ph.D. programs. I am grateful to Dr. Li for introducing the PCSP program for which I got the chance to study at UOP. I would also like to thank him for providing invaluable guidance and support during my leadership of AAPS – Pacific Student Chapter. I thank Dr. William K. Chan and Dr. John C. Livesey for providing access to instruments crucial for my research. I wish to express my gratitude to all the PCSP faculty for enriching my knowledge through the courses offered. I thank Lynda Davis, Kathy Kassab, and Sonya North for their help and suggestions.

I thank all my past and current lab mates for instilling a friendly and collaborative work environment in our lab. I thank Dr. Yifan Lu and Dr. Mallika Vadlamudi for providing training of formulation preparation, assistance on my project, and suggestions in organizing events of the student chapter. I thank Yingbo Huang for his training of cell culture and 3D MCS techniques. I thank Dr. Shen Zhao for his assistance and advice in chemical synthesis. I thank Xinyu Pei, who is a reliable partner in our AAPS student chapter and a best friend. I enjoyed the time that we

worked together and learned from each other. I thank Zhongyue Yuan, Zizhao Xu and Yong Zhu for their assistance and suggestions to my research project.

I am also grateful to all my friends in PCSP, without whom my time at pacific would not be so fun and memorable: Dr. Chao Feng, who helped with my research project with his excellent chemistry knowledges; Michael Ng, who helped with improving my oral and written English; my roommates Hao Wei, Fang liu, and You Li, with whom I had a lot of good time; and Xuequn Huang, Yiyuan Wang, Dr. Jinyun Chen, Qing Zhang, Jingda Wang, Yuntao Zhang, Jensen Spear, Guanming Jiang, Dr. Jieyun Cao, Arjun Patel, Md Tariqul Tuhin, Toufiq Ul Amin, for their friendship. I am grateful to my boyfriend Dengpan Liang, who always helps me to overcome whatever challenges I encounter. He has inspired me to find my interest in the field of pharmaceutical sciences. I cannot thank him enough for so much he has done for me.

At last but not the least, I am sincerely grateful to my parents and my family for their unconditional love and support.

IMIDAZOLE-BASED PH-SENSITIVE CONVERTIBLE LIPOSOMES
FOR ANTICANCER DRUG DELIVERY

Abstract

By Ruiqi Huang

University of the Pacific
2020

Solid tumors possess biological features that are different from those in healthy tissues, which provides opportunities of anticancer treatment by nanomedicines. Due to the presence of the fenestrated tumor vasculatures, nanomedicines can selectively accumulate in tumor tissues by the enhanced permeability and retention (EPR) effect. The acidic pH in tumor interstitium (pH 6.0-7.0) also provides a promising mechanism to trigger the nanomedicines to promote the cellular uptake of cargo drugs. The previously reported stealth liposomes coated with PEG are known to accumulate in tumors owing to their prolonged circulation time. The PEG coating on liposomes can hinder serum protein adsorption and thus prevent rapid elimination by the reticuloendothelial system, thus increasing the liposome circulation time. However, liposomal interaction with cancer cells can also be hindered by the PEG coating.

In order to improve the anticancer activity of stealth liposomes, novel synthetic imidazole-based lipids were introduced to the composition of stealth liposomes to develop the pH-sensitive imidazole-based convertible liposomes (ICL). At acidic pH, the imidazole-based lipids would protonate to acquire positive charges, thus clustering with the negatively charged PEGylated lipids. Such lipid-lipid electrostatic interaction would induce phase separation of the bilayer to generate a PEG-free domain that displays excess positive charges. Such newly converted, cationic liposomes at acidic pH in tumor interstitium would have better interaction

with negatively charged cancer cells and/or enhanced drug release, therefore overcoming the drawback of traditional stealth liposomes.

After synthesizing the imidazole-based lipids DHI, DHMI and DHDMI, we constructed doxorubicin (DOX)-loaded ICL formulations. The physicochemical properties of ICL were characterized, and factors influencing such properties were explored. The pH-triggered acquisition of positive charges of ICL was confirmed by the elevation of ζ- potentials and aggregation with negatively charged model liposomes that mimic bio-membranes at acidic pH 6.0-7.0. Acidic pH-triggered release of ICL was confirmed by drug release assays. It was also found that although the incorporation of cholesterol can remarkably reduce the size and increase the encapsulation efficiency (EE) of ICL, it also hinders the pH-sensitivity of ICL. The morphology of ICL at both pH 7.4 and pH 6.0 was characterized under transmission electron microscopy (TEM), which showed morphological changes in response to acidic pH 6.0, which further supported the proposed pH-sensitivity of ICL.

Cytotoxicity assays on 3D MCS of HeLa, A549, MDA-MB-231 and MDA-MB-468 cell lines were conducted to evaluate the anticancer activity of ICL formulations. ICL formulations without cholesterol showed considerably enhanced anticancer activities against MCS compared with the non-sensitive stealth liposomes (NSL). However, incorporation of cholesterol decreased such activities. The IC_{50} values of cholesterol-free ICL and ICL with cholesterol against MCS strongly suggested that the pH-sensitivity introduced by the imidazole-based lipids would enhance the anticancer activity of stealth liposomes, while the hindrance of the pH-sensitivity by cholesterol would reduce such activities.

Taken together, ICL's pH-sensitivity is correlated with their enhanced anticancer activity than non-sensitive stealth liposomes.

TABLE OF CONTENTS

LIST OF TABLES

Table

LIST OF FIGURES

Figure

LIST OF ABBREVIATIONS

AMF Alternating Magnetic Field

ATP Adenosine Triphosphate

Chol Cholesterol

CTX Chemotherapy

DHDMI and sn-2-((2,3-bis(hexadecyloxy)propyl)thio)-4,5-methyl-1Himidazole

DHG 1,2-Di-O-hexadecyl-rac-glycerol

DHI sn-2-((2,3-bis(hexadecyloxy)propyl)thio)-1H-imidazole

DHMI sn-2-((2,3-bis(hexadecyloxy)propyl)thio)-5-methyl-1Himidazole

DLPC 1,2-dilauroyl-sn-glycero-3-phosphocholine

DLPE 1,2-dilauroyl-sn-glycero-3-phosphoethanolamine

DMEM Dulbecco's Modification of Eagle's Medium

DMF N, N-Dimethylformamide

DMPC 1,2-dimyristoyl-sn-glycero-3-phosphocholine

DMPE 1,2-dimyristoyl-sn-glycero-3-phosphoethanolamine

DMSO Dimethyl sulfoxide

DOPC 1,2-dioleoyl-sn-glycero-3-phosphocholine

DOPE 1,2-dioleoyl-sn-glycero-3-phosphoethanolamine

DOX Doxorubicin

DPPC 1,2-dipalmitoyl-sn-glycero-3-phosphocholine

DPPE 1,2-dipalmitoyl-sn-glycero-3-phosphoethanolamine

DPPE-PEG 1,2-dipalmitoyl-snglycero-3-phosphoethanolamine-N-[azido(polyethylene glycol)-2000

DSPC 1,2-distearoyl-sn-glycero-3-phosphocholine

DSPE 1,2-distearoyl-sn-glycero-3-phosphoethanolamine

EE Encapsulation efficiency

EPR Enhanced permeability and retention

GI Gastrointestinal

HA Hyaluronic Acid

HEPES 2-[4-(2-hydroxyethyl)piperazin-1-yl]-ethanesulfonic acid

HPLC High-performance liquid chromatography

HTS High Throughput Screening

IC_{50} Fifty Percent Inhibitory Concentration

ICL Imidazole-based Convertible Liposomes

IV Intravenous

L-R-PI L-α-phosphatidylinositol

MCS Multicellular spheroids

MCTS Multicellular Tumor Spheroid

MDR Multidrug Resistance

MW Molecular Weight

NPs Nanoparticles

NSL Non-sensitive Liposomes

PBS Phosphate buffered saline

PC Phosphatidylcholine

PDI Polydispersity Index

PDX Patient-derived xenografts

PE Phosphatidylethanolamine

PEG Polyethylene glycol

pH_e Extracellular pH

pH_i Intracellular pH

POPC 1-palmitoyl-2-oleoyl-glycero-3-phosphocholine

POPE 1-palmitoyl-2-oleoyl-sn-glycero-3-phosphoethanolamine

POPS 1-palmitoyl-2-oleoyl-sn-glycero-3 phospho-L-serine

PPE Palmar-plantar Erythrodysesthesia

RES Reticuloendothelial System

RT Room Temperature

SD Standard Deviation

SEC Size Exclusion Chromatography

T Temperature

TEA Triethanolamine

TEM Transmission Electron Microscopy

TLC Thin-layer Chromatography

T_m Transition Temperature

TOP II Topoisomerase II

TPZ Tirapazamine

UA Uranyl Acetate

ULA Ultra-low Attachment

CHAPTER 1: INTRODUCTION

1.1 Cancer and Solid Tumor

 1.1.1 Introduction on cancer. Cancer is a generic term of a group of diseases that involves abnormal growth, migration, and invasion of cells [1]. Mostly, cancer is known as malignant tumors with the potential to invade to other parts of the body, which are in contrast to benign tumors that do not spread. Cancer is the second leading cause of death globally, and over 100 types of cancers have been found [2]. Five to ten percent of cancers are caused by genetic hereditary while vast majority of cancer are induced by external factors including tobacco use, obesity, lack of physical activity, excessive drinking of alcohol, and infections such as Helicobacter pylori, hepatitis and HIV [3]. Cancers show symptoms such as lumps, abnormal bleeding, weight loss, and can be diagnosed by screening tests, medical imaging, and biopsy [4]. Cancer is typically treated with combination of radiation therapy, chemotherapy, targeted therapy and surgery.

 1.1.2 Biological features of solid tumors. Neoplasm, also named solid tumors, is a type of abnormal and excessive growth of tissue in body, which can be classified into benign tumors, potential malignant tumors and malignant tumors. Malignant tumors will be the only type of solid tumors for discussion in this thesis.

 The physiology of solid tumors differs from that of normal tissues in a variety of aspects. Most of the biological features of solid tumors originate from the difference of vasculatures between normal and tumor tissues [5]. In contrast to the healthy, orderly vasculature of normal tissues, tumor blood vessels have more distended shape, more leaky walls and more sluggish blood flow. Due to the rapid growth of cancer cells, new blood vessels are grown in tumors in

order to maintain the basic supply of oxygen and nutrients. However, those blood vessels are usually poorly formed, which leads to several biological features in solid tumors, including hypoxia, necrosis, acidic microenvironment, unique extracellular matrix (ECM), and drug resistance.

1.1.2.1 Hypoxia in solid tumors. The metabolic hypoxia in solid tumors is a pathophysiological consequence of the disturbed vasculature and the deterioration of diffusion conditions [6]. When a tumor's oxygen supply is not restricted, its oxygen consumption rate and adenosine triphosphate (ATP) production is comparable with those in normal tissues. However, as the tumor grows larger, regions that lack microcirculation cannot obtain adequate supply of oxygen from blood vessels. Such regions enter a condition of hypoxia, which features progressive decrease of oxygen partial pressure and cellular ATP production. Hypoxia in tumors is largely associated with tumor propagation, malignant progression and resistance to therapy. Therefore, hypoxia has become a major issue in cancer treatment [6]. Hypoxia induces proteome changes in cancer cells and stromal cells in tumors, which in turn causes cellular quiescence, differentiation, apoptosis, and necrosis [7]. Evidence is accumulating that hypoxia in solid tumors drives malignant progression of cancer cells, which is marked by increasing probability of metastasis and increasing resistance against nonsurgical therapy (e.g. radiotherapy and chemotherapy) concomitant with tumor growth [8, 9].

1.1.2.2 Necrosis in solid tumors. Necrosis occurs in most solid tumors. The edges of necrotic regions in tumors were found to be parallel to the neighboring blood vessels, suggesting that the necrosis is caused by limited diffusion of adequate oxygen and nutrients into cancer cells as well as limited transfer of metabolites from cancer cells to the blood vessels [10]. A relatively constant distance between blood vessels and the edge of necrotic regions, typically 100 to 200

μm, was observed in tumors, which is consistent with the estimated distance of sufficient oxygen diffusion in tissues [11]. Such in-between areas contain cells that are still viable but with very low level of oxygen. This type of quiescent cells, together with the necrotic cells farther away from the blood vessels and the proliferative cells closer to the blood vessels, constitute the highly heterogeneous tumor tissues.

1.1.2.3 pH gradients in solid tumors. Acidic pH is a major feature of tumor tissues and is typically represented by two pH gradients in solid tumors: the reversed gradient between pH_i and pH_e, and the pH gradient between the outer and center region of tumors. Normal cells in healthy tissues have an intracellular pH (pH_i) of 7.2 and a slightly higher extracellular pH (pH_e) of 7.4. In contrast, cancer cells in tumor tissues are characterized by a relatively higher pH_i of 7.2 and a lower pH_e of 6.0-7.0 [12]. This "reversed" pH gradient in tumors not only provides essential support for the growth, invasion and migration of tumors, but also helps protect the tumors from anti-tumor immunity and apoptosis [13]. The pH_e of cancer cells also varies in different regions of solid tumors. The pH in the outer proliferative and quiescent areas average around pH 7.0, while the pH in the tumor cores generally drops to 6.1-6.4[14, 15].

The acidic pH in solid tumors results from the accumulation of the metabolic by-product of hypoxia – lactate. Under the condition of low oxygen and nutrient concentrations, cancer cells tend to produce lactate from the anaerobic glycolytic pathway more than oxidative phosphorylation for energy production [16]. In consequence, lactate accumulates in the tumor interstitium, especially in the tumor core where the oxygen penetration and waste removal are extremely restricted. The accumulation of the acidic lactate contributes to decrease of pH in tumor interstitium, leading to drug resistance [17]. Therefore, it has been considered a potential therapeutic strategy to inhibit the production and transport of lactate [18].

1.1.2.4 Extracellular matrix (ECM) in solid tumors. Extracellular matrix (ECM), a highly dynamic structure, is the major structural component in tumor microenvironment. The ECM of cancer cells provides both biochemical and physical support for the solid tumor, and is distinct in its composition and stiffness compared with normal ECM [19]. The dynamics of ECM in solid tumors becomes abnormal due to the disruption of equilibrium between the synthesis and secretion of ECM components and the expression of matrix-remodeling enzymes. The ECM in tumors contains a variety of proteins, including fibrous protein, glycoproteins, proteoglycans, and polysaccharides. The fibrous ECM proteins, such as collagen, partake in tumor tissue development by providing mechanical strength, altering cell adhesion, and promoting cell migration [20]. Glycoproteins in tumors make the ECM a cohesive network to link cells together with structural components, such as fibulin, fibrillin, and laminin. Proteoglycans play a crucial role in ECM assembly and cell signaling by binding with growth factors and acting as co-receptors of ligands. Polysaccharides, such as hyaluronic acid (HA), play a role in filling the interstitial space and buffering physical stress on the ECM. In addition to the biochemical effects, the tumor ECM also provides a physical barrier that hinders the transport of water, solutes and chemotherapeutics [21]. Due to the overexpression of many ECM components, tumor ECM is typically stiffer than ECM in healthy tissues.

1.1.2.5 Opportunities provided by biological features of solid tumors. Conversely, the aforementioned biological features of solid tumors, such as deformed vasculature, hypoxia and physical barriers from ECM also provide opportunities of anticancer treatment. For example, Tirapazamine (TPZ), can be activated by the hypoxia to selectively kill cancer cells in solid tumors [5]. Nanomedicines can diffuse across the more porous tumoral blood vessels to selectively accumulate in solid tumors [22]. The acidic pH in tumor interstitium can enhance

drug release from pH-sensitive drug delivery systems [23]. Some gene therapeutics have been developed to be activated by hypoxia or necrosis of solid tumors [24, 25].

1.2 Anticancer Drugs

1.2.1 Introduction on anticancer drugs. Generally, anticancer drugs are classified according to their mechanism of action. Major groups of anticancer drugs include cytotoxic drugs, hormonal drugs and targeted drugs. Correspondingly, three major modalities are included in cancer pharmacotherapy. The cytotoxic chemotherapy connotes the use of non-specific cytotoxic drugs to suppress cancer cell mitosis and division, but excludes therapeutic agents that are more targeted or block extracellular signals [26]. Therapies that inhibit tumor growth signals from endocrine hormones are called hormonal therapies, which are specifically applied in treatments of breast cancer and prostate cancer [27]. Therapies that inhibit tumor growth signals associated with specific targeted receptors are referred as targeted therapies [28]. Because anticancer drugs are administrated into the blood circulation, they represent a type of systemic therapy and could address cancer at any location in the body. Such systemic anticancer therapy is usually in conjunction with local anticancer therapy, such as radiation therapy, surgery, and hyperthermia therapy, which exert anticancer effects only where they are applied [29].

1.2.2 Challenges and limitations of cytotoxic chemotherapies. Chemotherapy, usually referred as chemo or CTX, is a type of cancer treatment that uses single or multiple cytotoxic drugs. Closely correlated to medical oncology, chemotherapy is one of the major categories of pharmacotherapy for cancers [30]. Conventional chemotherapeutic agents inflict toxicity to cells and interfere with their mitosis. The cytotoxic drugs in conventional chemotherapy are classified to antimetabolites (e.g. Methotrexate and Gemcitabine), alkylating agents (e.g. Cisplatin and Carboplatin), microtubule damaging agents (e.g. Vincristine and Vinblastine), topoisomerase

inhibitors (e.g. Etoposide and Topotecan), antibiotics (e.g. Doxorubicin and Bleomycin) and other miscellaneous agents (e.g. Tretinoin and Hydroxyurea). In general, chemotherapy using a combination of cytotoxic drugs have shown better efficacy than a single cytotoxic drug [31].

Poor selectivity is the major drawback of chemotherapy. Because cancer cells originate from normal cells, anticancer drugs that inhibit the growth of cancer cells are also cytotoxic to normal cells. Many of the side effects of chemotherapy are attributed to the damage of normal cells that are sensitive to anti-mitotic drugs, including those in digestive tract, bone marrow and hair follicles [32]. Therefore, common side effects of chemotherapy include decreased production of blood cells, mucositis in gastrointestinal tract and hair loss. For example, cyclophosphamide and methotrexate, which are commonly used agents for breast cancer are known to cause neutropenia, alopecia and emesis [33]. Moreover, cisplatin is widely known to have nephrotoxicity due to accumulation of transported cisplatin in the kidney [34], and doxorubicin has been known to have cardiotoxicity, which may induce arrhythmias, pericarditis, myocarditis and acute heart failure [35].

Besides poor selectivity, chemotherapy is also limited by drug resistance, which is a major cause of failure of chemotherapeutic drugs. One cause of drug resistance is that cancer cells overexpress transporters that that protect them from chemotherapeutics [36]. The transporters (e.g. p-glycoprotein) can be overexpressed on cancer cell surface to move drugs from cytosol to the interstitium. Agents that inhibit the transporters have been developed, but not yet approved for clinical use due to toxicity [37]. Another cause of drug resistance is gene amplification that induces multiple copies of a cancer cell, which is against the effect of chemotherapeutics on the gene expression in cell proliferation [36]. Furthermore, the cellular pathways of apoptosis can be defective in cancer cells, which increased cancer cell survival

when exposed to chemotherapeutics. Additionally, the DNA damage exerted by chemotherapy agents can be repaired by enzymes in some cancer cells [38]. Besides resistance against a single drug, cancer cells may also develop resistance against a group of drugs with similar mechanism and cross-resistance against several drugs of different targets and mechanisms [39]. Chemotherapy is also facing challenges in effective drug distribution and penetration due to the deformed vessels in tumors. New blood vessels are formed in tumors as they grow larger, but such tumoral blood vessels have poor structure and are only distributed in the peripheral region of a solid tumor. Therefore, the core of a solid tumor usually has inadequate blood supply, and consequently poor drug distribution[40].

1.2.3 Targeted anticancer drug delivery. Targeted drug delivery, also known as smart drug delivery, is a method that delivers drug(s) to a patient at higher concentration at the targeted site of action [41]. Targeted drug delivery systems aim to have prolonged and localized drug interaction with the diseased tissue to improve the efficacy. Moreover, targeted drug delivery aims to decrease the side effects of cytotoxic chemotherapy by decreasing the concentration of the cytotoxic anticancer drug in healthy tissues [42]. Targeted drug delivery systems have strong market prospects, because the reduced toxicity means significantly improved survival and life quality for cancer patients. The drawback of targeted delivery systems is the higher cost that makes production and dosage modification more challenging. Targeted drug delivery has been closely associated with the development of nanomedicines. Generally, the strategies of drug targeting in such drug delivery systems can be classified into passive targeting and active targeting [42, 43].

1.2.3.1 Passive targeting. Passive targeting, also known as physical targeting, increases drug accumulation in diseased tissues by taking advantage of the physical characteristics of the

delivery system [45]. The passive targeting for cancer treatment is directly related to the circulatory system and is assisted by the enhanced permeation and retention (EPR) effect. Translocation of molecules through vascular interspace is closely dependent on the sizes of molecules and the vasculature morphology. The short half-life of conventional chemotherapeutics in blood circulation and their indiscriminate accumulation in healthy tissues are attributed to their small size (generally < 1000 Da), which lead to extravasation through vascular pores in healthy tissues (50-150 nm) [44]. This mode of biodistribution constitutes poor selectivity and thus high general toxicity of conventional, small molecule chemotherapy agents. In comparison, blood vessels in tumors carry pores in the size range of 200-1200 nm [45], resulting in enhanced vascular permeability and lowered clearance of nanomedicines in the size range of 100-200 nm. Therefore, the fenestrated neovascular wall in tumors elicits selective accumulation of nanomedicines but not small molecular drugs (Figure 1.1). However, extended half-life of a nano drug delivery system in blood circulation is necessary for its passive targeting into tumors. In order to achieve the prolonged circulation in blood, a nano drug delivery system is often coated with hydrophilic polymers, such as polyethylene glycol (PEG) to hinder its recognition and elimination by the reticuloendothelial system (RES) [46].
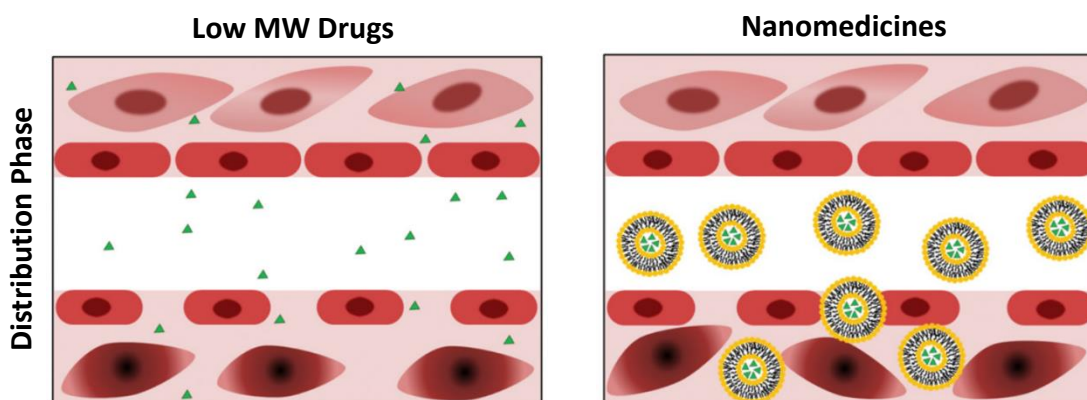
(Figure 1.1 Continued)
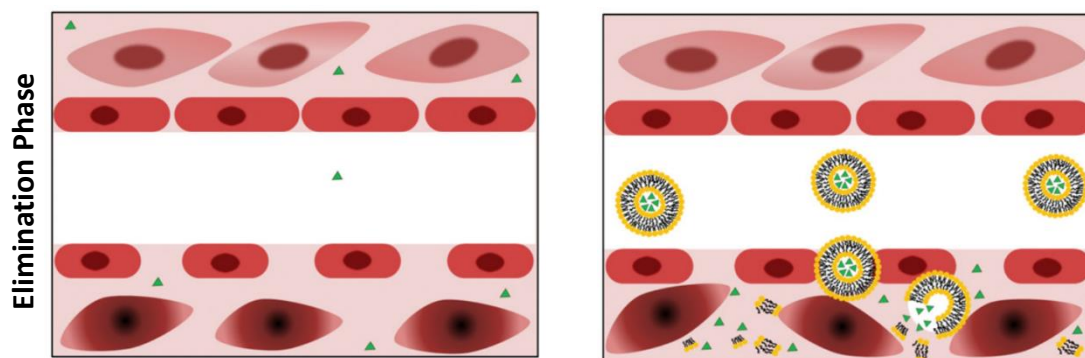
Figure 1.1. Conventional low molecular weight (MW) drugs versus nanomedicines: low MW drugs showed high accumulation in both healthy tissues (upper to the vessel, pink) and tumor tissues (lower to the vessel, dark red), while nanomedicines showed specific promoted accumulation in tumor tissues. [47]

Passive targeting provides great advantage in nanomedicine therapy but it also faces several challenges. One challenge for the EPR effect is the vascular features in tumors. The vascular density varies in different types of cancers. Specifically, it was found hepatic and renal carcinoma had stronger EPR effect than pancreatic and prostate cancers [47]. Moreover, the vessel distribution within a tumor is heterogeneous. It was reported that drug distribution is limited in the central necrotic regions in tumors, which are far from the blood vessels and therefore little impacted by EPR effect, which relies on vascular permeability [48]. Another challenge for the EPR effect is the stromal compartment in tumors, which is composed of ECM and stromal cells. The ECM components, such as collagen and hyaluronic, form a dense barrier against the penetration of nanomedicines from blood vessels to tumor interstitium [49]. Several studies have confirmed that nanomedicine accumulation is compromised in collagen-rich tumors, as the composition and distribution of collagen in tumors causes heterogenous distribution of drug delivery systems [50].

1.2.3.2 Active targeting. Active targeting takes effect based on the phenotypic and biochemical characteristics in diseased tissues. In addition to passive targeting, active targeting would help drug delivery systems take effect more specifically at targeted sites and spare healthy tissues [51]. Active targeting can be accomplished using several approaches, which are divided into ligand-receptor binding, activated targeting, and locally activated targeting.

The most common active targeting strategy is ligand-receptor binding, which employs biological interactions between ligand and its receptor [52]. Drug delivery systems containing specific ligands would selectively bind with their coupling receptors, which are overexpressed on the surface of tumor cells but not normal cells, in order to localize the payload drug to tumor tissues [53]. It was reported the ligand-receptor binding may trigger endocytosis and cellular drug uptake, which helps suppress the multidrug resistance of tumor [54]. For example, transferrin has been utilized to mediate endocytosis by conjugating with nano-formulations and then interacting with receptors on cell membranes. The transferrin-conjugated nano-formulations showed better cellular uptake than the non-conjugated counterparts [54]. One of the major challenges for the ligand-receptor mediated active targeting is the limited selectivity. Firstly, selectivity of such active targeting is compromised by the heterogeneity of receptor expression by cancer cells. Different receptors are expressed in various types of cancers; receptors are expressed differently in the same tumor at different developmental stages; cultured cancer cells *in vitro* may not express the same receptors as *in vivo* tumor cells – all these means that heterogeneity leads to imprecise evaluation of drug delivery systems [55]. Secondly, selectivity also relies on receptor density on cancer cells. Such active targeting would only take effect where the receptor is considerably over expressed by cancer cells than normal cells [55]. The third challenge for active targeting is the limited binding. The binding is associated with

both the distance and the affinity between a ligand and its receptor. The binding would occur only when the distance between the ligand and the receptor is smaller than 0.5 nm, beyond which the delivery system would not accumulate at the targeted site [56]. Moreover, excessive binding between the ligand and the receptor may generate a binding-site barrier, which would hinder the uptake of therapy agents by tumors [32].

One strategy to achieve active targeting is called locally activated drug delivery, which initiate the formulation-cell interaction and the drug release by signals that are specific to the diseased site such as pH, or by external stimuli such as temperature, ultrasound, light and magnetic field [57, 58]. This type of delivery systems is also known as stimulus-sensitive systems. Some locally active drug delivery systems are sensitive to specific signals generated by the abnormal biochemical properties of tumors, such as the acidic microenvironment and the lower redox potential due to hypoxia [59, 60]. Some locally active drug delivery systems can achieve enhanced release in response to external stimuli, such as ultrasound, light, magnetic field and electric field [61-64].

1.2.4 Anticancer nanomedicines. Nanomedicine, also named nanotherapeutic, is defined as the application of nanomaterials and nanotechnology for medical purposes [65]. Nanomedicine represents an emergent field address issues of conventional anticancer drugs. Designs of nano-drug delivery systems aim to maximize bioavailability both at specific sites and over a desirable period of time. Loading therapeutic agents into lipid- or polymer-based nanoparticles can help improve the pharmacokinetics of therapeutics, such as reduced distribution volume, lowered clearance rate and longer circulation time [65]. Targeted nanomedicines have lowered overall drug consumption and decreased toxicity by accumulating and releasing drugs selectively in the diseased regions at no higher dose than needed [66].

Nanomedicines have also been applied to improve anticancer immunotherapy by delivering specific tumor microenvironment (TME)-normalizing agents [67]. Nano-formulations can also deliver multiple drugs to counterdrug resistance and to achieve synergistic therapeutic effects [68]. Application of amphiphilic materials such as phospholipids in nano-formulations, helped enhance the solubility, stability and bioavailability of lipophilic drugs in blood circulation [69]. Furthermore, the 10-200 nm size range of nanomedicines significantly benefits their drug delivery. Compared with small molecule therapeutics, the larger surface area of nanomedicines improve their interaction with biological membranes [70]; compared with larger delivery systems such as microspheres and microcapsules, nanomedicines are less invasive and have shorter biochemical reaction time [71].

Nanomedicines are classified into lipid nanosystems, polymeric NPs, engineered NPs, dendrimers, nanotubes, fullerenes, quantum dots, and viral vectors. Among them, lipid nanosystems include liposomes, solid lipid nanoparticles (SLNs), lipid-based micelles, emulsions and lectin-modified SLNs [72]. Ideal nanocarriers of therapy agents are expected to possess high bio-capacity, low toxicity and low immunogenicity. However, the toxicity of nanocarriers themselves, namely nanotoxicity, has recently become a concern for their medical applications [73, 74]. Investigations on limitations of nanomaterials are still ongoing in order to broaden their applications in health sciences.

1.2.5 Doxorubicin (DOX) and DOX-loaded Nano-formulations. Doxorubicin (DOX or DXR) (Figure 1.2), with the brand name Adriamycin, was approved in U.S. in 1974. DOX is administrated by intravenous (IV) injection to treat a wide range of cancers, including breast cancer, ovarian cancer, bladder cancer, lymphoma, Kaposi's sarcoma, and acute lymphocytic leukemia [75]. DOX belongs to anthracyclines, a group of chemotherapy agents extracted from

Streptomyces bacterium, and is one of the most effective anticancer medications [76]. DOX is a

fluorescent molecule with a maximum excitation wavelength at ~485 nm and emission between

560-590 nm. The broad spectrum of anticancer activity and the fluorescence makes DOX one of

the most commonly used payload drugs in the development of anticancer drug delivery systems.

Cytotoxicity of DOX is based on two different mechanisms. Firstly, DOX intercalates into DNA

to inhibit the function of topoisomerase II (TOP II), which induces DNA breakage and cell death.

Furthermore, DOX is also known to generate free radicals that damage cell membranes, DNA,

and proteins, which is another mechanism to induce cell death [77].
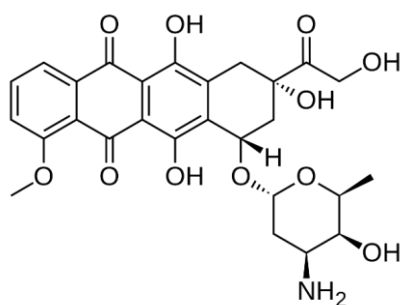
$C_{27}H_{29}NO_{11}$
Exact Mass: 543.17
Mol. Wt.: 543.52
m/e: 543.17 (100.0%), 544.18 (30.9%), 545.18 (6.8%), 546.18 (1.1%)
C, 59.66; H, 5.38; N, 2.58; O, 32.38

Figure 1.2. Chemical structure of DOX.

Common side effects of DOX include hair loss, nausea and vomiting, diarrhea, missed

menstrual periods, loss of appetite, weakness, tiredness, and reddish color in urine, tears and

sweat [75]. Moreover, DOX is known to cause severer and possibly life-threatening

cardiotoxicity. To mitigate the dose-limiting side effects, DOX-loaded nanomedicines have been

developed, including Doxil®, Myocet™, ThermoDox®, LipoDox®, and Caelix® [78-80].

Doxil, the DOX-encapsulated long-circulating stealth liposomes, was the first nano-sized

liposomal product to obtain regulatory approval [79]. It was approved in the U.S. in 1995 for the treatment of ovarian cancer and AIDS-related Kaposi's sarcoma. The mean diameter of Doxil liposomes is 80-90 nm and each lipid vesicle can encapsulate up to 15000 DOX molecules [81]. Many studies have demonstrated that, compared with free DOX, Doxil has a drastically lower cardiotoxicity and substantially higher efficacy, both owing to its preferred accumulation at tumor sites [82, 83]. Owing to the nanometer size, Doxil can accumulate at tumor sites based on the mechanisms of passive targeting (1.2.3.1). The PEG coating of Doxil hinders its recognition by the RES system (1.3.4.2), thereby increasing its circulation time to consolidate the passive targeting.

1.3 Liposomes

1.3.1 Introduction of liposomes. As one of the nanocarriers, liposome is a type of nano-scaled spherical vesicles which consist of a lipid bilayer shell and an aqueous interior. The bilayer structure is attributed to the special properties of lipids. Most liposomes are composed of phospholipids, which are amphiphilic molecules carrying a hydrophilic head consisting of a phosphate group and a lipophilic tail consisting of two fatty acid chains. When phospholipids are dispersed in water, they spontaneously form enclosed bilayer structures. The amphiphilicity of phospholipids makes liposome a versatile carrier for both hydrophilic and hydrophobic drugs. Composition of liposomes may also include other lipids such as cholesterol, as long as they are compatible with the lipid bilayer [84]. There are currently more than ten clinically used liposome-based products and hundreds of new liposome formulations in clinical trials. So far liposomal formulations of anticancer and antifungal agents have been commercialized [85].

1.3.2 Preparation of liposomes. Liposomes can be prepared by several types of methods. Thin-film hydration is the most widely used preparation method in research labs in

which a dry film of lipids is prepared and then hydrated in an aqueous medium [78]. Ethanol injection method is commonly used in industrial manufacturing of liposomes, in which an ethanol solution of lipids is rapidly injected into an aqueous medium through a needle to disperse the lipids and promote the vesicle formation [78]. Other methods include reverse-phase evaporation and freeze-drying [79]. Techniques such as freeze-anneal-thawing, membrane extrusion, sonication and homogenization are applied to control the size and size distribution of liposomes [78].

In preparation of drug-loaded liposomes (Figure 1.3), hydrophobic drugs can be mixed with the compositional lipids in the thin film to incorporate into the lipid bilayer during film hydration/ethanol injection, while hydrophilic drugs can be encapsulated either passively by using an aqueous drug solution for film hydration/ethanol injection or actively by remote loading with an ion gradient. Many liposome formulations encapsulate DOX by the remote loading method [81]. Remote loading, also known as active loading, efficiently drives DOX molecules into the liposomes by a transmembrane ion gradient from a highly concentrated salt solution in the aqueous interior of liposomes. Traditionally, DOX is loaded by a pH gradient established by a concentrated ammonium sulfate solution in the aqueous liposome interior (Figure 1.4), which maintained the pH at pH 4-5. The remote loading occurs when DOX molecules diffuse from the bulk media to the liposome aqueous interior, where they are protonated at the acidic pH and then form a sulfate salt precipitate, which enables high drug loading and stable drug retention [85]. This remote loading driven by ammonium sulfate is less effective when the intraliposomal pH is neutral or slightly basic. As improved alternatives, metal salts such as manganese sulfate and copper gluconate have been reported to achieve high loading efficiency at pH > 6.5 [86, 87] by forming DOX-metal complexes inside the liposomes.
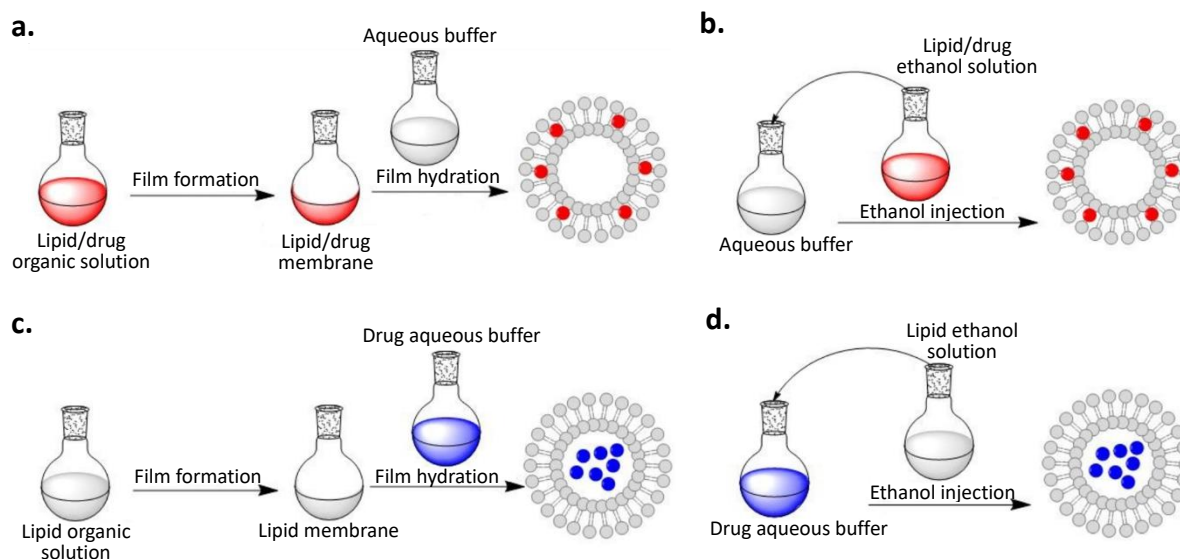
Figure 1.3. Schematic of preparation methods of drug-loaded liposomes. (a) Hydrophobic drug-loaded liposomes with film hydration method. (b) Hydrophobic drug-loaded liposomes with ethanol injection method. (c) Hydrophilic drug-loaded liposomes with film hydration method. (b) Hydrophilic drug-loaded liposomes with ethanol injection method. [86]
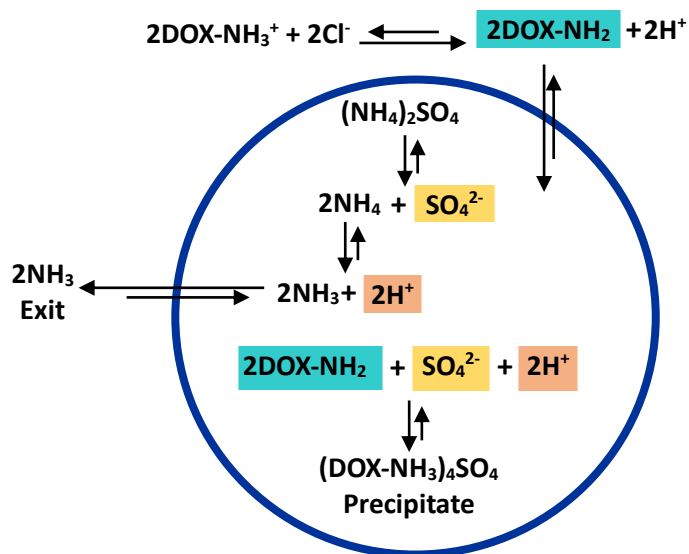
Figure 1.4. Remote loading of DOX into liposomes by ammonium sulfate gradient. (a) Reactions occurring inside and outside of the vesicles which caused $(DOX-NH_3)_4SO_4$ precipitate. (b) Spatial structure of $DOX-NH_2$ and $(DOX-NH_3)_4SO_4$.

1.3.3 Advantages of liposomal drug delivery systems. The liposomal drug delivery system was first proposed in 1961, and now has shown many applications in delivery of small molecule drugs, biomolecules and genes [87]. Liposomes are the most commonly utilized nanocarriers for targeted drug delivery due to a number of advantages [88]. Firstly, liposomes are able to carry a variety of cargo molecules, including small molecules, proteins, nucleotides and plasmids [85]. Specifically, liposome can encapsulate hydrophilic molecules in the aqueous interior, incorporate hydrophobic molecules in cavities of fatty acid chains, and carry drugs conjugated on the surface (Figure 1.5). Secondly, because both external and internal surfaces of the bilayer are outlined by the hydrophilic headgroups of phospholipids, liposomes represent a colloidal system to stabilize diverse payload molecules in aqueous media. Encapsulated hydrophilic payload molecules can be protected by the lipidic bilayer from deactivation in physiological media. Hydrophobic molecules that are incorporated in the liposome membrane can improve the solubility, stability and bioavailability in blood circulation [69, 89]. Thirdly, due to their generally biocompatible components, liposomes tend not to inflict severe immunoreaction or toxicity [90].
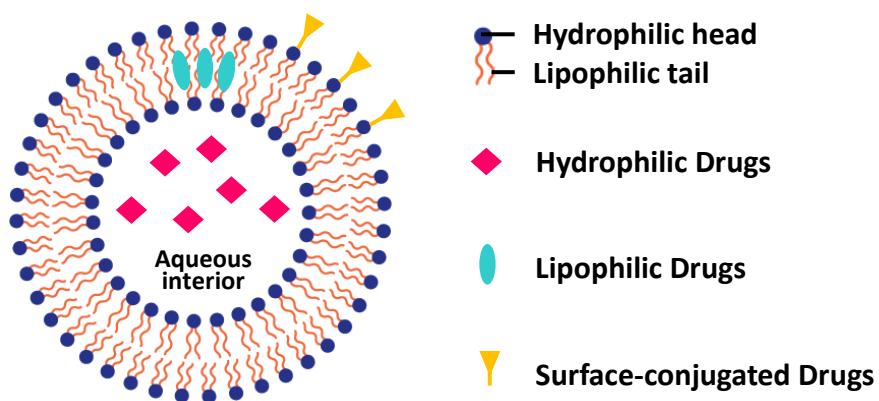
Figure 1.5. Schematic of liposome loaded with hydrophilic, lipophilic and surface-conjugated drugs.

1.3.4 Liposomal drug delivery and drug release. The pharmacokinetic profile and efficacy of liposomal drug delivery systems are largely correlated to: a) physicochemical characteristics including size, surface charge, steric hindrance, stability, and drug loading efficiency, b) successful delivery of drugs to the targeted sites, and c) successful release of drugs. Complex mechanisms have been developed to improve the precision of liposomal drug delivery and drug release, which can occur both extracellularly and intracellularly. The extracellular delivery by liposomes include passive targeting and active targeting (1.1.2.2). The liposomes are circulated in blood and then extravasate to accumulate in the interstitium of diseased tissues, followed by either drug release or endocytosis. Liposomes are often designed to release the payload more quickly in response to specific signals at the target site (aka triggered release), such as the acidic pH_e in tumors. The intracellular delivery of liposomes is needed for protein and nucleic acid therapeutics, because those molecules need to reach appropriate subcellular organelles to exert activity but cannot cross cell membranes by diffusion due to their large size and high hydrophilicity [91]. One of the major mechanisms of delivering large molecules into cells is endocytosis, the means of which include clathrinmediated endocytosis, phagocytosis, micropinocytosis and caveolae-mediated endocytosis. Endocytosis provides a mechanism to cross the plasma membrane but can result in varying levels of lysosomal degradation and exocytosis [92]. In order to avert these processes, some liposomal systems are designed to escape the endosome in response to a local stimuli such as acidic pH and enzymatic activities in the endosome [93, 94]. Besides endocytosis, lipid-mediated fusion with cell membrane is another major pathway for liposomes to release drugs into cells [95, 96].

1.3.5 Classification of liposomes. Liposomes can be formulated and processed to differ in size, lamellarity, composition, and surface charge. Besides these features, various molecules

can be grafted on the surface of liposomes to cater to various applications in drug delivery

(Figure 1.6). Major classes of liposomes are summarized in Table 1.1.

Table 1.1
Types of liposomes based on size and lamellarity, composition and charge, and application. [97, 98]

Classification Principals	Types	Properties
Size and Lamellarity	Small Unilamellar Vesicles (SUV)	With a single bilayer. Size ranges from 20 to 100 nm
	Large Unilamellar Vesicles (LUV)	With a single bilayer. Size ranges from 100 to 1000 nm
	Multilamellar Vesicles (MLV)	With multiple bilayers
Composition and Charge	Conventional Liposomes	Simply contain neutral/anionic phospholipids and cholesterol
	Cationic Liposomes	Contain cationic lipids such as DOTAP
Application	Stealth Liposomes	Contain a PEG coating to improve circulation time
	Stimulus-sensitive Liposomes	Physicochemical changes in response to specific stimuli
	Ligand Targeted Liposomes	Grafted with targeting ligands to interact with receptors on cells
	Immunoliposomes	Grafted with monoclonal antibodies for targeted drug delivery
	Transferosomes	With high elasticity to improve skin permeation following topical delivery
	Ethosomes	Utilize ethanol's penetration properties to improve skin penetration
	Pharmacosomes	Contain drugs that bind to phospholipids to improve their bioavailability
	Emulsomes	Contain a solid fat core to improve stability and entrapment efficiency
	Niosomes	Contain nonionic surfactants to improve oral bioavailability of drugs
	Vesosomes	Contain multiple compartments with an external bilayer to protect drugs from degradation and immune defense
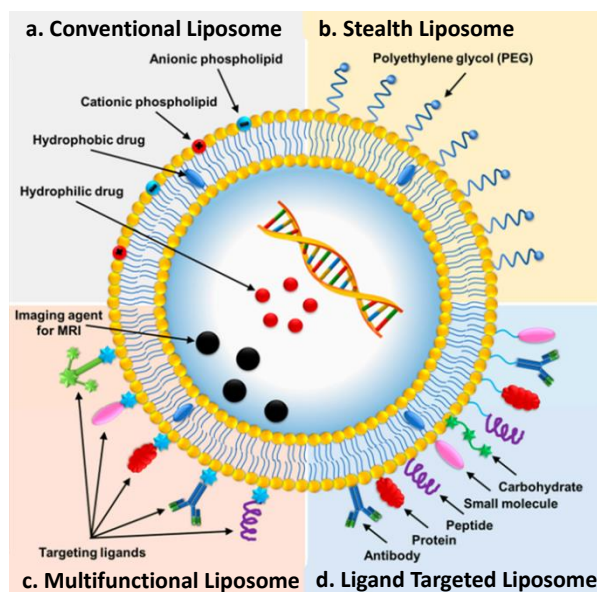
Figure 1.6. Schematic of liposome surface modification strategies. (A) Conventional liposomes. (B) Stealth liposomes (PEGylated liposomes). (C) Multifunctional liposomes. (D) Ligand targeted liposomes. [99]

1.3.5.1 Conventional liposomes. Conventional liposomes, also referred as the 'first generation liposomes", are usually composed of neutral or anionic phospholipids and cholesterol [83, 100]. Although their lipid bilayers are similar as biological membranes, they are detected by the immune system as foreign objects. After administrated through IV injection, conventional liposomes are recognized and rapidly captured by the reticuloendothelial system (RES), leading to their quick clearance and short half-life [46]. Conventional liposomes have been utilized for antiparasitic and antimicrobial drug delivery [101]. Nevertheless, RES becomes the major site of conventional liposome accumulation, resulting in their minimal effect on cells beyond RES. Conventional liposomes with larger size showed enhanced RES uptake, especially in the liver, which elevated the hepatic clearance [102]. Furthermore, conventional liposomes, especially those without cholesterol, displayed poor stability and poor extravasation after injection, due to their physical interaction with lipoproteins other serum proteins [83, 103].

1.3.5.2 Stealth liposomes. In order to overcome the aforementioned drawback of conventional liposomes, the surface of liposomes was modified to prolong their circulation in blood. The extended circulation time can be achieved by coating the liposomes with inert, hydrophilic polymers, such as polyethylene glycol (PEG), which provides a protective shell to hinder adsorption of serum proteins and elimination by RES. Owing to the PEG coating, the liposomes are less "visible" to RES, thus earning them the distinction as stealth liposomes [80] [83]. The hydrophilic PEG is also known to bind with water molecules via hydrogen bonding, which results in a hydration film that surrounds the liposome to mitigate its interaction with RES [51]. Moreover, the long chains of PEG surrounding a liposome provide a strong repulsion to the bilayer of other liposomes and thus prevent liposome aggregation, leading to improvement of liposome stability [104]. These multiple mechanisms of the PEGylated liposomes help them stay in the blood circulation for a longer period of time. Stealth liposomes have demonstrated dose-independent and non-saturable kinetics, as well as improved bioavailability [105].

PEG can be introduced onto liposome surface in multiple ways, including a) physical adsorption onto liposomes, b) covalent binding to liposomes, and c) addition of PEGylated lipids in the bilayer composition during liposome preparation. Stealth liposomes can be prepared using various lengths of PEG chains, which can substantially influence the liposome properties. Generally, the higher molecular weight of PEG leads to longer circulation time, except that liver clearance is found to be increased when the average molecular weight of PEG goes over 50000 Da [106]. PEG molecules ranging 2000 – 5000 Da have been extensively utilized in the preparation of stealth liposomes [107]. Besides PEG length, the performance of stealth liposomes *in vivo* is also influenced by other physicochemical properties, such as their size. It was found that 275 nm is the maximum limit of stealth liposome size, beyond which the stealth

property is significantly compromised [108]. Stealth liposomes with diameter of 100-150 nm were found to display notably reduced interaction with opsonins and other proteins in plasma [79, 109, 110].

Stealth liposomes are important in cancer treatment because their properties support passive targeting of their payload drugs. By minimizing the interaction of with RES, the stealth liposomes are targeted to tumor tissues more than RES. With PEG functionalization, the half-life of liposomes in blood circulation was extended from a few minutes to several hours [79]. The EPR effect is principally correlated to circulating time, and thus can be enhanced in stealth liposomes thanks to the sufficient time for such liposomes to circulate and to accumulate in tumor tissues. The preferential accumulation of stealth liposomes in tumor tissues leads to highly concentrated payload drugs at the target site and hence improvement in therapeutic efficacy over conventional liposomes.

Despite the prolonged circulation time and improved passive targeting of stealth liposomes, the steric hindrance of PEG chains decreases the interaction of liposomes with tumor cells [111], which in turn decreases intracellular uptake of the liposomal drug. To overcome this challenge, active targeting strategies, either ligand-receptor binding or locally activated drug delivery, has been applied along with the passive targeting to improve the drug delivery. The ligand-receptor mediated active targeting can be introduced by modifying the surface of stealth liposomes with targeting ligands. With the targeting ligands attached, the stealth liposomes would have significantly more interaction with tumor cells that overexpress the corresponding receptor [85]. Moreover, because the stealth liposomes can lodge in the interstitial spaces between the tumor cells, some elaborate targeting ligands were utilized to deliver the liposomes further into cancer cells [83]. The locally activated targeting can be achieved by incorporating

molecules that can trigger the liposomes in response to specific local stimuli. Stimulus-triggered release is the most common mechanism of action by stimulus-sensitive systems.

It must be noted that long circulation time is not always desirable for liposomes because it may also cause additional toxicity other than that of the cytotoxic payload [98]. For example, Doxil®, the approved stealth liposomal DOX, has much longer half-life (2-3 days) than free DOX (0.2 hour). The prolonged circulation time and passive targeting makes Doxil a suitable medicine for skin treatment of localized cancers such as Kaposi's sarcoma [83]. However, despite its significantly lower cardiotoxicity, myelosuppression and nausea than free DOX, Doxil has other significant side effects, such as Palmar-plantar erythrodysesthesia (PPE) and mucositis [81], which are largely attributed to its reduced clearance and tendency to accumulate at the skin [112]. In contrast, Myocet™, the approved conventional liposomal DOX with a much shorter half-life (2-3 hours) is not associated with PPE and has remarkably reduced incidence of mucositis [113]. Still, Myocet has sufficient circulation time to allow effective passive targeting to tumor sites, as demonstrated in studies on its use against metastatic breast cancer [80]. Stealth liposome-based and conventional liposome-based delivery systems are both under heavy development and have both yielded approved nanomedicines. These two types of liposomes are used to treat different diseases due to their different features so neither one would be able to substitute the other.

1.3.5.3 Stimulus-sensitive liposomes. Triggered release is a strategy to enhance the payload drug exposure to target cells and hence to improve the therapeutic outcome of liposomal formulations [114]. To achieve triggered release, liposomes are functionalized with specific molecules, thus become sensitive to target-specific stimuli and can release the cargo agents upon activation by those stimuli, which can be either internal or external.

The internal stimuli are endogenous signals that are specifically presented at or near the diseased sites, including pH, redox potentials, temperature, and enzymes. The pH gradients in tumor interstitium and endosomes have been widely utilized to trigger extracellular and intracellular release of payload agents from pH-sensitive liposomes [23, 114]. Liposomes can also be triggered in tumor tissues by their lower redox potential due to their hypoxia condition [60]. Thermo-liposomes can elevate their drug release when stimulated by higher temperature in inflammatory tissues [115] or by hyperthermia treatment of tumors [116]. In endosomes, hyaluronidase, the enzyme that degrades hyaluronic acid (HA), can trigger endosomal escape of HA-coated liposomes [94].

The external stimuli include ultrasounds, light, magnetic field and electric field. Such stimuli are applied for spatiotemporal control. It was found alternating magnetic field (AMF) can trigger the self-heating of liposome-encapsulated iron oxide nanoparticles to permeate the liposome membrane and hence to enhance the content release [117]. Ultrasound was found to expand gas pockets and thus was used to permeate the membrane of liposomes that co-encapsulate drugs and gas bubbles [118].

1.3.5.4 pH-sensitive liposomes. pH-sensitive liposomes have been developed to respond to the change of pH in specific biological microenvironments. pH gradients in the body have been investigated as an internal stimulus for drug delivery systems. The gastrointestinal (GI) track has a broad range of pH, from 1-3 in stomach, to 6 in duodenum, and to 7-8 in jejunum and ileum [119]. The tumor tissues have lower pH_e than normal tissues (pH 7.4), ranging from 5.8 to 7.6 and averaging around 7.0 [14]. The highly hypoxic core in tumors generally displays pH_e 6.1-6.4 [15]. pH decrease is also found during endosome maturation: from 7.4 to 6.5 in early endosomes, then to 5.5 in late endosomes, and then to 4.5 in lysosomes [120].
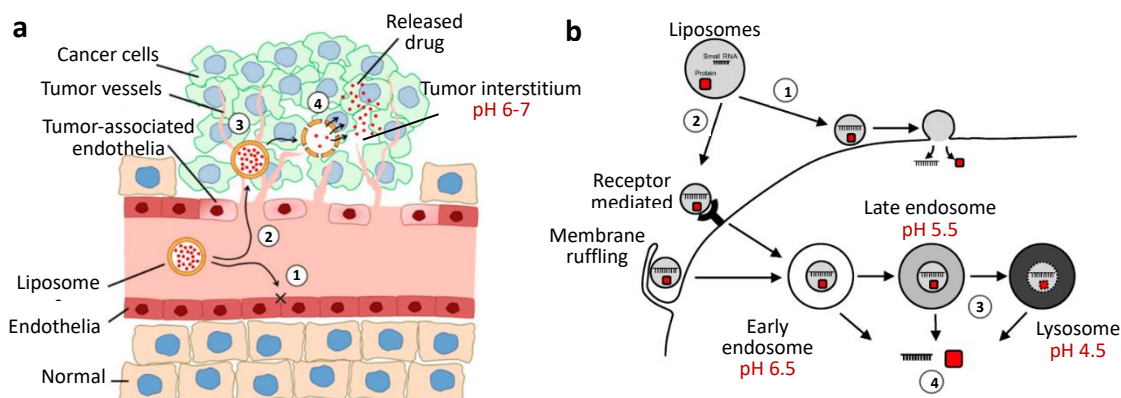
Figure 1.7. Schematic of two levels of pH-triggered responses of liposomes. (a) pH-triggered drug release in tumor interstisium [121]. 1) Liposomes are not able to extravasate to healthy tissues. 2) Liposomes extravasate to tumor tissues through the more porous tumor blood vessels. 3) Liposomes are retained in the tumor microenvironment. 4) Triggered release in response to acidic pH in tumor interstitium. (b) pH-triggered endosomal escape in cytoplasm [122]. 1) Direct fusion pathway of liposomes. 2) Endocytosis pathway of liposomes. 3) Maturation process of endosomes. 4) pH-Triggered endosomal/lysosomal escape.

Mechanistically, pH-sensitive liposomes undergo rapid destabilization in acidic environments to exert their biological activities [114]. The methods of inducing pH-sensitivity include incorporation of pH-sensitive lipids (such as DOPE or synthetic novel lipids) in the liposome membrane, conjugation with pH-sensitive molecules such as polymers and peptides, and encapsulation of pH-sensitive substances such as nanoparticles and peptides [23]. The pH-triggered actions of liposomes include content release, interactions with cells (such as binding, membrane fusion, and endocytosis), and endosomal escape. For some examples, pH-induced conformational flip of cyclohexane ring was utilized to produce a novel pH-sensitive lipid, which can permeate liposome membranes when exposed to the acidic microenvironment in tumor interstitium, thereby enhancing the release of the cargo drugs [123]; pH-sensitive alkylated N-isopropylacrylamide (NIPAM) copolymers enhanced the liposomal release after being grafted

onto liposome surface as a polymer coating [124]; magnesium phosphate nanoparticles that were co-encapsulated in liposomes were found to dissolve at lowered pH in endosomes to increase the osmotic pressure, which in turn help the cargo agents to escape the endosome [93].

1.3.6 Imidazole-based convertible liposomes (ICL). Although the PEG coating of liposomes helps to overcome the short circulation time and RES clearance to enhance tumor accumulation, the steric hindrance of the PEG coating also reduces the liposome's interaction with the cancer cells [125]. An ideal liposomal formulation is expected to carry not only high stability and sufficient accumulation in tumor tissues, but also good interaction with cancer cells to improve their penetration into solid tumors and their cargo's intracellular uptake. If a liposome carries the PEG coating in blood circulation and yet removes the coating upon exposure to cancer cells, then it can first accumulate at tumor sites and then interaction with cancer cells. Specific stimuli from tumor sites, such as acidic pH, can trigger this conversion. Previously, various PEG-shedding strategies were reported [126]. pH-sensitive linkers that can be hydrolyzed at acidic pH were used to detach the PEG molecules from liposome surface. However, such hydrolysable liposomes showed either poor stability at physiological pH 7.4 or insufficient pH-sensitivity at the mildly acidic pH 6.0 in tumor interstitium. Recently, our group developed a novel pH-sensitive liposome, whose grafted PEG chains are clustered rather than shed at acidic pH, is expected to be stable at physiological pH 7.4 but also activated to improve interaction with cancer cells in acidic tumor interstitium (Figure 1.8).
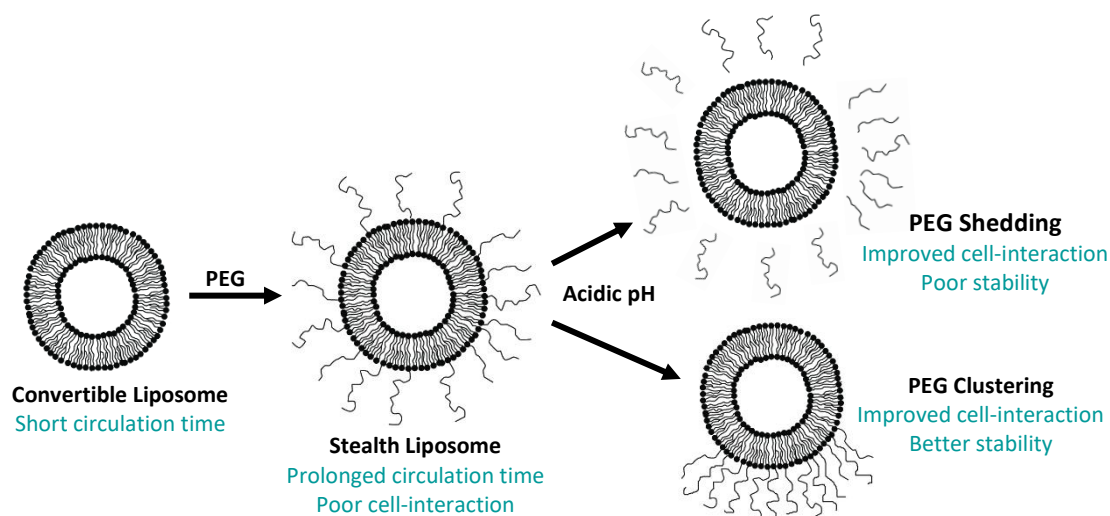
Figure 1.8. Schematic of two strategies to reduce the steric hindrance of PEG coating of stealth liposomes at acidic pH: PEG shedding (right upper) and PEG clustering (right lower).

Instead of using hydrolysable linkers to shed the PEG coating at acidic pH, this novel liposome contains 25 mol% of a synthetic lipid with an imidazole headgroup and two C16 hydrocarbon chains, which can protonate to display positive charges in response to acidic pH (Figure 1.9). This novel liposome also consists of DPPE-PEG (5 mol %), which is a PEGylated C16 phospholipid with a negative charge on the Phosphatidylethanolamine (PE) headgroups. The liposome also consists of a neutrally charged C18 phospholipid DSPC (70 mol %) (Figure 1.9). Due to electrostatic attraction between the headgroups and Vander Waals forces between the lipid tails of the same length [127], the positively charged imidazole-based lipids (C16) can cluster with the negatively charged DPPE-PEG (C16) (Figure 1.8) to expose part of the liposome surface free of PEG coating to interact with cancer cells. Moreover, the protonated imidazole-based liposomes display excess positive charges to interact more with cell membranes, which are negatively charged [128] (Figure 1.10). Such novel liposomes would show the stealth properties at physiological pH 7.4 but converts into cationic liposomes at acidic pH in tumor interstitium. Such liposomes are named imidazole-based convertible liposomes (ICL) [129].
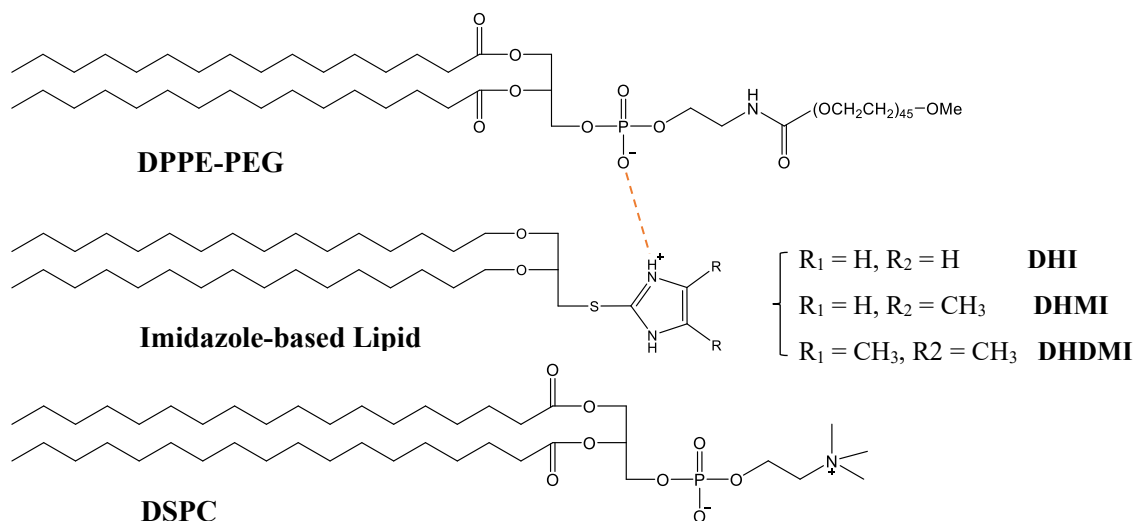
Figure 1.9. Chemical structures of lipids that constitute ICL: (1,2-dipalmitoyl-sn-glycero-3-phosphoethanolamine-N-[methoxy(polyethylene glycol)-2000 (DPPE-PEG) (C16, negatively charged), the imidazole based lipids DHI/DHMI/DHDMI (C16, positively charged at acidic pH), and 1,2-distearoyl-snglycero-3-phosphocholine (DSPC) (C18, neutral). At acidic pH, the imidazole-based lipids would be protonated and cluster with DPPE-PEG due to the electrostatic interaction.
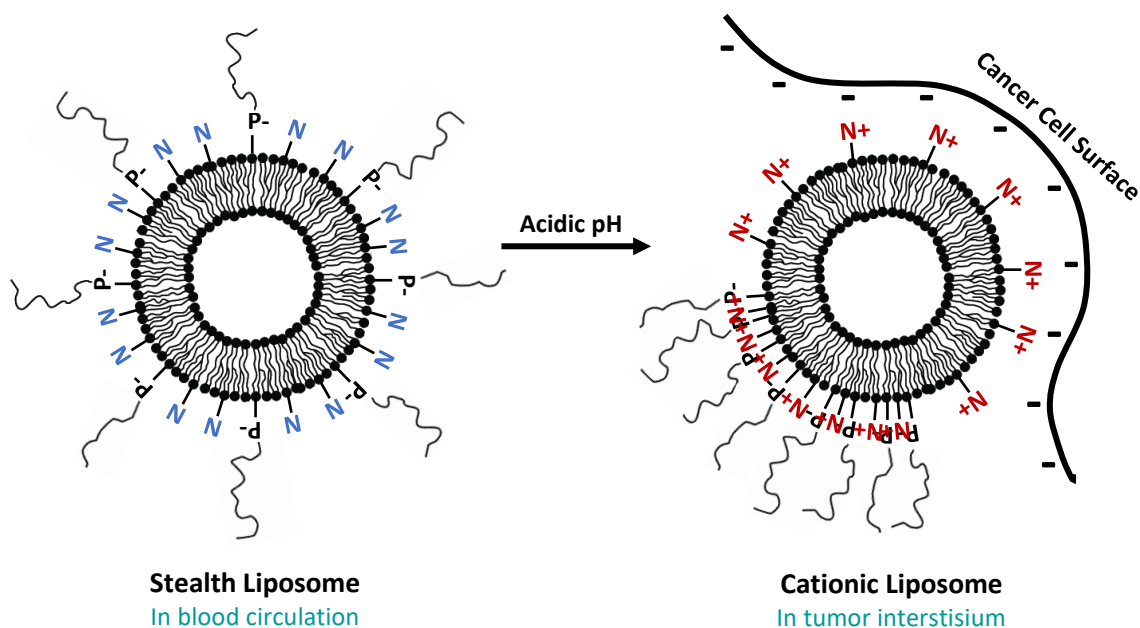
Figure 1.10. Schematic of ICL turning from stealth liposomes into cationic liposomes. ICL contains negatively charged DPPE-PEG (shown by 'P'), imidazole lipids (shown by 'N'), and neutral DSPC. In blood circulation (at pH 7.4), the ICL are coated with a PEG shell to prolong their circulation time (left). When the ICL are delivered into tumor tissue (at pH 6.0-7.0), the

(Figure 1.10 Continued)
imidazole lipids are protonated (shown by 'N+') and therefore cluster with DPPE-PEG to expose
a domain with excess positive charges and without the PEG shell. Such cationic liposomes would
have greater interaction with cancer cells.

1.4 3D Multicellular Spheroids (MCS)

1.4.1 2D and 3D cell culture systems. Traditionally, the *in vitro* processes which are

used to assess the activity of anticancer drug are two-dimensional (2D) monolayer cancer cells.

Besides cancer research, 2D cell culture systems have also been broadly applied in other fields of

biological and medical sciences, such as basic cellular research, stem cell research and

regenerative medicine. 2D cell culture systems have many advantages, including high efficiency,

low cost and convenient operation. However, the 2D monolayers cell culture cannot adequately

simulate many features of solid tumors, such as cell-cell interactions, tissue hypoxia and ECM

[130, 131]. It has been found the 2D cell culture systems are not always predictive of the clinical

performance of new drug candidates. Poor correlation is also noted between the outcomes from

2D monolayer cell models *in vitro* and on those from animal models *in vivo*. Because 2D

monolayer cells lack the solid structures or the complex dynamics of material transport in real

tumors, they are also substantially different in many other functions such as proliferation and

responses to external stimuli [132].

However, *in vitro* cell culture models are still widely used because of their low cost and

high efficiency, especially in high throughput screenings (HTS) [133]. Three-dimensional (3D)

cell cultures allow the cells can grow and interact with their surroundings in all three dimensions,

similar to how they would *in vivo* [134]. 3D culture systems are usually conduced in small

capsules or bioreactors where the growing cells would form spheroids or 3D cell colonies. 3D

cell culture systems have been used in research since 1970s but are emerging as attractive *in vitro*

models for drug discovery owing to their huge translational potentials [135, 136]. The establishment of 3D cell culture models is focused on the physiologically relevant multicellular structures and the ECM, which is more relevant than 2D cell culture systems for validating cell responses to therapeutics. 3D cell culture models are able to resemble not only the 3D morphology of solid tissues but also the complex tissue properties including cell connectivity, tissue architecture, and even gene expression, all serving to better bridge between *in vitro* and *in vivo* models.

Among the 3D models, multicellular spheroids (MCS) are the most accessible, economical and versatile due to their diverse and relatively simple preparation methods [136]. 3D MCS, also known as spheroids, are spherical constructs composed of self-assembled cells. Many 2D monolayer cell cultures have been adapted to construct spheroids systems, including multicellular tumor spheroids (MCTS), neurospheres, mammospheres, hepatospheres and embryoid bodies [133, 137]. Besides cancer research, 3D cell culture techniques have also been commonly applied to stem cell research and tissue engineering.

1.4.2 Similarity between MCTS and solid tumors. The best-characterized 3D cell culture technique in anticancer research is MCTS, which is derived from cancer cell lines commonly used in 2D culture [138]. MCTS are more representative *in vitro* models of solid tumors than 2D monolayer cells, due to their solid morphology, gradients of oxygen, nutrients and pH, heterogeneous cell viability, cell-cell interaction, and complex ECM [138, 139]. Owing to the above biological features, MCTS have been utilized to study solid tumor biology and to establish platforms to screen for anticancer drugs.

1.4.2.1 Three gradients and three layers of cell organization. Similar with *in vivo* solid tumors, MCTS have three gradients – oxygen, nutrients, and pH gradients, and a three-layer cell

organization – proliferating, quiescent, and necrotic cell layers. Owing to the dense solid constructs of aggregated cells, penetration of oxygen and nutrients are limited in MCTS. The hypoxic characteristic of MCTS has been well adapted to assess oxygen-dependent therapeutics. For example, many studies explored the sensitivity of MCTS to radiation in order to effectively predict the clinical responsiveness of solid tumors to radiotherapy, because hypoxia was found to be a major contributor to the radio-resistance of tumor cells [140, 141].

The pH gradients in MCTS are attributed to insufficient penetration of oxygen and nutrients. Without adequate oxygen and nutrients, metabolic pathways in MCTS to favor anaerobic metabolism while the removal of metabolic waste is enfeebled, jointly leading to an accumulation of metabolic by-products of hypoxia, mostly lactate [142]. Thus, similar with solid tumors, MCTS carry acidic interstitial pH, especially in the core. Such lowered pH of MCTS allows better understanding of tumor biology and better evaluation of anticancer therapeutics. The vasculature-free "microtumors" mimicked by MCTS are composed of three layers of cells - proliferating cells at the periphery, quiescent cells right below the proliferating cells, and necrotic cells in the MCTS core. Such a three-layer cellular structure of MCTS is similar to the avascular regions in solid tumors (Figure 1.11) [22]. The three-layer cell organization of MCTS is closely correlated to the gradients of oxygen, nutrients and pH, and primarily relies on the volume and growth rate of spheroids. MCTS larger than 500 μm were found to assume this three-layer cell organization [143, 144]. MCTS with diameter below 120 μm were found well oxygenated, but as they grow larger, the concentrations of oxygen and nutrients in the inner core decrease rapidly. Subsequently, the MCTS interstitial pH also decreases, followed by the decrease of cell viability [145]. Both the hypoxia and the necrosis characteristics of MCTS closely mimic their corresponding gene expression profiles in solid tumor [146].
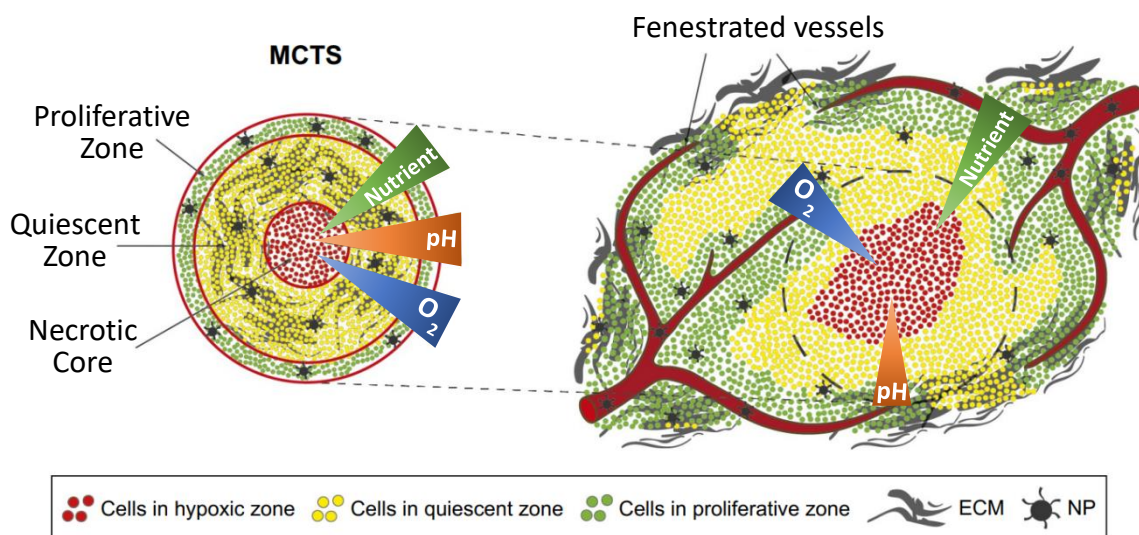
Figure 1.11. Schematic representation of bio-similarity between MCTS (left) and solid tumor (right). [22]

1.4.2.2 ECM, cell-cell and cell-ECM interactions. The extracellular matrix (ECM) is a major structural component in tumor microenvironment. ECM contains proteins and polysaccharides to provide cells with essential physical and biochemical support. The traditional 2D monolayer cell cultures cannot mimic the microenvironment in solid tumors because of their much weaker cell-cell and cell-ECM interactions, which often makes them unreliable models to evaluate drug efficacy and toxicity [147]. The *in vivo*-like MCTS models would overcome some of these limitations. Various types of ECM components, including structural (collagen and elastin) and adhesive (fibronectin and laminin) proteins, are found in MCTS in similar proportions as those in solid tumors. Such components have been found as critical factors to define the interaction between MCTS and drugs [148, 149]. Because of the importance of ECM to cell survival, proliferation, and migration, MCTS have been utilized to investigate not only the mechanisms of cell migration and invasiveness in tumors but also the therapeutics applied to prevent them [150]. The ECM components in MCTS depend on the cell lines and techniques of

MCTS construction. Some cancer cells can produce adequate ECM substrates for self-assembling while some cancer cells cannot [151]. Cancer cells that do not produce sufficient ECM substrates can be assisted by scaffold materials to establish their MCTS. Biocompatible, natural polymers such as collagen, fibrin and Matrigel are utilized as scaffolds to construct ECM-embedded MCS models because those polymers intrinsically contain ECM components, including growth factors (GFs) and laminin [136]. Despite the advantages of 3D MCTS over 2D cell culture from their ECM, it should be noted that the ECM substrates in MCTS originate differently compared to those in solid tumors in that the former are generated by cancers cells or added extrinsically, while the latter are secreted by fibroblasts [152]. To better study the cell-ECM interactions in tumors as well as their impact on anticancer treatments, MCTS co-cultured with stromal components (e.g. fibroblast, macrophages and endothelial cells) have been developed as the more *in vivo*-like models that mimic the heterogeneity of tumor tissues [153].

1.4.2.3 Drug penetration and drug resistance. 3D MCTS models have become more predictive tools for drug screening because they can mimic the restricted intratumoral drug penetration, which is a large contributor for drug resistance *in vivo* [137]. The microenvironment forcell-cell and cell-ECM interactions in MCTS closely mimics the permeability barriers in solid tumors [149]. Moreover, the hypoxic regions seen in both solid tumors and MCTS was found to limit the penetration of anticancer drugs by boosting their local degradation/metabolism [154, 155]. Drug penetration into MCTS was studied under tunable hypoxic conditions that were controlled by extrinsic hypoxia-reoxygenation cycling, which showed poor drug penetration into hypoxic spheroids and increased penetration and cellular uptake of drugs in reoxygenated spheroids [156]. Together, hypoxia, necrosis and acidic pH all contribute to drug resistance in solid tumors, which are all replicated in MCTS but not in 2D cell culture [13].

3D MCTS should greatly benefit the development and clinical translation of anticancer nanomedicines due to their unique physicochemical properties. MCTS provide a solid construct, which can provide the *in vivo*-like interaction with nano drug carriers. Because the physicochemical properties (size, shape, surface, etc) of nano drug carriers greatly affect their interaction with tumor cells, such properties can be optimized according to their effects in MCTS models [157, 158]. MCTS also contains ECM which provides highly *in vivo*-like physical and biochemical barriers for nanomedicines. Nanomedicines can be designed and developed to overcome such impediment from ECM based on the *in vitro* data from the ECM of MCTS. Lastly, MCTS containing ECM stromal cells are considered even more clinically relevant. For example, Doxil® was reported to have reduced penetration into MCTS of breast cancer cells when the MCTS also contains fibroblasts [159].

1.4.3 3D cell culture techniques. 3D cell culture can be constructed by many techniques, which can be grouped into scaffold-based techniques and scaffold-free techniques.

1.4.3.1 Scaffold-based techniques. Scaffold-based techniques are also known as matrix-based techniques, which refer to the utilization of solid scaffolds, hydrogels and other materials to provide the structural support. For example, hydrogels, which provide high moisture retention and interconnected pores, allows adequate gas exchange and nutrient supply in a way similar to natural ECM structures in tissues [160]. Agarose gel was used to generate a 3D model to understand the bone ossification process and potential of human CD34+ stem cells. Scaffolds can also play as vehicles to control the delivery of drugs, proteins and DNA [151, 161].

Scaffold-based 3D cell culture still faces several challenges, including poor initial cell density in the constructed tissues, and improper usage of scaffold materials [162]. Some scaffolds may interfere with the behavior of the cells such as their interaction with drugs. Some

scaffolds may also induce biodegradation, which is triggered by inflammatory responses of the cultured cells. Scaffolds with too small pores would limit transport of oxygen, nutrients, and waste, resulting in poor cell survival and proliferation. The surface properties of scaffold materials would also affect cell adhesion, proliferation, aggregation, and functions [163]. Taken together, significant factors to consider when choosing scaffold materials include their cell interaction, porous size, and surface properties. Matrix materials such as Matrigel and HA are considered as ideal scaffolds for 3D cell culture, which are biocompatible and can provide growth factors and signal factors to promote cell proliferation [137, 164].

Scaffold-based techniques have been extensively applied in tissue regeneration and cell transplantation. They have limited capability to construct 3D MCS, due to the inhomogeneous distribution of cells seeded in the porous scaffold and the lower initial seeding density compared with scaffold-free techniques [165]. However, the scaffold-free methods with the addition of scaffold/matrix materials, such as collagen and Matrigel, have been extensively applied to construct MCS tumor models using cancer cells that produce limited ECM substrates [136, 166].

1.4.3.2 Scaffold-free techniques. Scaffold-free techniques are methods to construct 3D culture models without dependence on scaffold materials. This strategy relies on the inherent ability of the culturing apparatus to assemble cells into larger structures [165]. Available scaffold-free methods (Figure 1.2) include hanging-drop, forced-floating (low adhesion surface), agitation-based bioreactors (spinning flask and rotating culture), force-driven approaches (magnet, electric and acoustic), cell sheets and bioprinting [137, 164].

Scaffold-free techniques have been developing faster than scaffold-based techniques due to a number of advantages[167]. With external rigid support, scaffold-free techniques can overcome the challenges of scattered cells to construct solid 3D assemblies. It takes less time to

construct 3D models by scaffold-free methods because the initial cell seeding density is much

higher than scaffold-based methods. Consequently, cell proliferation and migration are not

crucial factors for the 3D MCS construction. Compared with time-consuming scaffold-based

methods, which use scaffold materials that may be biodegradable, scaffold-free methods are

considered as faster, safer, and more reliable techniques [168].

Furthermore, scaffold-free methods have been used to construct not only 3D MCS of one

type of cells but also those of multiple types of co-cultured cells in order to simulate the

complexity of tissue and organ architecture [167]. Some 3D co-culture spheroids are composed

of both cancer cells and other cells known to be involved in tumor progression, such as

fibroblasts, macrophages, monocytes, endothelia and immune cells. Such co-culture MCTS can

provide more pertinent assessments of anticancer therapeutics [153, 169, 170].
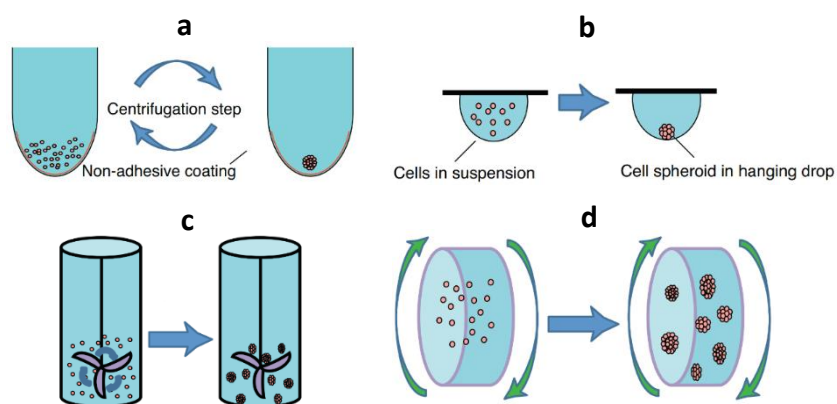
Figure 1.12. Common methods to construct 3D MCS. (a) Low adhesion plates. (b) Hanging-drop. (c) Spinning flask. (d) Rotating culture. [164]

1.5 Hypothesis and Specific Aims.

Based on the foregoing, the hypothesis of this thesis is that compared with conventional

stealth liposomes, the convertible liposomes with pH-sensitivity introduced by the imidazole-

based lipids can express better anticancer activity *in vitro*. To test this hypothesis, this project

has the following specific aims:

1. To prepare, optimize and characterize the imidazole-based convertible liposomes (ICL).

2. To test the pH-sensitivity of ICL.

3. To study the morphology of ICL using transmission electron microscopy (TEM)

4. To evaluate the anticancer activity of ICL on 3D multicellular spheroids (MCS).

CHAPTER 2: PREPARATION AND PHYSICOCHEMICAL CHARACTERIZATION OF IMIDAZOLE-BASED CONVERTIBLE LIPOSOMES

2.1 Introduction

Liposomal formulations have been reported to carry considerable advantages, including high loading capacity of drugs, capability to carry either hydrophilic or lipophilic payload drugs, relatively long half lives in blood circulation, and targeting to tumors [171]. The stealth liposomes, which contain PEGylated lipids to form a surface coating of the PEG polymers, can achieve longer half-life in blood circulation than conventional liposomes by sterically hindering their recognition by reticuloendothelial system (RES) [172]. The increased half-life allows the stealth liposomes to accumulate more in the perivascular environment in solid tumors, a phenomenon known as the enhanced permeation and retention (EPR) effect. However, the steric hindrance of the PEGylated stealth liposomes also decreases their interaction with cancer cells [125]. To increase the liposome-cancer cell interaction and thus to improve the intracellular delivery of the payload drug, three imidazole-based ether lipids were developed in our group to be protonated at the acidic microenvironment of the tumor interstitium. At acidic pH, the PEGylated stealth liposomes containing the imidazole-based lipids would convert to cationic liposomes, thus given the name imidazole-based convertible liposomes (ICL). The cationic liposomes thus formed at acidic pH in the tumor microenvironment would then better interact with the negatively charged cell membrane [40].

The studies reported in this chapter aim to develop more robust methods to prepare DOX-loaded ICL for anticancer drug delivery. Various PEGylated liposomes containing imidazole-based ether lipids were constructed to investigate the effect of multiple factors on the physicochemical properties of ICL and to discover more robust methods of preparing ICL.

2.1.1 Design of the imidazole-based ether lipids. The imidazole headgroup has been chosen to conjugate with the two C16 hydrocarbon chains due to its unique properties. The N3 of the imidazole moiety is basic (estimated pK_a 5.5-6.8) and thus would protonate at mildly acidic pH. The protonation of imidazole would then provide positive charges to the lipid molecules, which would then interact with the negatively charged PEGylated lipid molecules. The imidazole lipids and the PEG-lipid conjugate (DPPE-PEG) all carry C16 hydrocarbon chains to further enhance their Van Der Waals interactions.
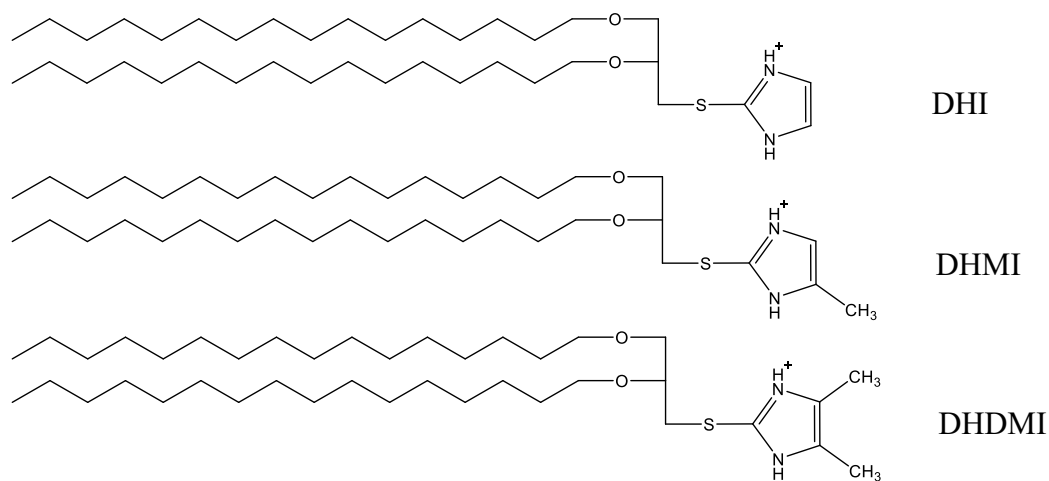
Figure 2.1. Structures of the imidazole-based ether lipids.

2.1.2 The composition of ICL. The imidazole-based convertible liposomes (ICL) contain DSPC (C18), imidazole-based lipids (C16) and DPPE-PEG (2000) (C16). In our studies that investigated the influence by cholesterol, 25% cholesterol were added in place of the same mole percentage of DSPC. ICL were studied in comparison with a non-sensitive liposomes (NSL), which contains no imidazole-based lipids. The lipid composition of ICL and NSL without and with cholesterol are shown in Table 2.1.

Table 2.1
Lipid composition of ICL and NSL formulations without and with cholesterol

Formulations	DHI	DHMI	DHDMI	DSPC	DPPE-PEG	Chol
			Mol %			
I	25	-	-	70	5	-
II	-	25		70	5	-
III	-	-	25	70	5	-
IV	-	-	-	95	5	-
V	25	-	-	45	5	25
VI	-	25	-	45	5	25
VII	-	-	25	45	5	25
VIII	-	-	-	70	5	25

2.1.3 The phase transition temperature of ICL. The phase behavior of lipid bilayers has been widely acknowledged as property about the mobility of individual lipid molecules in response to temperature [173]. Generally, a lipid bilayer can exist in either gel phase or fluid phase at a certain temperature. The gel phase is commonly known as lipid bilayers composed of lipids in solid state. The fluid phase, also known as the liquid crystal phase, is known as lipid bilayers composed of lipids in liquid state. Same as in gel phase, the lipid molecules in fluid phase bilayers are constrained to the lateral plane of membranes. However, the lipid molecules in the fluid phase, but not those in the gel phase, have free lateral diffusion within their monolayer. The temperature at which a specific lipid transits from the ordered gel phase to the disordered fluid phase is defined as its phase transition temperature (T_m) [174]. The T_m value of a lipid was found to be a function of the length of its acyl chains and its saturation [175]. Table 2.2 shows that phospholipids with longer acyl chains and less unsaturated bones bonds would possess higher T_m.

Table 2.2. *Hydrocarbon length, unsaturated and T_m of lipids with PC and PE headgroups [176]*

Lipids	Length of Acyl Chains	Unsaturated Bones	T_m (˚C)
DLPC	12	0	-2
DMPC	14	0	24
DPPC	16	0	41
DSPC	18	0	55
DOPC	18	1	-17
DLPE	12	0	29
DMPE	14	0	50
DPPE	16	0	63
DSPE	18	0	74
DOPE	18	1	-16

According to Table 2.2, the T_m of DSPC and DPPE are 55˚C and 63˚C, respectively. The T_m of a liposomal bilayer is determined by the T_m of the component lipids [177]. Concisely, T_m of a bilayer system was defined as the temperature at which half of the substance is in its fluid state, while the other half is in its gel state [177]. The shift of T_m of a lipid bilayer after incorporation of PEGylated lipids can be attributed to the mismatch of acyl chain length and the negative effect of PEG [178]. For PEGylated lipids containing shorter polymers (up to 3000), their acyl chains determine their effect on the T_m, while for PEGylated lipids containing longer polymers (> 3000), their PEG chains determine their effect on the T_m. Accordingly, the T_m of DPPE-PEG (2000) should be close to the T_m of DPPE (63˚C). The T_m of imidazole-based lipids (C16) is estimated to be lower than that of DSPC (55˚C), due to their shorter acyl chains. Based on the foregoing, we estimated that the T_m of our ICL liposomal bilayer would be around 63˚C. Therefore, the temperature during the ICL preparation was set at 70˚C to ensure that the bilayer was to be completely kept in the fluid phase.

2.2 Materials and Methods

2.2.1 Materials. 1,2-Di-O-hexadecyl-*rac*-glycerol (DHG), 2- Mercaptoimidazole, 4-Methyl-1H-imidazole-2-thiol and 4,5-Dimethyl-1H-imidazole-2-thiol were purchased from Santa Cruz Biotechnology (Dallas, TX, US). pToluenesulfonyl chloride, dichloromethane (anhydrous), pyridine (anhydrous), DMF (anhydrous) and 2-[4-(2-hydroxyethyl)piperazin-1-yl]-ethanesulfonic acid (HEPES) were purchased from Fisher Scientific (Hampton, NH, US). Triethylamine (TEA) and Silica Gel 60 (230-450 mesh) were purchased from Alfa Aesar (Haverhill, MA, US). The lipids 1,2-distearoyl-sn-glycero-3-phosphocholine (DSPC), 1,2-dipalmitoyl-snglycero-3-phosphoethanolamine-N-[azido(polyethylene glycol)-2000 (DPPE-PEG (2000)), and 1,2 dipalmitoyl-sn-glycero-3-phosphocholine (DPPC) were purchased from Avanti Polar Lipids, Inc. (Alabaster, AL, USA). Cholesterol, Dowex® 50WX-4 (50-100 mesh), and Sephadex G-25 were purchased from Sigma-Aldrich (St. Louis, MO, USA). Doxorubicin Hydrochloride was purchased from Biotang (Waltham, MA, USA). All other organic solvent and chemicals were purchased from Sigma Aldrich, Fisher Scientific or VWR.

2.2.2 Synthesis of imidazole-based ether lipids.

2.2.2.1 Synthesis of 1,2-Di-O-hexadecyl-rac-glyceryl tosylate (DHG Tosylate). 1,2-Di-O-hexadecyl-*rac*-glycerol (DHG) (2.30 g, 4.25 mmol, 1 equiv) was dissolved in 20 mL anhydrous dichloromethane, coupled with pyridine (18.6 mL, 225 mmol, 50 equiv). *p*-Toluenesulfonyl chloride (1.90 g, 9.97 mmol, 2 equiv) was dissolved in small amount of dry dichloromethane and transferred to the above solution. The apparatus and solid reagents were dried under high *vacuo* at room temperature for over 4 hours the dry solvents and solutions were transferred by Hamilton syringe or double-pointed needles under argon. The reaction mixture was stirred under argon at room temperature for 8 to 12 hours. The reaction was monitored by

silica gel TLC (Fisher Scientific, Hampton, NH, US) using dichloromethane as the mobile phase. The reaction mixture was then mixed well with 10 ml anhydrous dichloromethane and washed with saturated sodium carbonate solution for 3 times. The organic phase was separated from the aqueous phase and was then dried with magnesium sulfate. The dried solution of the reaction mixture was filtered and then evaporated into dryness under vacuum. The resultant residue was then seperated by silica gel chromatography with dichloromethane as the mobile phase to yield 2.53 g DHG-tosylate solid. (Yield 86%).

2.2.2.2 Synthesis of sn-2-((2,3-bis(hexadecyloxy)propyl)thio)-1H-imidazole (DHI), sn-2-((2,3-bis(hexadecyloxy)propyl)thio)-5-methyl-1Himidazole (DHMI) and sn-2-((2,3-bis(hexadecyloxy)propyl)thio)-4,5-methyl-1Himidazole (DHDMI). In order to achieve the anhydrous conditions for the reactions, the glass apparatus and reagents were pre-dried in high vacuum for over 4 hours, and transfers of liquid were handled by air-tight Hamilton syringe and double-pointed needles under argon. 2- Mercaptoimidazole (0.91 g, 9.06 mmol, 5 equiv.), 4-Methyl-1H-imidazole-2-thiol (1.03 g, 9.03 mmol, 5 equiv.), or 4,5-Dimethyl-1H-imidazole-2-thiol (1.15 g, 9.03 mmol, 5 equiv.) was dissolved in 8-9 mL N,N-Dimethylformamide (DMF). DHG-tosylate (1.265 g, 1.82 mmol, 1 equiv) was dissolved in 7-8 ml of dry dichloromethane and transferred into the above-mentioned solution, followed by addition of Triethylamine (TEA) (1.27 mL, 9.08 mmol, 5 equiv.). The reaction mixture was stirred under argon at 55°C for 48 hours. The reaction was monitored by TLC (silica gel plate) and UV with 5/95 (v/v) methanol/dichloromethane or ethyl 3/7 (v/v) acetate/hexane as the mobile phase. The solvent was evaporated under vacuum and the resultant residue was dissolved in dichloromethane. The solution was washed with saturated sodium bicarbonate solution for 3 times, dried with sodium carbonate, filtered and then evaporated into dryness under vacuum. The resultant residue was

then separated by silica gel chromatography with 1-5% (v/v) methanol/dichloromethane as the

mobile phase to yield DHI, DHMI and DHDMI. (Yield 25-30%).

DHI $\quad$ R_1 = H, R_2 = H
DHMI $\quad$ R_1 = H, R_2 = CH$_3$
DHDMI $\quad$ R_1 = CH$_3$, R2 = CH$_3$
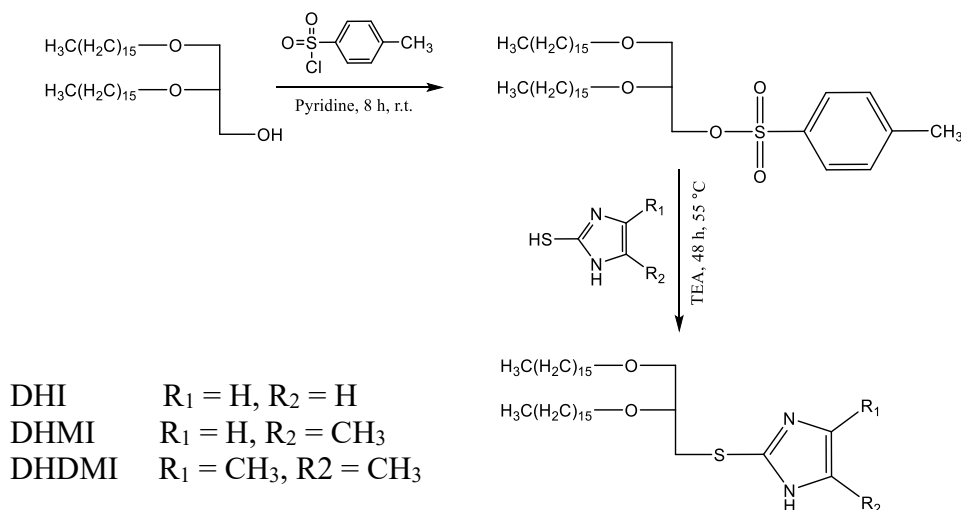
Figure 2.2. Synthesis of imidazole-based lipids DHI, DHMI and DHDMI.

2.2.3 Preparation of ICL formulations.

2.2.3.1 Preparation of liposomes. Generally, the liposomes were prepared using film

hydration, freeze-anneal-thawing and extrusion methods. A dichloromethane solution of

imidazole-based ether lipids and a chloroform solution of other lipids were mixed in a recovery

flask. The organic solvents were evaporated under reduced pressure to form a lipidic film on a

Buchi rotavapor at 70˚C. The lipidic film was further dried in vacuum for over 4 hours at room

temperature to remove the residual solvent completely. The lipidic film was then hydrated with

isotonic HEPES buffer (pH 7.4, 5 mM HEPES, 140 mM NaCl) by intermittent agitation in a

70˚C water bath to obtain a liposomes suspension containing 20 mM total lipids. The flask was

filled with argon and sealed with parafilm. The Liposome suspension was freeze-anneal-thawed

by rapidly freezing in liquid nitrogen, emerging in ice-water mixture for 2 min and incubating in

70˚C water bath for 4 min. The freeze-anneal-thawing was repeated for 11 times. The liposome suspension was sequentially extruded 21 times each though 400 nm, 200 nm and 100 nm polycarbonate membranes (Nucleopore Corp., Pleasanton, CA, US) using a hand-held Mini-extruder (Avanti Polar Lipids Inc., Alabaster, AL, US) at 70° C to reduce and homogenize the sizes of liposomes. The resultant liposome suspensions were stored at 4˚C in glass vials filled with argon and sealed with parafilm until further studies.

2.2.3.2 DOX loading into liposomes by manganese sulfate gradient. The transmembrane manganese sulfate gradient was used to load DOX into liposomes. The lipidic film in 2.2.3.1 was hydrated with HEPES buffer (pH 7.4, 30 mM HEPES) containing 300 mM manganese sulfate by intermittent agitation in a 70˚C water bath to obtain a liposomes suspension containing 20 mM total lipids. The freeze-anneal-thawing and extrusion were similar as mentioned in 2.2.3.1. To establish the transmembrane gradient, the extruded liposomes were separated from the unencapsulated manganese sulfate by size exclusion chromatography (SEC) using a Sephadex G-75 column (Sigma Aldrich, St. Louis, MO, USA)) pre-equilibrated with isotonic HEPES buffer (pH 7.4, 5 mM HEPES, 140 mM NaCl). DOX (0.75-3 mg/ml) dissolved in the same isotonic HEPES buffer was then mixed with the purified liposome suspension (approximately 10 mM total lipids) in 1:2 (v/v) ratio and mixture was incubated at 70˚C water bath for 90 min. The cation-exchange resin Dowex® 50WX-4, 50-100 mesh (Sigma Aldrich, St. Louis, MO, USA) was converted to the sodium form by sequential washing with 400 ml 2 M NaOH per 100 g of dry resin on filter paper with a Buchner funnel. The NaOH was removed by washing with 1 M NaCl until the pH returned to neutrality. The resin was then washed several times with 0.9% (w/v) NaCl and dried overnight on filter paper in vacuum and stored at room temperature. Such pretreated resin was then mixed with the DOX-liposome mixture at DOX:

resin = 1:60 (w/w) and shaken on an orbital shaker (Thermo Fisher Scientific, Waltham, MA) at approximately 100 rpm, room temperature for 25 min to remove the unencapsulated DOX from the DOX-loaded liposomes. The resin was then separated from the DOX-loaded liposomes by filtration through glass wool in a syringe. The resultant DOX-loaded liposome suspension (approximately 7 mM total lipids) was stored at 4°C in an amber glass vial filled with argon and sealed with parafilm until further studies.

2.2.4 Physicochemical characterizations of liposomes.

2.2.4.1 Size measurement. An aliquot (2.5-5 µL) of a liposome suspension was diluted in 150 µL DI water or isotonic buffer and the sizes of liposomes were measured at room temperature by dynamic light scattering (Zetasizer ZS90, Malvern Instruments Ltd., UK). The size values are analyzed from the intensity of hydrodynamic diameters.

2.2.4.2 Quantitation of payload DOX concentration and liposome encapsulation efficiency (EE). An aliquot (10 µl) of DOX-loaded liposome suspension was lysed with 90 µL lysis buffer (90% (v/v) isopropanol, 0.075 M HCl) [179] in a 96-well Black Clear Bottom Polystyrene microplate (Corning®, NY, US), together with 10 µL DOX standard solutions (1, 2, 5, 10, 20, 50, 100 µg/ml) diluted in the same lysing buffer (90 µL). All samples in the quantitation were triplicated. The microplates were covered with foil, and the fluorescence of the samples was measured at 486 nm (excitation) and 590 nm (emission) on a Synergy HT microplate reader (Biotek, Winooski, VT, US). Concentration of the payload DOX of liposomes was estimated using a standard calibration curve from the fluorescence of the above-mentioned DOX standard solutions. The encapsulation efficiency (EE) of the liposomes was then calculated by the following formula.

$$EE = \frac{Encapsulated\ DOX\ Conc.}{Input\ DOX\ Conc.\ for\ drug\ loading} \times 100\%$$

2.2.5 Concentrating the liposome formulations. The DOX-loaded formulations need to be concentrated before testing on biological systems if their DOX concentration are not sufficient for the treatment. A diafiltration column (MicroKros®, Spectrum, Stamford, CT, US) was used to concentrate the liposome suspension by partially removing the extra-liposomal buffer. The liposome suspension was slowly extruded by two syringes through the diafiltration column to be condensed to the needed concentration. Typically, a 2 ml liposome suspension was extruded 14 times to yield a 0.5 ml concentrated formulation.

2.3 Results and Discussions

2.3.1 Synthesis of imidazole-based ether lipids DHI, DHMI and DHDMI. The synthesis of DHG Tosylate and imidazole-based lipids were carried out to yield three pH-sensitive convertible lipids with similar structures. The synthesis methods were based on the tosyl activation of the lipid DHG and the substitution of the tosylate group with the imidazole moiety using mercaptoimidazole compounds. Tosylate was known as a reliable leaving group, so it was used for the conjugation of lipid chains and the imidazole headgroups. The anhydrous conditions were essential for the high yield of the conjugation reaction. Besides, to purify the imidazole-based lipids, the mobile phases 1-5% (v/v) methanol/dichloromethane and 3/7 (v/v) ethyl acetate / hexane were utilized respectively, and the former led to higher yield (30%) than the latter (10%).

2.3.2 Physicochemical characterization of ICL.

2.3.2.1 Size and PDI before and after DOX-loading. After preparation by lipidic film hydration, freeze-anneal-thawing and sequential extrusion through 400 nm, 200 nm and 100 nm polycarbonate membranes, imidazole-based convertible liposomes containing 25% DHI, DHMI or DHMI were successfully prepared with mean hydrodynamic diameter smaller than 130 nm.

The Polydispersity Index (PDI), a measure of the heterogeneity of the size of particles in a mixture, was lower than 0.3 for all the formulations. After the sequential extrusion and before the loading with DOX, the mean size and PDI of the ICL are shown in Table 2.3 together with NSL for comparison.

Table 2.3
Size and PDI of empty ICL and NSL after sequential extrusion with 400 nm, 200 nm and 100 nm polycarbonate membranes and before DOX loading

Lipid Compositions	Mol Ratio	Ext by 400 nm		Ext by 200 nm		Ext by 100 nm	
		Size (nm)	PDI	Size (nm)	PDI	Size (nm)	PDI
DHI/DSPC/DPPE-PEG	25/70/5	219.6	0.310	189.1	0.283	124.4	0.195
DHMI/DSPC/DPPE-PEG	25/70/5	179.2	0.149	170.0	0.271	118.7	0.205
DHDMI/DSPC/DPPE-PEG	25/70/5	176.2	0.179	146.5	0.226	105.7	0.178
DSPC/DPPE-PEG	95/5	226.0	0.227	136.9	0.152	104.7	0.050

Note. Size values are the cumulative intensity of hydrodynamic diameters.

After the sequential extrusions, each formulation was passed through a SEC column (Sephadex G-75) equilibrated with the isotonic HEPES buffer (pH 7.4, 5 mM HEPES, 140 mM NaCl) to generate the manganese sulfate gradient (300 mM) from inside of liposomes. Such liposome suspensions were then mixed with DOX in the same buffer at 1000 μg/ml final DOX concentration in the DOX-liposome mixture. After 90 min incubation at 70˚C and resin removal of the unencapsulated DOX, the sizes of ICL and NSL significantly increased (Table 2.4). The DHI/DSPC/DPPE-PEG (last extruded by 100 nm membrane) showed the most increase in the mean size value from 124.4 nm to 802.7 nm while DHMI/DSPC/DPPE-PEG (last extruded by 100 nm membrane) showed the increase from 118.7 nm to 693 nm. The mean size of the formulation DHDMI/DSPC/DPPE-PEG increased from 105.7 nm to 404.9 nm after the DOX-

loading. The non-pH-sensitive control liposome DSPC/DPPE-PEG had similar increase in mean

size from 104.7 nm to 372.7 nm. The liposomes last extruded by the 200 nm polycarbonate

membrane had similar augment in size. The PDI of each formulation also increased after the

drug loading.

Table 2.4
*Size and PDI of DOX-loaded ICL and NSL that were last extruded by 200 nm and 100 nm
polycarbonate membranes*

Lipid Compositions	Mol Ratio	Extruded by 200 nm		Extruded by 100 nm	
		Size (nm)	PDI	Size (nm)	PDI
DHI/DSPC/DPPE-PEG	25/70/5	807.6.0	0.845	802.7	0.721
DHMI/DSPC/DPPE-PEG	25/70/5	550.0	0.644	693.0	0.605
DHDMI/DSPC/DPPE-PEG	25/70/5	266.8	0.501	246.1	0.501
DSPC/DPPE-PEG	95/5	401.4	0.246	372.7	0.620

Note. Size values are the cumulative intensity of hydrodynamic diameters.

The pharmacokinetics and tissue distribution of drug delivery systems are remarkably

affected by their size [180]. For PEGylated nano-carriers, it is preferred to keep the size under

200 nm to take advantage of the EPR effect in tumor tissues. In this study, we developed the

methods to prepare drug-free formulations with sizes under 200 nm, but their sizes significantly

increase after being loaded with the payload drug DOX. It was reported that, during drug

loading, DOX induced aggregation of negatively charged liposomes when the temperature is

cooled down to the liposome's phase transition temperature (T_m) [181]. It was suggested that the

aggregation resulted from the electrostatic interactions between the unencapsulated DOX

molecules (positively charged) and the negatively charged lipids on the liposome surface. It was

also suggested that the DOX molecules that bind to different liposomes may also stack with one

another to induce the liposome aggregation. In this study, the aggregation of our ICL and NSL during drug loading may also result from their electrostatic attraction with DOX. The particle size of the formulations after drug loading reflected the extent of aggregation. This speculation is also supported by the ζ- potential measurements of ICL and NSL at pH 6.0-7.4 (Figure 2.4), which showed that all the three ICL and NSL formulations carried a negative ζ- potential at pH 7.4. The further formulation studies in this chapter aimed to keep the size of the DOX-loaded formulation under 200 nm by reducing the aggregation while maintaining the pH-sensitivity. The resultant convertible liposomes would then serve as a viable anticancer drug delivery system.

2.3.2.2 Encapsulation efficiency (EE)and DOX concentration of ICL. After separating the DOX-loaded liposomes from unencapsulated DOX in the suspensions, the payload DOX concentration was measured (Table 2.5) and the EE was calculated from the payload DOX concentration and the input DOX concentration. The EE of the formulations ranged from 40% to 80%, depending on the lipid compositions.

Table 2.5
Encapsulation efficiency and DOX concentration of ICL and NSL that had been extruded by 200 nm and 100 nm polycarbonate membranes

Lipid Compositions	Mol Ratio	Extruded by 200 nm		Extruded by 100 nm	
		EE (%)	DOX Conc. (μg/ml)	EE (%)	DOX Conc. (μg/ml)
DHI/DSPC/DPPE-PEG	25/70/5	45.79±0.44	457.92±4.44	41.28±0.45	412.80±4.50
DHMI/DSPC/DPPE-PEG	25/70/5	51.64±0.35	516.40±3.51	52.17±1.52	521.68±15.23
DHDMI/DSPC/DPPE-PEG	25/70/5	75.54±1.00	755.44±10.07	65.55±0.65	655. 51±6.50
DSPC/DPPE-PEG	95/5	62.35±0.80	623.49±8.02	52.80±0.69	527.96±6.94

Note. Data presented as mean ± SD, N = 3.

EE of liposomes is considered a very important characteristic, because higher EE would allow higher concentration of the payload drug to be delivered to biological systems [177]. The anticancer activity studies on MCS models needed 250 μg/ml or higher DOX concentration in the formulations. The results in this study indicated the above formulations were capable of loading sufficient DOX for the later anticancer activity studies (Chapter V). To achieve a high loading capacity and efficiency, the manganese sulfate gradient was applied to generate the transmembrane ion gradient [182], which was acknowledged as one of the well-developed remote loading methods. At T_m, the membrane of liposomes became more permeable, which allowed the DOX molecules to diffuse into the liposome aqueous interior, wherein the concentration of manganese sulfate is much higher than in the extra-liposomal medium. Manganese formed a complex with DOX, which drove the drug loading and the drug retention in the liposome aqueous interior.

2.3.2.3 Factors affecting size, PDI and EE. To reduce the sizes of DOX-loaded ICL while keeping sufficient DOX encapsulation, several methods have been attempted to improve the formulations. The following sections will discuss a number of formulation conditions that affect the ICL properties such as size, PDI and EE. Such formulation conditions include drug loading time, lipid compositions, drug-loading pH, temperature mixing with resin and input DOX concentration.

2.3.2.3.1 Effect of longer time of drug-loading. To investigate the kinetic changes of size and EE in drug loading, an aliquot of liposome suspension was taken at different time point of drug loading (20, 30, 40, 50, 60, 70, 80 and 90 min) to measure its size and EE. As shown in Figure 2.3 (a), the size of ICL and NSL increased with longer drug-loading time. Compared with DHDMI/DSPC/DPPE-PEG and NSL, DHI/DSPC/DPPE-PEG and DHMI/DSPC/DPPE-PEG

showed higher extent of aggregation, where the size increased to 200 nm after 40 min incubation and 500 nm after 90 min incubation. As shown in Figure 2.3 (b), the EE of ICL and NSL increased with longer incubation time. The convertible liposomes DHDMI/DSPC/DPPE-PEG showed the smallest size and the highest EE than the other formulations in this study, which suggests that the DHDMI/DSPC/DPPE-PEG formulation possesses better stability than the other formulations.
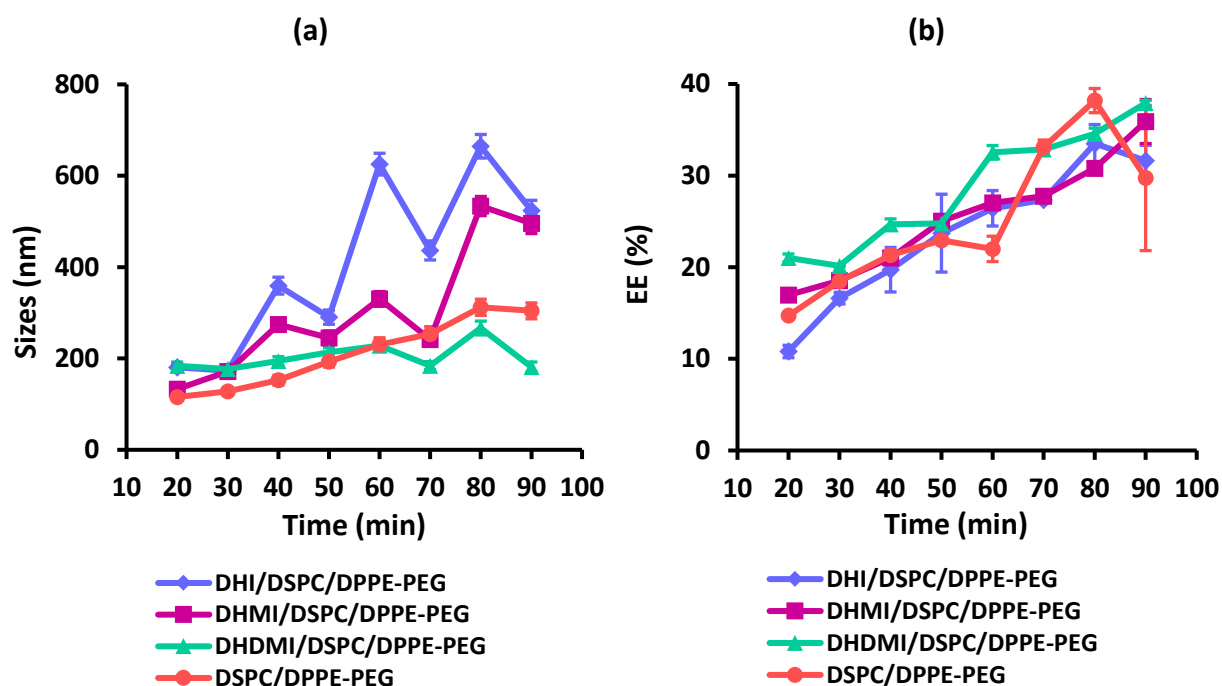
Figure 2.3. (a) Change of liposome sizes with incubation time in drug loading. Data presented as mean ± SD, N = 7. (b) Change of EE of liposomes with incubation time in drug loading. Data presented as mean ± SD, N = 3.

The study obtained the result revealing the correlation between longer incubation time and larger size of DOX-loaded ICL, which suggested the size of liposomes can be decreased by shortened incubation time. Nevertheless, based on the result, the aggregation of convertible DHI and DHMI liposomes started in 40 min, while the EE in 30 min was below 20%. Liposomes

with EE of 20% contained 200 μg/ml encapsulated DOX, which needed TFF concentrating to reach the concentration demanded in the cytotoxicity studies on MCS.

      2.3.2.3.2 Effect of lipid composition – C18 phospholipid versus C16 phospholipid. To investigate the influence of phospholipid on DOX-loaded liposomes, liposomes consisting of 70% C16 phospholipid DPPC (DHI/DPPC/DPPE-PEG) were prepared in comparison to liposomes consisting of 70% C18 phospholipid DSPC (DHI/DSPC/DPPE-PEG). As shown in Table 2.6, DHI/DPPC/DPPE-PEG liposomes extruded by both 200 nm and 100 nm polycarbonate membranes showed dramatically larger sizes (over 2000 nm in hydrodynamic diameter) than the DHI/DSPC/DPPE-PEG liposomes. Interestingly, the larger DHI/DPPC/DPPE-PEG liposomes carried a smaller PDI than the DHI/DPPC/DPPE-PEG liposomes, indicating that the DHI/DPPC/DPPE-PEG liposomes are more homogeneous than the DHI/DSPC/DPPE-PEG liposomes.

Table 2.6
Effect of phospholipid the on the size and PDI of DOX-loaded ICL

Lipid Compositions	Mol Ratio	Extruded by 200 nm		Extruded by 100 nm	
		Size (nm)	PDI	Size (nm)	PDI
DHI/DSPC/DPPE-PEG	25/70/5	706.3	0.833	429.0	0.788
DHI/DPPC/DPPE-PEG	25/70/5	2355.0	0.354	2126.0	0.343

(*Note.* Size values are the cumulative intensity of hydrodynamic diameters.

The EE result in Table 2.7 showed that the DHI/DPPC/DPPE-PEG liposomes contained more payload DOX than the DHI/DSPC/DPPE-PEG liposomes, which demonstrated the higher extent of aggregation in DPPC-containing ICL didn't negatively impact the EE. The higher EE of DHI/DPPC/DPPE-PEG liposomes was consistent with the earlier speculation that the aggregation result from the liposome-DOX-liposome stacking, which would complex more DOX

molecules in between the aggregated liposomes. These complexed DOX molecules could not be removed by the ion-exchange resin, and thus would contribute to the EE.

Table 2.7

Effect of phospholipid on EE and DOX Conc. of ICL

Lipid Compositions	Mol Ratio	Ext by 200 nm		Ext by 100 nm	
		EE (%)	DOX Conc. (µg/ml)	EE (%)	DOX Conc. (µg/ml)
DHI/DSPC/DPPE-PEG	25/70/5	40.99±0.44	409.93±4.36	46.63±0.73	466.29±7.28
DHI/DPPC/DPPE-PEG	25/70/5	72.28±0.98	722.80±9.88	65.22±7.10	652.15±71.00

Note. Data presented as mean ± SD, N = 3.

2.3.2.3.3 Effect of lipid composition - 25% cholesterol. To investigate the influence of cholesterol, DOX-loaded ICL liposomes containing 25% cholesterol were prepared to compare with the corresponding cholesterol-free liposomes. As shown in Table 2.8, before DOX loading, the sizes of liposomes containing cholesterol were below 130 nm after extrusion through the 100 nm polycarbonate membranes, similar to the cholesterol free liposomes in Table 2.8. Based on the PDI results in Table 2.3 and 2.8, furthermore, the PDI values of ICL with cholesterol (Table 2.8) were all smaller than 0.1 while those of cholesterol-free ICL were all larger than 0.1, indicating that cholesterol improved the homogeneity of ICL.

Table 2.8

Size and PDI of liposomes consisting of 25% cholesterol after sequential extrusion through 400 nm, 200 nm and 100 nm polycarbonate membranes and before DOX loading

Lipid Compositions	Mol Ratio	Ext by 400 nm		Ext by 200 nm		Ext by 100 nm	
		Size (nm)	PDI	Size (nm)	PDI	Size (nm)	PDI
DHI/DSPC/DPPE-PEG/Chol	25/45/5/25	271.1	0.212	164.0	0.197	124.1	0.088
DHMI/DSPC/DPPE-PEG/Chol	25/45/5/25	233.6	0.119	145.4	0.145	114.5	0.041

(Table 2.8 Continued)

DHDMI/DSPC/DPPE-PEG/Chol	25/45/5/25	247.0	0.125	159.6	0.181	115.7	0.066
DSPC/DPPE-PEG/Chol	70/5/25	217.3	0.124	172.6	0.212	120.3	0.108

Note. Size values are the cumulative intensity of hydrodynamic diameters

As shown in Table 2.9, after 90 min DOX loading, the sizes and PDI of ICL with cholesterol didn't have obvious change. The DOX-loaded cholesterol liposomes had sizes smaller than 150 nm and PDI below 0.3, which means no significant aggregation took place during the drug loading, while the EE of all the ICL liposomes with cholesterol reached above 60%.

Table 2.9
Size, PDI and EE of ICL liposomes containing 25% cholesterol after extrusion by 100 nm polycarbonate membrane and DOX-loading

Lipid Compositions	Mol Ratio	Size (nm)	PDI	EE (%)
DHI/DSPC/DPPE-PEG/Chol	25/45/5/25	133.6	0.145	71.38±0.61
DHMI/DSPC/DPPE-PEG/Chol	25/45/5/25	120.0	0.075	89.86±1.27
DHDMI/DSPC/DPPE-PEG/Chol	25/45/5/25	120.7	0.115	92.97±1.10
DSPC/DPPE-PEG/Chol	70/5/25	144.1	0.266	60.98±1.66

Note. Size values are the cumulative intensity of hydrodynamic diameters. EE data presented as mean ± SD, N = 3.

Compared with DOX-loaded cholesterol free ICL and NSL, the DOX-loaded ICL and NSL containing 25% cholesterol showed significantly smaller sizes and higher EE. Thus, the aggregation during DOX-loading was averted by the introduction of cholesterol.
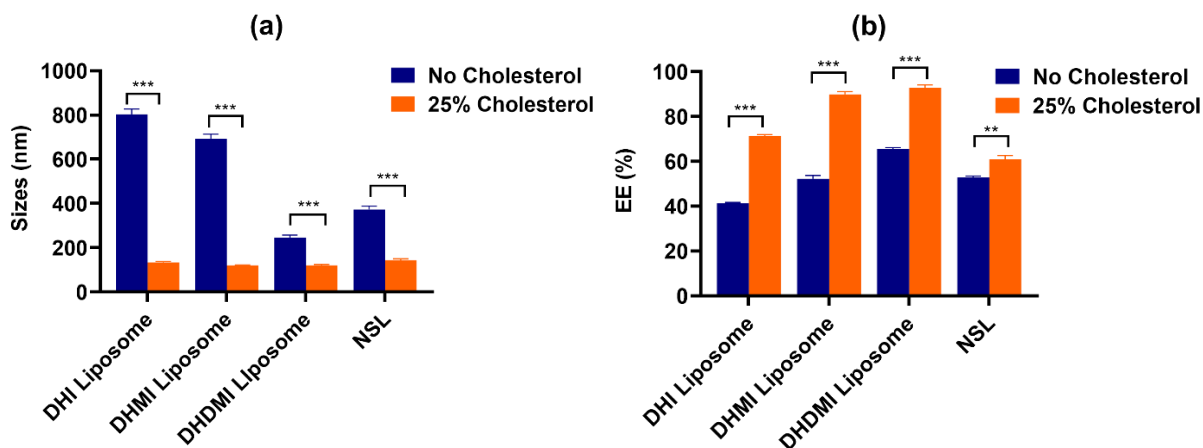
Figure 2.4. Effect of cholesterol on sizes and EE of ICL and SNL. (a) Sizes of liposomes with and without 25% cholesterol. Data presented as mean ± SD, N = 7. *** p < 0.001. (b) EE of liposomes with and without 25% cholesterol. Data presented as mean ± SD, N = 3. ** p < 0.01, *** p < 0.001.

It was reported that incorporation of cholesterol into the lipid bilayer structure can improve the stability of liposomal formulations [183, 184]. At $T > T_m$, the lipid bilayer was in fluid phase, in which the lipid molecules were restrained to the surface of membranes but nonetheless free to diffuse within this surface. Each lipid molecule had the process of random walk to exchange locations with its neighboring lipid molecules. Due to its unique physicochemical characteristics, cholesterol helps the lipid bilayers exert their thermodynamic properties. The hydrophilic domain of cholesterol molecule is little (a single hydroxyl group), which makes it barely resemble phospholipids. The addition of cholesterol was found to help control the mobility of lipid bilayers in fluid phase and to reduce their permeability to water [185, 186]. Cholesterol was found to reduce the fluidity of lipid bilayers and to increase their mechanical rigidity by intercalating between phospholipids and filling in the cavities to decrease the flexibility of hydrocarbon chains of the surrounding phospholipids [187]. Furthermore, the inhibition of lipid mobility also reduced the lateral diffusion coefficient of lipid bilayers in fluid phase. Consequently, the introduction of cholesterol helped stabilize the phospholipid bilayer

structures when the temperature was elevated above T_m. Conversely, the addition of cholesterol was also found to interfere with phospholipid bilayers in gel phase by disrupting the local packing order of their lattice structures. This interaction increased the diffusion coefficient and decreased the elastic modulus of lipid bilayers in the gel phase [188].

In this study, liposomes were incubated with DOX at 70˚C ($T > T_m$) for 90 min, and a protective effect of cholesterol against aggregation was observed while the temperature cooled down. The above-mentioned studies on cholesterol suggest that on the one hand, cholesterol would stabilize the fluid state of the liposome bilayers, which would increase the drug retention of liposomes during drug-loading, while one the other hand, cholesterol would mobilize the lipids in the bilayers at the gel state bilayers to hinder the aggregation from liposome-DOX-liposome stacking. The addition of cholesterol remarkably improved the size and EE. Therefore, ICL containing no cholesterol and 25% cholesterol were subjected to further studies to test their pH-sensitivity, stability and anticancer activity *in vitro*.

2.3.2.3.4 Effect of pH during drug loading. To explore the effect of drug loading pH on size and EE of DOX-loaded liposomes, liposomes with or without 25% cholesterol were prepared and loaded with DOX at pH 7.4 or 8.0. As shown in Table 2.10, for both DHI/DSPC/DPPE-PEG and DSPC/DPPE-PEG, the sizes after DOX loading at pH 8.0 were dramatically larger than pH 7.4, together with smaller PDI and higher EE. This implies that loading DOX at pH 8.0 induced higher percentage of aggregated liposomes than at pH 7.4, similar as the higher extent of aggregation observed in ICL and NSL consisting of DPPC (Table 2.6 and 2.7). For the liposomes consisting of 25% cholesterol, DOX loading at pH 8.0 also yielded larger liposomes than pH 7.4 but the size increase is not as large as liposomes without cholesterol.

Table 2.10

Effect by loading pH. Size, PDI and EE of liposomes loading DOX at pH 7.4 and 8.0

Lipid Compositions	Mol Ratio	Loading pH	Size (nm)	PDI	EE (%)
DHI/DSPC/DPPE-PEG	25/70/5	7.4	808.3	0.857	40.56±4.54
DHI/DSPC/DPPE-PEG	25/70/5	8.0	3260.0	0.643	65.97±1.15
DSPC/DPPE-PEG	95/5	7.4	304.2	1.000	36.69±0.53
DSPC/DPPE-PEG	95/5	8.0	1842.0	0.448	65.61±1.00
DHI/DSPC/DPPE-PEG/Chol	25/45/5/25	7.4	159.9	0.105	91.27±1.97
DHI/DSPC/DPPE-PEG/Chol	25/45/5/25	8.0	208.0	0.278	84.48±2.31
DSPC/DPPE-PEG/Chol	70/5/25	7.4	148.4	0.293	52.95±0.95
DSPC/DPPE-PEG/Chol	70/5/25	8.0	361.0	0.592	69.76±1.58

Note. Size values are the cumulative intensity of hydrodynamic diameters. EE data presented as mean ± SD, N = 3.

Based on this result, DOX-loading pH considerably affects the sizes of ICL liposomes. The addition of cholesterol restrained the interaction between liposomes and DOX at both pH 7.4 and 8.0. For the liposomes with cholesterol loading at pH 8.0, the slightly increase of sizes was the composite outcome of aggregation intensified by the elevated pH and protection effort by cholesterol.

2.3.2.3.5 Effect of the temperature for mixing with resin to remove unencapsulated DOX. It was reported that under certain conditions, liposomes can aggregate in the gel phase but not in fluid phase [181]. In our studies, the ICL aggregated during the cooling down process after incubation with DOX at $T > T_m$. To confirm this, size of NSL was measured at 70˚C immediately after 90 min incubation with DOX at 70˚C before cooling down and compared with the size of NSL measured at room temperature after cooling down. As shown in Table 2.11, the cumulative hydrodynamic diameter of NSL before cooling down stayed below 250 nm, which is

smaller than the cooled downed NSL. The detailed dynamic light scattering result of the size of NSL after cooling showed a peak of above 1000 nm size, which confirmed aggregation. In comparison, NSL before cooling down, only showed peaks of sizes similar to or smaller than the cumulative size. These data confirmed that NSL aggregated when the liposomes were cooled down and turned into gel phase.

Table 2.11

Cumulative size and intensity of each peak of DOX-loaded liposomes measured at 70˚C immediately after DOX loading, and at room temperature after suspension cool-down

Lipid Compositions	Mol Ratio	Measurement T (˚C)	Cumulative Size (nm)	PDI	Peak 1 (nm)	Peak 2 (nm)
DSPC/DPPE-PEG	95/5	70	241.1	0.361	234.3	60.23
DSPC/DPPE-PEG	95/5	RT	486.5	1.000	1465.0	121.0

Note. Cumulative size values are the cumulative intensity of hydrodynamic diameters.

Based on the above observation, the DOX-loaded liposomes was mixed with resin at T > T_m to remove unencapsulated DOX from liposome before the liposomes were cooled down to form the gel phase in an effort to reduce the aggregation. As shown in Table 2.12, the liposomes that were mixed with resin at 50˚C had similar average size as those that were mixed with resin at room temperature, while the liposomes mixed with resin at 60˚C and 70˚C had slightly smaller average size than at room temperature. The peak 1 (largest peak) of the size measurement of the liposome mixed with resin at 60˚C and 70˚C showed more evident decrease in the diameter from that at room temperature compared with liposomes after drug-loading at 50˚C. The EE of liposomes after being mixed with resin at 60˚C and 70˚C were lower than at room temperature and 50˚C, which was probably caused by less stacking of DOX on liposomes in fluid phase at higher temperature.

Because the percentage of aggregated liposome was reduced after mixing the liposomes with resin at $T \geq T_m$, filtration was attempted to remove the large liposome-DOX aggregates to further reduce the formulation size. The liposome suspensions were filtered with nylon syringe filters of 400 nm pore. As shown in Table 2.12, the cumulative size of liposomes after mixing with resin at different temperature and filtration were decreased below 150 nm. The PDI also decreased considerably, which indicated the aggregated liposomes were removed. However, the filtration significantly decreased the EE and the filtered liposomes suspension became more transparent, indicating that a substantial portion of the liposomes were trapped in the syringe filters. EE for the liposomes that were mixed with resin at 60°C or 70°C followed by filtration were higher than those that were mixed with resin at 50°C or room temperature, which is in line with the results that their extent of aggregation is lower (Table 2.12).

Table 2.12
Size and EE of DOX-loaded liposomes after being mixed with resin at room temperature, 50°C, 60°C or 70°C and the effect of filtration on the size and EE

Composition	Mol Ratio	Mixing T (°C)	Filtered	Cumulative Size (nm)	PDI	Peak 1 (nm)	Peak 2 (nm)	EE (%)
DSPC/DPPE-PEG	95/5	RT	×	486.5	1.000	1465.0	121.0	53.01±0.47
			√	208.2	0.184	260.0	44.91	4.61±0.84
DSPC/DPPE-PEG	95/5	50	×	493.5	0.605	1240.0	118.1	48.23±0.47
			√	118.2	0.172	136.1	-	5.99±0.34
DSPC/DPPE-PEG	95/5	60	×	348.8	0.647	680.6	135.4	28.47±0.60
			√	144.7	0.191	184.2	40.7	10.92±0.16
DSPC/DPPE-PEG	95/5	70	×	428.1	0.684	639.0	118.1	31.17±0.30
			√	116.5	0.184	141.8	-	7.58±0.18
DHI/DSPC/DPPE-PEG	25/70/5	RT	×	455.4	0.661	1152.0	139.5	44.36±1.23
			√	116.7	0.321	170.8	4233	5.48±1.37

(Table 2.12 Continued)

DHI/DSPC/ DPPE-PEG	25/70 /5	70	×	427.0	0.719	724.0	76.08	46.43±0.66
			√	125.6	0.370	95.66	256.9	5.01±0.05

Note. Cumulative size values are the cumulative intensity of hydrodynamic diameters. EE data presented as mean ± SD, N = 3.

The above results indicated mixing liposomes with resin at $T \geq T_m$ moderated the aggregating of liposomes but did not sufficiently decrease the average sizes of the formulations. The Dowex 50WX-4 was known as a cationic ion-exchange resin which bounds with the unencapsulated DOX and yet leave the DOX molecules that are entrapped by liposome [179]. The result that resin partially diminished the aggregation was in line with the finding that the stacking of DOX and their binding with liposomes can cause aggregation. In this study, the resin appeared to have limited capability in removing DOX that were stacked on the surface of liposomes. Adding resin into the liposome suspension at T_m or even higher temperature only moderated the aggregation but did not totally prevent it.

The filtration method was commonly used to sterilize liposomal formulations in industrial manufacturing [189, 190]. Our study indicate that the filtration method can cause considerable loss of the liposomes when the sample contains liposome aggregates of too large size (diameter larger than 500 nm).

2.3.2.3.6 Effect of input DOX concentration. To study the effect of input DOX concentration on size and EE of liposomes, liposomes were mixed with 1000, 500, 250 µg/ml DOX solutions and incubated for 90 min of drug loading. As can be seen in Figure 2.5 (a), the sizes of liposomes decreased after incubation with lower and lower DOX concentration, which was consistent with the prior report that the aggregation resulted from stacking of DOX and their association with liposomes. As shown in Figure 2.5 (b), the EE remained at the same level in

liposomes that were incubated with different concentrations of input DOX. Because the input

DOX concentration was reduced, the encapsulated DOX concentration was further considered as

a characteristic of the drug loading, in consideration that the minimum concentration of the DOX

concentration for anticancer studies in MCS models. Although the lower input DOX decreased

the liposome size, the encapsulated DOX concentration of the resultant DHI and NSL liposomes

also dropped below 200 µg/ml, which is required for MCS studies. Therefore, the resultant

formulations were concentrated with a diafiltration column. After extrusion through the

diafiltration column for 14 times, the volume of each liposome suspension was reduced from 2

mL to 0.5 mL while the encapsulated DOX concentration was raised above 300 µg/ml for further

anticancer investigations in MCS.
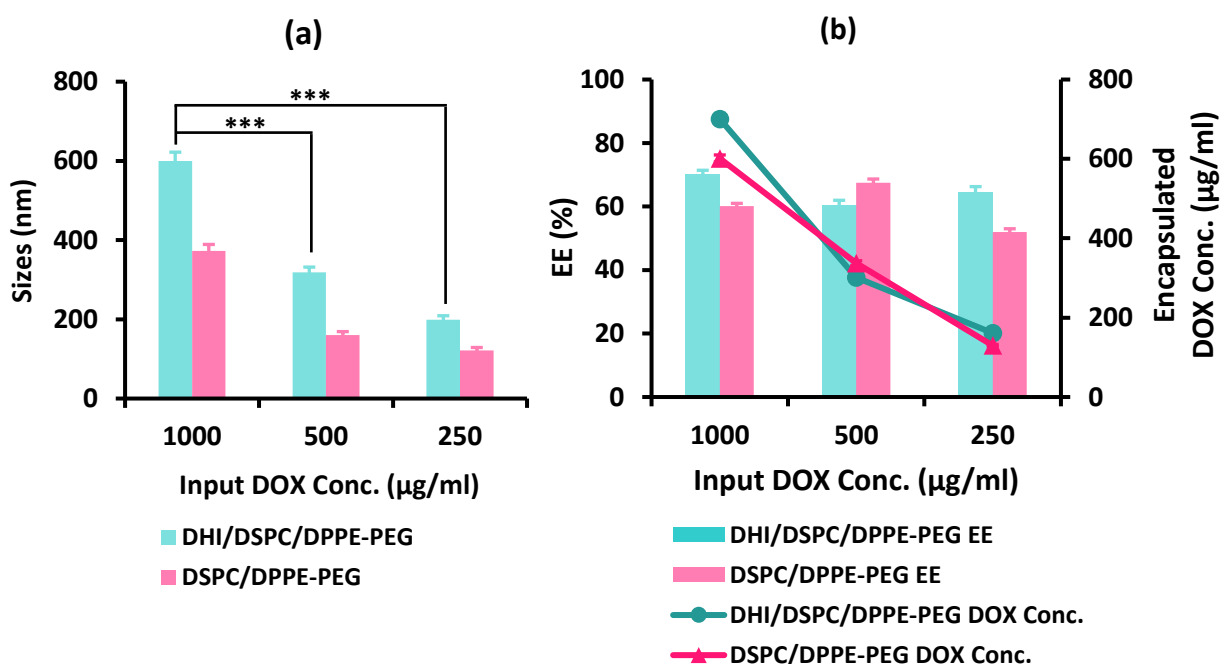
Figure 2.5. Effect of input DOX concentration on sizes and EE of ICL and SNL. (a) Sizes of liposomes after DOX loading at different input concentrations. Data presented as mean ± SD, N = 7. *** $p < 0.001$. (b) EE and encapsulated DOX concentration of liposomes after DOX loading at different input concentrations. Data presented as mean ± SD, N = 3. ** $p < 0.01$, *** $p < 0.001$.

Based on the results in Table 2.4 and Figure 2.3 (a), the ICL consisting of DHI was more prone to aggregation during drug loading than ICL consisting of DHMI or DHDMI. Drug loading at a lower DOX concentration of 200 µg/ml yielded smaller ICL consisting of DHI (198.8 nm in diameter) and NSL (121.2 nm in diameter), indicating that the input DOX concentration during drug loading was a significant factor to influence the sizes of DOX-loaded ICL and NSL. With such method, ICL formulations containing DHI, DHMI and DHDMI were prepared and characterized with sizes around or below 200 nm (Table 2.13). TFF concentrating was needed for those formulations before applied in MCS treatment.

Table 2.13

Size, PDI and EE of ICL liposomes lasted extruded by 100 nm polycarbonate membrane and loaded with 200 µg/ml DOX for 90min.

Lipid Compositions	Mol Ratio	Size (nm)	PDI	EE (%)
DHI/DSPC/DPPE-PEG	25/70/5	198.8	0.531	56.62±2.06
DHMI/DSPC/DPPE-PEG	25/70/5	179.6	0.573	53.18±1.12
DHDMI/DSPC/DPPE-PEG	25/70/5	202.9	0.115	59.54±0.59
DSPC/DPPE-PEG	95/5	121.2	0.266	57.74±0.98

Note. Size values are the cumulative intensity of hydrodynamic diameters. EE data presented as mean ± SD, N = 3.

2.4 Summary

The imidazole-based ether lipids DHI, DHMI and DHDMI were successfully synthesized. Using film hydration, freeze-anneal-thawing and extrusion methods, ICL were successfully prepared with sizes smaller than 130 nm and PDI under 0.3. With manganese sulfate gradient method at the input DOX concentration of 1000 µg/ml, ICL were loaded with DOX at EE of at least 40%. The sizes and PDI of DOX-loaded ICL significantly increased

during DOX-loading due to aggregation. Factors influencing the sizes and EE of ICL were studied to improve the ICL formulations, including drug loading time, length of acyl chains of phospholipids, addition of cholesterol, drug-loading pH, temperature of mixing with the resin and input DOX concentration. Reducing drug loading time, adding cholesterol, mixing with resin at $T \geq T_m$ followed with filtration and reducing the input DOX concentration decreased the sizes of DOX-loaded ICL by inhibiting or preventing the liposome aggregation. Among these methods, adding 25% cholesterol and reducing the input DOX concentration from 1000 μg/ml into 200 μg/ml most effectively decreased the sizes of DOX-loaded ICL to about 200 nm in diameter without dramatically reducing EE. The advantages and disadvantages of these improvement methods are summarized in Table 2.13.

Table 2.14
Comparison of methods to improve the size and EE of DOX-loaded ICL

Methods	Pros	Cons
Reducing drug loading time	Size ~200 nm	Lowered EE
Incorporation with cholesterol	Size ~140 nm, EE ~70%	
Mixing with resin at $T \geq T_m$ and filtration	Size ~120 nm	Lowered EE
Reducing input DOX Conc.	Size ~200 nm	Lowered DOX Conc.

The addition of cholesterol seems to be the most effective method to improve the size and EE. However, modified composition of ICL formulations could also impact their pH-sensitivity. Thus, pH-sensitivity studies were carried out on both the cholesterol-free ICL and the ICL containing cholesterol in the next chapter.

CHAPTER 3: TESTING OF PH-SENSITIVITY OF IMIDAZOLE-BASED CONVERTIBLE LIPOSOMES

3.1 Introduction

A pH-sensitive liposome is a modified form of liposomes that shows high stability at physiological pH (pH 7.4) while undergoing destabilization or physicochemical changes under acidic conditions [23]. pH-sensitive liposomes can serve as viable drug delivery systems because many physiological and pathological scenarios involve acidic pH, including endosomal/lysosomal vesicles solid tumors and sites of inflammation [23, 114]. The composition of the imidazole-based convertible liposomes was designed to protonate in response to the acidic extracellular pH in tumor (pH 6.0-7.0). The protonated imidazole lipids would then interact with the negatively charged DPPE-PEG on the liposome membrane to condense them laterally and thus to unveil the excessive positive charges on the surface of ICL. Such pH-triggered ICL would in turn have stronger electrostatic interaction with cancer cells and/or release more of the payload drug.

Based on the results of Chapter II, two methods were discovered to considerably improve the physicochemical properties of ICL: reduction of input DOX concentration during drug loading and addition of cholesterol in lipid composition. Studies in this chapter aim to test the pH-sensitivity of ICL by exposing them to aqueous solutions of pH 6.0-7.4 *in vitro*. Based on the aforementioned properties of ICL, the pH-sensitivity studies include pH-dependent change of liposome surface charge (ζ-potential) and pH-dependent DOX release, which would test ICL's potential to interact more with negatively charged cells and to release more payload drug at lower pH, respectively.

3.1.1 Calculated pK$_a$ of the imidazole-based ether lipids. The pK$_a$ of the imidazole-based ether lipids DHI, DHMI and DHDMI were calculated using ACD/pK$_a$ DB software (Advanced Chemistry Development, Inc., Ontario, Canada) [191]. Calculation by software was chosen instead of experimental methods for pK$_a$ determination of imidazole-based lipids due to the assembly of these lipids in aqueous solutions, which makes it hard to trace the protonation status of each lipid molecule in water. The calculated pK$_a$ values of the imidazole-based lipids are evaluated together with the ζ- potentials measurements of ICL liposomes containing these lipids to assess the protonation of these lipids in response to different pH. As shown in Table 3.1, the estimated pK$_a$ of the imidazole-based lipids ranges from 5.36 to 6.75. As a lipid with a basic headgroup, each imidazole-based lipid would protonate more in an acidic environment than neutral pH. Based on their pK$_a$, their extent of protonation would be ranked DHDMI > DHMI > DHI.

Table 3.1
Calculated pK$_a$ of DHI, DHMI and DHDMI using ACD/pK$_a$ DB software. [129]

Imidazole Lipids	pK$_a$
DHI	5.53±0.5
DHMI	6.20±0.5
DHDMI	6.75±0.5

3.1.2 Phase separation of ICL in response to acidic pH. Due to the significantly strong electrostatic interaction between the imidazole-based lipids and DPPE-PEG, phase separation was observed in the ICL bilayer at acidic pH, which was reported in our prior studies [129]. The liposome membrane can separate into multiple phases when interaction between its lipid components are sufficiently strong [192]. The phase separation in lipid bilayers can be

monitored by differential scanning calorimetry (DSC), a thermoanalytical technique developed in 1962 [193]. DSC measures the heat a sample absorbs to increase its temperature (aka, heat capacity) as a function of temperature. Therefore, DSC can attest to lipid phase separation by recording multiple peaks of higher heat capacities that are generated from the gel-to-liquid transition of the separated lipid phases at different temperatures (Figure 3.1). The DSC thermogram of the convertible liposome DHI/DSPC/DPPE-PEG (Figure 3.2) in prior studies of our group showed a single broad peak at pH 7.4 between 56°C and 65°C, which indicated the gel-to-liquid transition of only one phase and therefore the homogeneous mixing of the lipid components of ICL (DSPC (C18), DPPE-PEG(C16) and imidazole-based lipids (C16)) at pH 7.4. At pH 6.0, the DSC thermogram showed an additional broad peak at around 52 °C (Figure 3.1), which indicated the formation of at least two lipid phases on the liposome membrane. The new lipid phase was probably rich in DSPC because liposomes of only DSPC has a very similar gel-to-liquid phase transition temperature of 54°C. The newly formed lipid phase on the liposomes supports our proposed mechanism of the pH-sensitivity, where interaction between the protonated imidazole-based lipids and the negatively charged DPPE-PEG would expulsed the DSPC to form two phases, one rich in DSPC, and the other in DPPE-PEG.
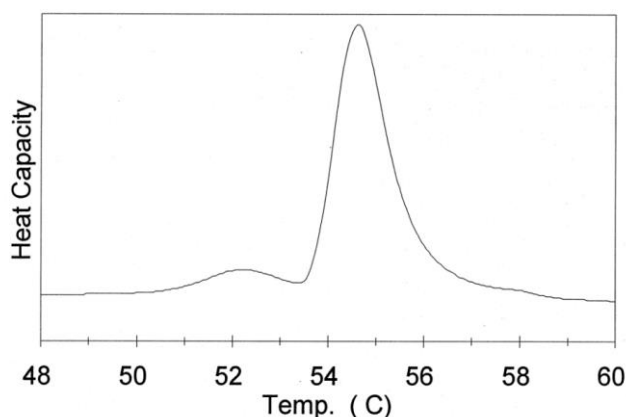
(Figure 3.1 Continued)
Figure 3.1. DSC Thermogram of DSPC. [194]
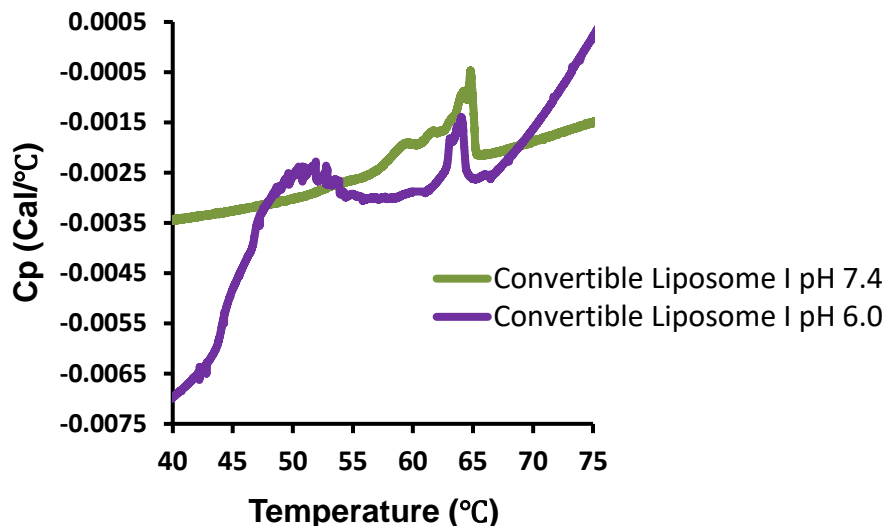
Figure 3.2. DSC Thermogram of Convertible Liposome I (DHI/DSPC/DPPE-PEG) at pH 7.4 and 6.0. [129]

The acidic pH-triggered phase separation of DOX-loaded ICL would enhance the anticancer activity in bio-systems. Firstly, the clustering of negatively charged PEGylated lipids expulsed DSPC doped with positively charged imidazole lipids to form a domain displaying positive charges. This domain would not only have excess positive charges, but also would be cleared from steric hindrance of PEG, both of which would strengthen its electrostatic interaction with negatively charged cell surface. Furthermore, the fractures of the liposome membrane between the DPPE-PEG-rich phase and the DSPC-rich phase would be more permeable to diffusion, which would enhance drug release at acidic pH.

3.2 Materials and Methods

3.2.1 Materials. 2-[4-(2-hydroxyethyl)piperazin-1-yl]-ethanesulfonic acid (HEPES) and 2-(N-morpholino)ethanesulfonic acid (MES) were purchased from Fisher Scientific (Hampton, NH, US). The lipids 1,2-distearoyl-sn-glycero-3-phosphocholine (DSPC), 1,2-dipalmitoyl-

snglycero-3-phosphoethanolamine-N-[azido(polyethylene glycol)-2000 (DPPE-PEG (2000)), 1-palmitoyl-2-oleoyl-glycero-3 phosphocholine (POPC), 1-palmitoyl-2-oleoyl-sn-glycero-3-phosphoethanolamine (POPE), 1-palmitoyl-2-oleoyl-sn-glycero-3 phospho-L-serine (sodium salt) (POPS) and L-α-phosphatidylinositol (Soy) (L-R-PI) were purchased from Avanti Polar Lipids, Inc. (Alabaster, AL, USA). Cholesterol, Dowex® 50WX-4 (50-100 mesh), Sephadex G-25 were purchased from Sigma-Aldrich (St. Louis, MO, USA). Doxorubicin Hydrochloride was purchased from Biotang (Waltham, MA, USA). All other organic solvents and chemicals were purchased from Sigma Aldrich, Fisher Scientific or VWR.

3.2.2 pH-triggered acquisition of positive charges by ICL. The ζ- potential of ICL and the mean sizes of ICL mixed with equimolar model liposomes at pH 6.0, 6.5, 7.0 7.4 were measured to monitor the pH-triggered acquisition of positive charges by ICL.

3.2.2.1 ζ- potential measurement at pH 6.0, 6.5, 7.0, 7.4. In order to enhance the detection of changes in liposome surface charge, ICL and NSL were prepared by hydration in an isotone buffer of low ionic strength (pH 7.4, 5 mM HEPES, 5% (w/v) Glucose) [195]. The liposome preparation methods were similar as in 2.2.2.1. An aliquot (50-100 μL) of the resultant suspension of ICL or NSL was diluted in 900 μL isotonic MES buffer (pH 6.0 and 6.5, 10 mM MES, 5% (w/v) Glucose) and isotonic HEPES buffer (pH 7.0 and 7.4, 10 mM HEPES, 5% (w/v) Glucose), and the ζ- potentials was measured at 37˚C based on electrophoresis mobility under applied voltage (Zetasizer ZS90, Malvern Instruments Ltd., UK).

3.2.2.2 Interaction of ICL with model liposomes. The model liposomes [196, 197] mimicking the lipid composition of biomembranes were prepared using film hydration, freeze-thawing and extrusion. Briefly, a chloroform solution of POPC: POPE: POPS: L-R-PI: cholesterol = 50:20:5:10:15 (mol%) in a recovery flask was evaporated under reduced pressure

to form a lipidic film on a Buchi rotavapor at room temperature. The lipidic film was further dried in vacuum oven for over 4 hours at room temperature to remove the residual of solvent completely. The lipidic film was then hydrated with isotonic HEPES buffer (pH 7.4, 5 mM HEPES, 140 mM NaCl) by intermittent agitation to obtain a liposomes suspension containing 20 mM total lipids. The flask was filled with argon and sealed with parafilm. The Liposome suspension was freeze-thawed by rapidly freezing in liquid nitrogen, emerging in ice-water mixture for 2 min and thawing in water at room temperature for 5 min. The freeze-anneal-thawing was repeated for 11 times. The liposome suspension was extruded 11 times though 400 nm polycarbonate membranes (Nucleopore Corp., Pleasanton, CA, US) at room temperature using a handling Mini-extruder (Avanti Polar Lipids Inc., Alabaster, AL). The mean size of the resultant model liposomes was 192.7 nm in diameter as measured by Zetasizer ZS90. Liposome suspension of ICL and NSL were mixed with the model liposome containing equimolar total lipid and 5 μL of the mixture was diluted in 150 μL isotonic MES buffer (pH 6.0 and 6.5, 10 mM MES, 140 mM NaCl) and isotonic HEPES buffer (pH 7.0 and 7.4, 10 mM HEPES, 140 mM NaCl). The size of the particles in the diluted mixtures was measured at 37°C by dynamic light scattering (Zetasizer ZS90, Malvern Instruments Ltd., UK).

3.2.3 pH-triggered drug release of ICL.

3.2.3.1 Qualification of initial DOX Concentration in liposomes diluted with buffers at pH 6.0, 6.5, 7.0, 7.4. Liposome formulation (100 μL) was severally diluted with 500 μL MES buffer (pH 6.0 and 6.5, 100 mM MES, 1.7% (w/v) Glucose) and HEPES buffer (pH 7.0 and 7.4, 100 mM HEPES, 1.7% (w/v) Glucose) in 1.5 mL Amber glass vials. An aliquot (10 μL) of each diluted sample was immediately lysed with 90 μL lysing buffer (90% (v/v) isopropanol, 0.075 M HCl) in a 96-well Black Clear Bottom Polystyrene microplate (Corning®, NY, US) and the

initial DOX concentration C_i (as at time point 0 hour) was qualified with a standard calibration curve generated from the standard DOX solutions as mentioned in 2.2.4. All samples in 96-well microplate were triplicated. The microplates with samples were covered with foil before reading.

3.2.3.2 pH-triggered drug release from liposomes determined by direct resin adsorption. The liposome samples diluted by buffer at different pH (6.0, 6.5, 7.0, 7.4) as in 2.2.5.1 were mixed with cation-exchange resin Dowex® 50WX-4 (50-100 mesh) at DOX: resin = 1:200 (w/w) ratio. The mixtures were incubated and gently shaken in an incubator at 37˚C. An aliquot (10 µL) of supernatant was taken from each sample at time points 1, 3, 6, 12, 24, 48 hours to be lysed with 90 µL lysing buffer (90% (v/v) isopropanol, 0.075 M HCl) in a 96-well Black Clear Bottom Polystyrene microplate(Corning®, NY, US). The DOX concentration of supernatant C_s, which is the concentration of DOX retained in liposome was qualified by fluorescent spectrometry using a standard calibration curve generated from the standard DOX solutions as mentioned in 2.2.4. All samples in 96-well microplate were triplicated. The microplates with samples before recording were covered with foil. The percentage of released DOX was determined by the following equation,

$$\% \ Released \ DOX = \left(1 - \frac{C_s}{C_i}\right) \times 100\%$$

Where C_s = concentration of DOX retained in liposome after resin absorption, C_i = initial liposomal DOX concentration.

3.3 Results and Discussions

3.3.1 pH-triggered acquisition of positive charges by ICL.

3.3.1.1 Acidic pH-triggered elevation of ζ- potentials of ICL. ζ- potentials of drug-free ICL and NSL at pH 6.0, 6.5, 7.0, and 7.4, at 37˚C were measured to evaluate the pH-sensitivity of ICL. As shown in Figure 3.3 (a), all three of the cholesterol-free ICL (DHI, DHMI and

DHDMI) showed significant increase of ζ- potential when pH was adjusted from 7.4 to 6.0. Particularly, the ICL containing DHMI and DHDMI were converted to possess positive surface charges at pH 6.0. The extent of the ζ- potential increase of ICL was correlated with the pK$_a$ of their imidazole-based lipids (pK$_a$: DHDMI > DHMI > DHI). This result demonstrated that the pH-sensitivity of ICL was rendered by the protonation of the imidazole-based lipids DHI, DHMI and DHDMI. By contrast, the NSL (DSPC/DPPE-PEG) displayed negative ζ- potentials below -10 mV at both physiology and acidic pH. However, as can be seen in Figure 3.3 (b), the three ICL containing 25% cholesterol didn't show noticeable rise of ζ- potentials at any of the pH under this study but instead fluctuated between -5 mV and -20 mV. This result indicated that the pH-sensitivity of ICL, as displayed by the acidic pH-triggered acquisition of positive surface charges, was prohibited by the addition of 25% cholesterol.
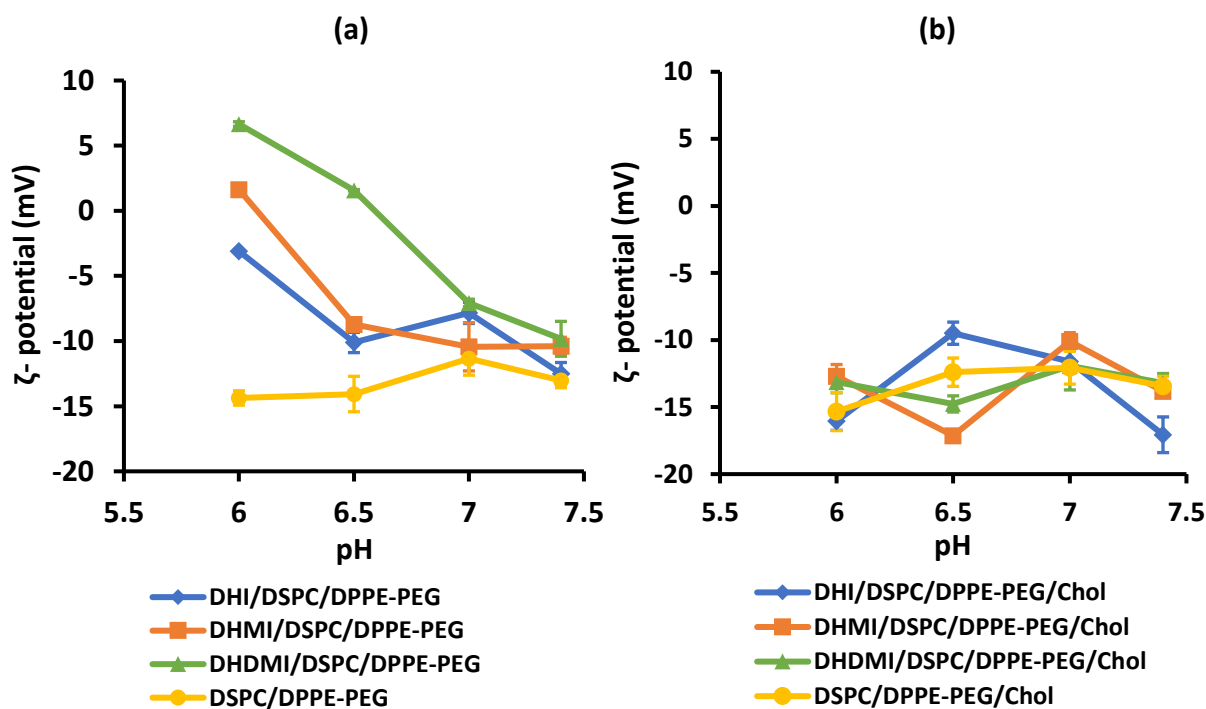
Figure 3.3. ζ- potential of ICL without (a) or with (b) 25% cholesterol at 37 °C, pH 6.0, 6.5, 7.0, and 7.4. Data presented as mean ± SD, N = 3.

3.3.1.2 Acidic pH-triggered interaction between ICL and model liposome. The acidic

pH-triggered interaction of ICL with model liposomes was characterized based on prior studies

in our group [129]. The negatively charged model liposomes, utilized as a simple and fast model

to simulate the components and electrostatic property of biomembranes, were successfully

prepared as shown in Table 3.2.

Table 3.2
Size, PDI and ζ- potential of model liposomes

Lipid Compositions	Mol Ratio	Size (nm)	PDI	ζ- potential (mV)
POPC/POPE/POPS/L-R-PI/Chol	50/20/5/10/15	192.7	0.180	-51.77±1.18

The stock preparation of the model liposomes was diluted in isotonic buffer at pH 6.0,

6.5, 7.0 and 7.4, and then mixed with equimolar drug-free ICL and NSL. The particle size of the

mixture was measured at 37°C. As shown in Figure 3.4 (a), the DHDMI/DSPC/DPPE-PEG

showed remarkable increase of the cumulative size at pH 6.0 compared with pH 7.4. The size

increase indicated the aggregation between ICL and model liposomes due to the electrostatic

interaction. By contrast, as shown in Figure 3.4 (b), the mixture of model liposomes and ICL

consisting of cholesterol did not show noticeable size increase, which indicated no aggregation

between ICL containing cholesterol and the model liposomes.
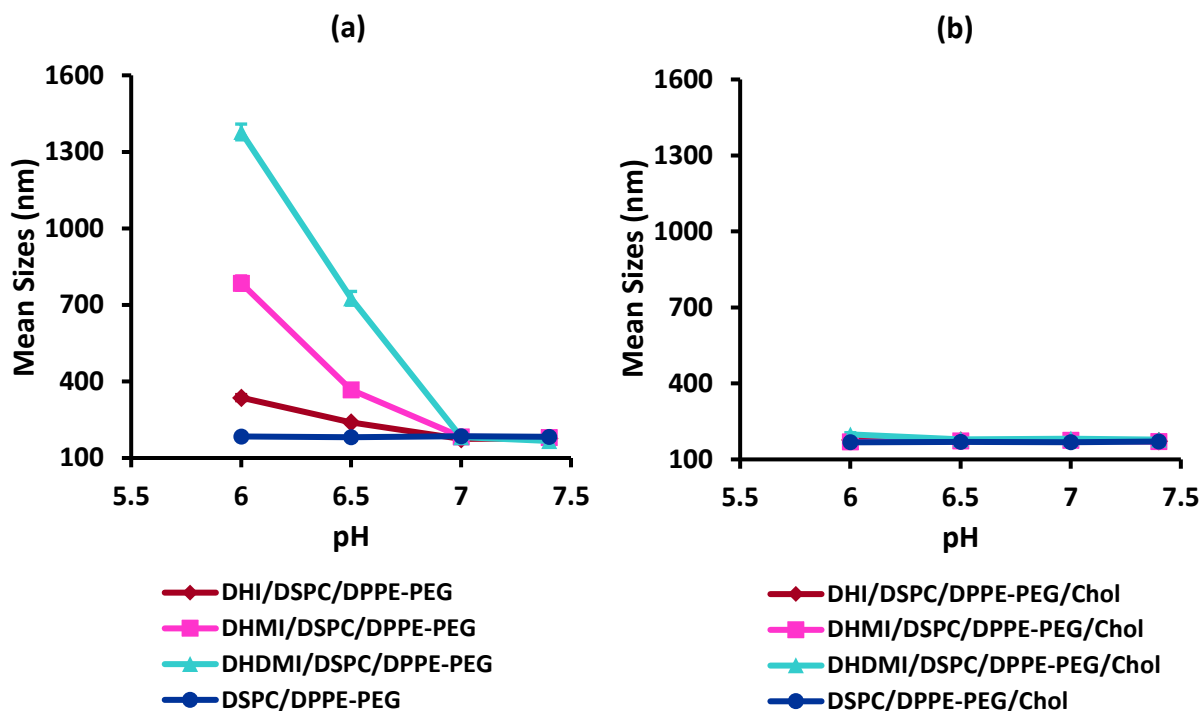
Figure 3.4. (a) Mean sizes of equimolar mixture of model liposome and DHDMI/DSPC/DPPE-PEG at pH 6.0, 6.5, 7.0, and 7.4. Data presented as mean ± SD, N = 3. (b) Mean size of equimolar mixture of model liposome and liposome containing cholesterol at pH 6.0, 6.5, 7.0, and 7.4. Data presented as mean ± SD, N = 3.

Based on the results in 3.3.1, the introduction of imidazole-based convertible lipids introduced pH-sensitivity to liposomes, while the addition of cholesterol was found to suppress the pH-sensitivity. As directly displayed by the pH-triggered rise of ζ- potentials and further supported by the pH-triggered interaction with model liposomes, the cholesterol-free ICL were negatively charged at pH 7.4 and yet converted to cationic liposomes at acidic pH, while the ICL containing cholesterol showed negative surface charges at both pH 7.4 and acidic pH. As discussed in 2.3.2.3.3, cholesterol was reported to help stabilize the fluid phase bilayer structures of liposomes by inserting into cavities between phospholipids to control the flexibility of the hydrocarbon chains. However, at $T < T_m$, incorporation of cholesterol obstructed the movements of phospholipids within the surface of bilayers. An "umbrella model" was proposed to explain

the multibody interaction between cholesterol and phospholipid headgroups in phospholipid bilayers containing cholesterol [192, 198]. Even though cholesterol has a high solubility in phospholipids (about 67 mol % at saturation for many types of PC), the cholesterol molecules are prone to tie up their neighboring phospholipids to accommodate in a lattice structure that is stable in water [192]. In a bilayer structure, the nonpolar cholesterols must be covered by polar phospholipid headgroups to minimize its thermodynamically unfavorable exposure to water at the membrane-water interface. Such required coverage substantially limits the lateral diffusion of the lipids compared to the corresponding cholesterol-free bilayers. Furthermore, it was also demonstrated that as phospholipid headgroups cover cholesterol to form the "umbrella", the hydrophobicity of the liposome membrane increases, which further reduces its affinity with cations [199].

This "umbrella model" is consistent with the results in our studies. The distinct display of surface positive charges by ICL would need not only protonation of the imidazole-based lipids but also the phase separation that was implemented by the lateral redistribution and assembly of negatively charged DPPE-PEG and positively charged imidazole-based lipids. In our study, the pH-sensitivity was recorded in conditions at 37˚C, which is below the T_m of ICL (estimated 63˚C). Therefore, based on the "umbrella model", DPPE-PEG and imidazole-based lipids would not be able to cluster at acidic pH when cholesterol prohibits the lipid lateral redistribution by tying up the surrounding phospholipids. Furthermore, the addition of cholesterol increases the hydrophobicity of the liposome membrane, which would reduce its affinity with protons, and thus reduce the protonation of imidazole-based lipids. Such speculation is supported by the observation that ICL with cholesterol maintained negative a ζ-potentials at acidic pH. In our studies, the stabilization effect by the incorporated 25% cholesterol at $T \geq T_m$ improved the

physicochemical properties of DOX-loaded ICL. However, the inhibition of the lipid lateral diffusion by cholesterol at $T < T_m$ also inhibited the pH-triggered display of positive charges by ICL. Therefore, further drug release and cytotoxicity studies were carried out to evaluate ICL with and without cholesterol.

      3.3.2 pH-triggered drug release of ICL. Drug release studies were carried out to further test the stability and pH-sensitivity of ICL without or with cholesterol. After extrusion by 200 nm and 100 nm polycarbonate membrane, ICL without or with cholesterol were loaded with DOX and then incubated at 37˚C, pH 6.0, 6.5, 7.0, and 7.4 for 12 hours, and the change of fluorescence of DOX was recorded to calculate the drug release. As shown in Figure 3.5, the DHI, DHMI, DHDMI and NSL liposomes without cholesterol released 62.91±7.15%, 47.15±4.98%, 19.02±3.27% and 24.15±1.28%, respectively, of the encapsulated DOX after incubation at pH 7.4 for 12 hours, which indicated that the stability of DHDMI and NSL liposomes were higher than DHI and DHDMI liposomes at the physiological pH 7.4 environment. Figure 3.5 (b) showed the DHMI liposomes released more DOX at pH 6.0 than other higher pH, which again illustrated that the DHMI formulation was sensitive to the acidic pH. According to Figure 3.5 (c) and (d), the DHDMI and NSL liposomes showed no evident low pH-triggered increase in drug release. Figure 3.5 (a) showed the DHI liposomes released more DOX at pH 6.0 than pH 6.5 and 7.0 but not more than pH 7.4, which might be due to its relatively low stability at pH 7.4.
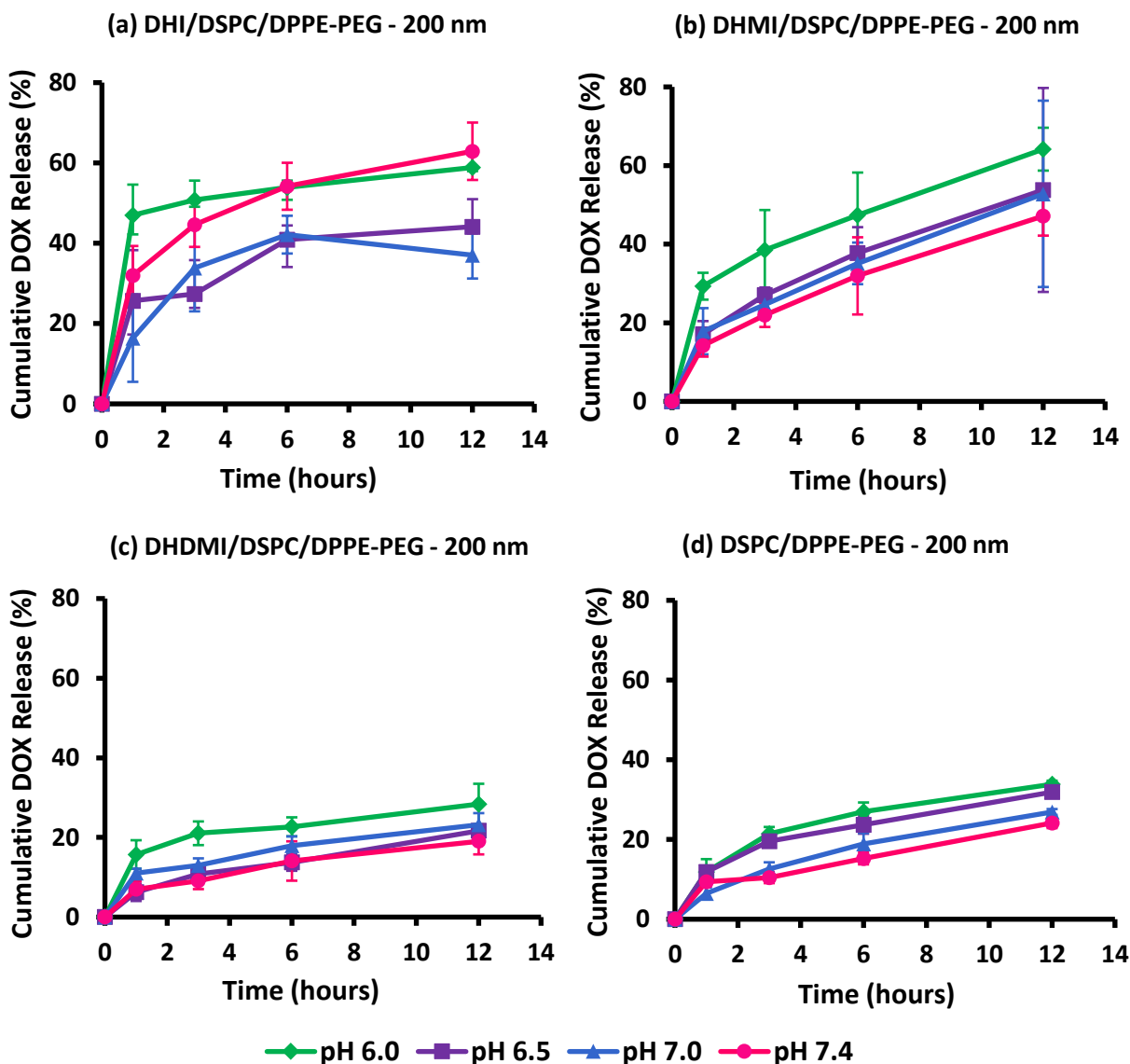
Figure 3.5. The percentage of DOX release from liposomes extruded by 200 nm over 12 hours at 37 °C, pH 6.0, 6.5, 7.0, 7.4. Data presented as mean ± SD, N = 3.

As shown in Figure 3.6, for cholesterol-free liposomes that had been extruded by 100 nm polycarbonate membrane, the DHI, DHMI, DHDMI and NSL liposomes incubated released 64.53±1.74%, 53.65±2.27%, 20.36±0.83% and 29.56±0.70% DOX in 12 hours at pH 7.4, which was in consistence with the formulations extruded by 200 nm. Specifically, Figure 3.6 (b) showed remarkable enhanced drug release of DHMI liposomes at pH 6.0 compared with higher

pH. However, Figure 3.6 (a) (c) and (d) showed no obvious acidic pH-triggered enhancement of drug release from DHI, DHDMI and NSL liposomes.
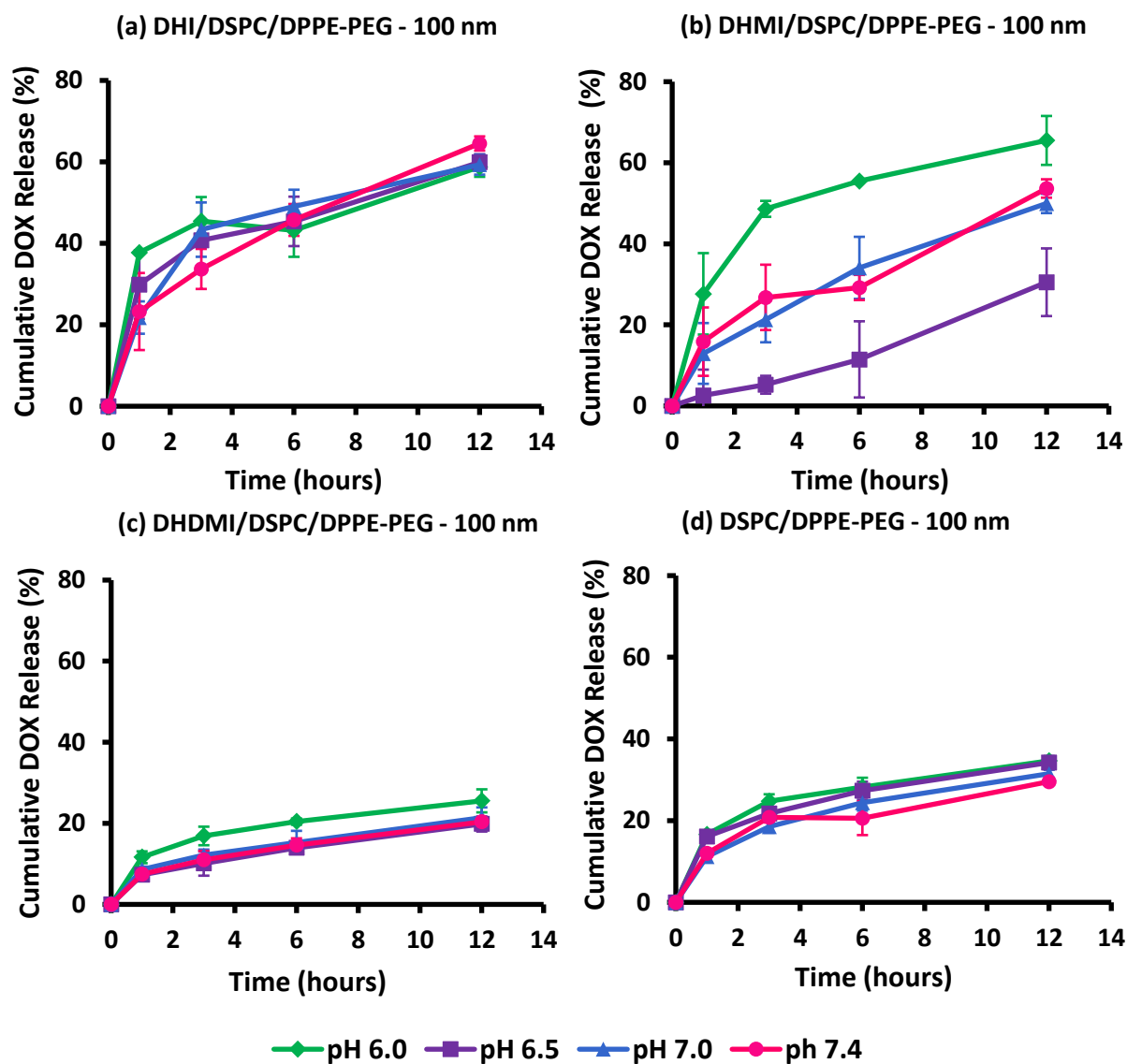
Figure 3.6. The percentage of released DOX of liposomes extruded by 100 nm over 12 hours of incubation at 37 °C, pH 6.0, 6.5, 7.0, and 7.4. Data presented as mean ± SD, N = 3.

As shown in Figure 3.7, after incorporation of 25% cholesterol and extrusion through 100 nm polycarbonate membrane, the DHI, DHMI, DHDMI and NSL liposomes released

56.19±0.78%, 47.11±0.60%, 40.32±0.99% and 57.70±3.03% DOX, respectively after incubation at pH 7.4 for 12 hours. Compared with the cholesterol-free counterparts, the DHI and DHMI liposomes with cholesterol showed similar level of drug release, while the DHDMI and NSL liposomes with cholesterol showed increased drug release. None of the formulation with cholesterol showed pH-triggered enhancement in drug release, which indicates that the addition of cholesterol prevented the acidic pH-triggered drug release from ICL.
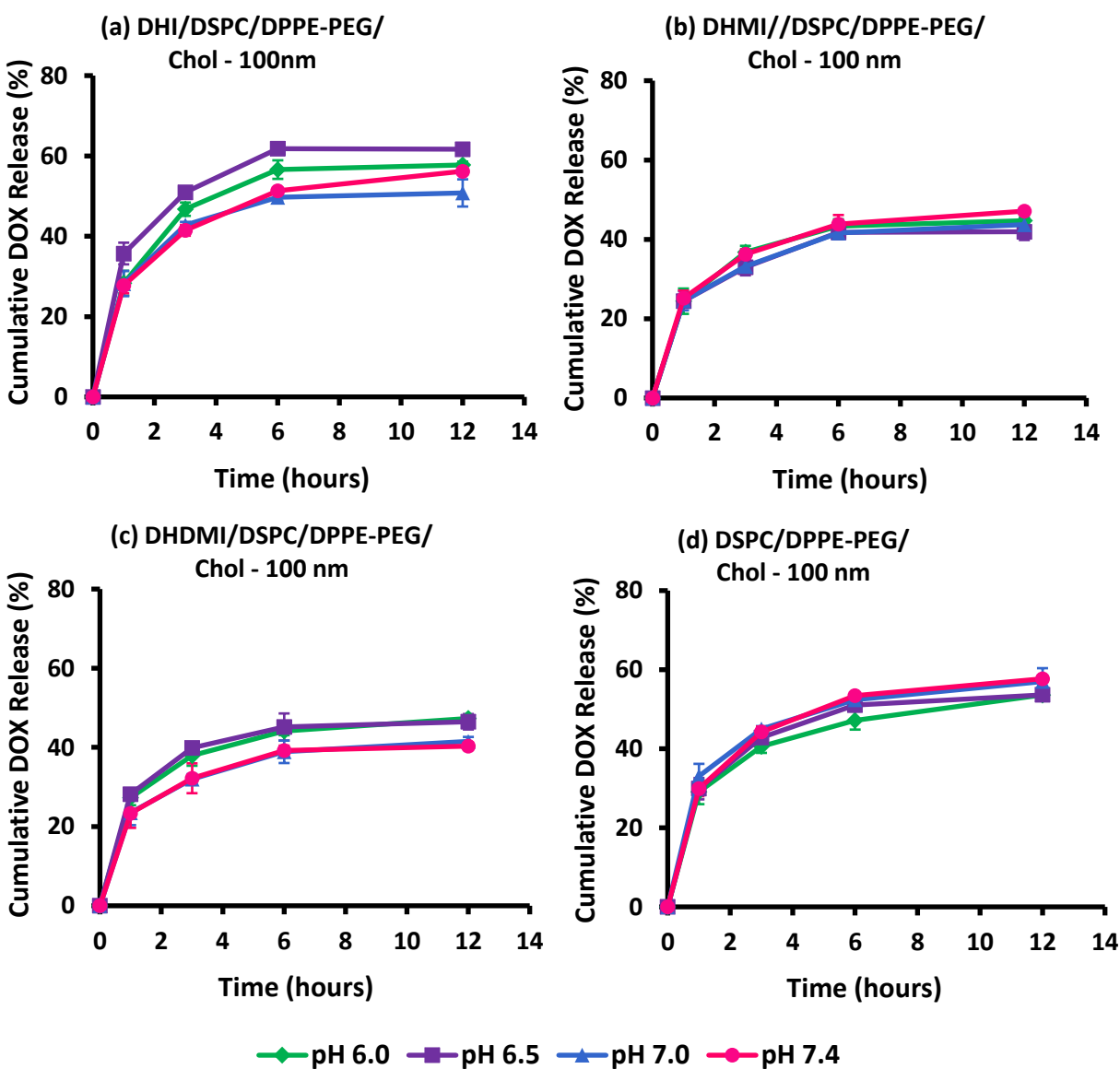
Figure 3.7. Release of DOX from liposomes consisting of 25% cholesterol and extruded by 100 nm over 12 hours of incubation at 37 °C, pH 6.0, 6.5, 7.0, and 7.4. Data presented as mean ± SD, N = 3.

In the drug release study, the stability (presented as drug retention at physiology pH 7.4) and pH-sensitivity of ICL and NSL at 37°C were characterized, and the effect of cholesterol incorporation was investigated. In this study, the cholesterol-free ICL containing DHMI showed pH-triggered increase of drug release, which would favor its anticancer activity in the acidic tumor microenvironment. The ICL consisting of DHI showed some enhanced drug release however also released substantial percentage of the drug at pH 7.4, which suggests that DHI ICL are less stable than DHMI ICL. The drug release of DHDMI and NSL liposomes showed no sensitivity to acidic pH but better stability than DHI and DHMI liposomes at pH 7.4, 37°C. The sensitivity to acidic pH in the drug release study could be explained by the phase separation of ICL at acidic pH, which resulted in destabilization of liposomes. It was reported the release of content entrapped in liposomes was the consequence of accelerated diffusion through the liposomal membranes [200]. The release of content would occur when liposomes lose some or all of their membrane integrity, thus leaking out some or all of the entrapped content to the external media over time. The stability of liposomes was reported to be correlated with the length of acyl chains of lipids [177]. The release kinetics can be controlled by the addition of different lipid components possessing different T_m, because the lateral diffusion coefficient depends on lipid packing and acyl chain ordering [201]. The liposomes containing phospholipids with longer acyl chains would have a higher T_m and higher stability. In our study, at pH 6.0, the liposome membrane would consist of the imidazole-based lipids (C16)/DPPE-PEG (C16)-rich phase and the DSPC (C18)-rich phase, owing to the electrostatic interaction between

positively charged imidazole-based lipids and the negatively charged DPPE-PEG. Based on the correlation between liposome stability and the length of acyl chains of lipids, the C16-rich phase in ICL would possess less stability compared to the phase of evenly distributed C16 and C18 at pH 7.4, therefore the entrapped DOX would leak out faster through the C16 rich phase.

Based on the results of the drug release study, the addition of cholesterol hindered the sensitivity to acidic pH of ICL but enhanced the drug release of ICL at 37°C. Similar with cholesterol's prohibition of pH-triggered display of positive surface charges, the prohibition of pH-triggered drug release can also be explained by cholesterol's inhibition of the phase separation of ICL. According to the "umbrella model" [199] that is explained in 3.3.1, the cholesterol molecules associate with the neighboring phospholipids because of their poor polarity, hence hindering the lateral redistribution of the lipids to form separate phases. Moreover, the addition of cholesterol to lipid bilayers in gel phase was reported to disrupt the original packing of lipids, thus increasing the lateral diffusion coefficient of the bilayers at $T <$ T_m [188, 202]. This can explain the enhancement of drug released from ICL with cholesterol compared with cholesterol-free ICL at pH 7.4.

The physical stability of liposomes concerns the maintenance of liposome size against aggregation and fusion and the retention of entrapped drug against premature leakage [177]. Therefore, evaluation of ICL stability needs comprehensive assessment of their size, encapsulation efficiency (EE), and drug release. In our case, EE is determined both by the efficiency of the drug loading that is driven by ion gradient and by drug leaking out during the drug loading. Therefore, both size and EE of DOX-loaded liposomes reflects their stability at the temperature during drug loading ($T \geq T_m$). On the other hand, drug release of ICL indicates their stability at 37°C ($T < T_m$), at which the drug release is assessed. Among the DOX-loaded

cholesterol-free liposomes (ICL and NSL) (Table 3.3), the liposome of better stability at T ≥ T_m

(smaller sizes and higher EE) also showed more stability at 37˚C (slower drug release in 12

hours at 37˚C). DHDMI/DSPC/DPPE-PEG showed the highest stability among all the

cholesterol-free liposomes. The addition of cholesterol appeared to increase the stability of

liposomes at T ≥ T_m but decrease their stability at 37˚C. This is consistent with the prior findings

that for the bilayers incorporated with cholesterol, their lateral diffusion coefficient is reduced at

T ≥ T_m due to the decrease of lipid mobility [125, 186], but increased at T < T_m due to the

disturbance of lattice arrangement [188]. This effect induced the formulations to leak the

entrapped DOX faster than the cholesterol-free counterparts at 37˚C.

Table 3.3
Comparison of sizes, EE and DOX release (at pH 7.4 in 12 hours) reflecting stability of
liposomes at T ≥T_m and at 37˚C

Lipid Compositions	Lipid Mol Ratio	T ≥T_m		37˚C (T < T_m)
		Sizes (nm)	EE (%)	DOX Release (%)
DHI/DSPC/DPPE-PEG	25/70/5	802.7	41.28±0.45	64.53±1.74
DHMI/DSPC/DPPE-PEG	25/70/5	693.0	52.17±1.52	53.65±2.27
DHDMI/DSPC/DPPE-PEG	25/70/5	246.1	65.55±0.65	20.36±0.83
DSPC/DPPE-PEG	95/5	372.7	52.80±0.69	29.56±0.70
DHI/DSPC/DPPE-PEG/Chol	25/45/5/25	133.6	71.38±0.61	56.19±0.78
DHMI/DSPC/DPPE-PEG/Chol	25/45/5/25	120.0	89.86±1.27	47.11±0.60
DHDMI/DSPC/DPPE-PEG/Chol	25/45/5/25	120.7	92.97±1.10	40.32±0.99
DSPC/DPPE-PEG/Chol	70/5/25	144.1	60.98±1.66	57.70±3.03

Note. Size values are the cumulative intensity of hydrodynamic diameters. EE and DOX release
data presented as mean ± SD, N = 3.

3.4 Summary

The pH-dependent ζ- potential measurement assays, model liposome-interaction assays, and drug release assays were carried out to characterize the pH-sensitivity of ICL with and without cholesterol. The cholesterol-free ICL formulations containing DHI, DHMI or DHDMI showed substantial pH-sensitivity by elevation of ζ- potentials and by interaction with model liposomes, indicating their conversion in response to acidic pH (pH 6.0-7.0). The ICL containing DHMI also showed low pH-enhanced drug release. However, the incorporation of cholesterol hindered both the pH-triggered display of positive surface charge and the pH-triggered drug release of ICL.

Based on the results of Chapter II and Chapter III, it is found that although incorporation of cholesterol seems to be highly effective in improving the sizes and EE of ICL, it has the disadvantage of prohibiting the pH-sensitivity. In comparison, reducing the input DOX concentration during drug-loading appears to be a more practical way to decrease the size of ICL while maintaining their pH-sensitivity. ICL of smaller size, higher EE and higher pH-sensitivity would favor the anticancer activity of ICL in biological systems.

CHAPTER 4:   MORPHOLOGICAL STUDIES ON IMIDAZOLE-BASED CONVERTIBLE
LIPOSOMES USING TRANSMISSION ELECTRON MICROSCOPY (TEM)

4.1 Introduction

Transmission electron microscopy (TEM) is a microscopy technique using a beam of electrons to transmit through a specimen to obtain an image. As the beam transmits through a specimen, its electrons interact with the sample to form the image. Compared with light microscopy, TEM is capable of imaging in outstandingly higher resolutions. The smaller de Broglie wavelength [203] of electrons enables the TEM instrument to capture fine morphological details, such as structures of nanotubes and virus. Therefore, TEM finds applications in cancer research, virology, nanotechnology and material science. In conventional TEM, the specimen must be either cut into ultrathin sections (< 100 nm thick) or suspended and then coated onto a grid [204] to allow the transmission of the electron beam. Specimen preparation is specific to the materials to be analyzed and types of information to be obtained from the images. The samples/sample areas with heavy metals would appear darker and have greater contrast against the background while the samples consisting of non-metals would not scatter electrons and thus cannot be distinguished from the background. Hence, such non-metal samples need to be stained with a heavy metal stain during specimen preparation [205]. The stain absorbs the passing electrons which would otherwise be projected onto the imaging detector. Solutions/suspensions of salts of heavy metals such as osmium, lead, uranium and gold can be used as the stain of TEM imaging (7). TEM samples can be stained with either positive stains that bind to the actual specimen and visualize the internal components or negative stains that bind to the background and visualize the size and shape of the specimen [206].

In this chapter's studies, we aimed to utilize TEM techniques to record the morphology of ICL at physiological pH 7.4 and acidic pH. Comparison of the images at different pHs will test and monitor ICL's morphological changes in response to acidic pH.

4.1.1 Negative staining techniques in TEM. Negative staining is a technique applied in microscopy to contrast a specimen against the background, in which the background is stained, and the actual specimen is excluded from the staining. In the case of TEM, opaqueness to electrons is affected by number of protons in the nuclei of the sample. Commonly used negative stains include ammonium molybdate, uranyl acetate (UA), uranyl formate (UF), phosphotungstic acid (PTA), osmium tetroxide and osmium ferricyanide [15], owing to their capability to scatter electrons and adsorption to biological matter. Negative staining technique has been applied to image virus, bacteria, biological membrane structures and protein, due to their low capacity to scatter electrons [207]. Beside biological samples, negative staining has also been employed to study lipidic colloids in aqueous media, such as lamellar liposomes and inverted micelles [208]. Negative staining was reported to lead to flattening of specimen [209, 210]. As shown in Figure 4.1, a liposome which possesses spherical structure would be flattened but still intact in negative stain.

Liposome in solution   **Flattened intact liposome in negative stain**
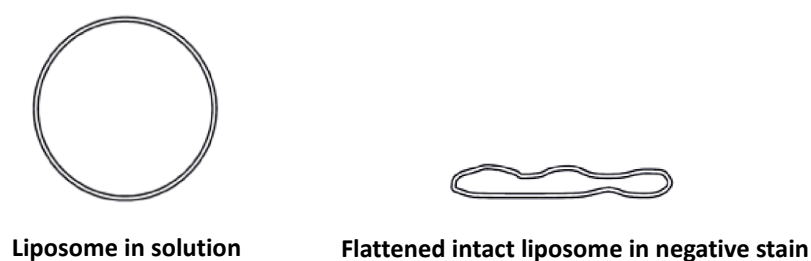
Figure 4.1. Schematic of liposome in solution and flattened intact liposome in negative stain under TEM. [211]

4.1.2 Application of TEM in characterization of nanomedicines. The development of microscopic techniques has made the studies on the surface and inner structure of nanocarriers more straightforward and attractive [212]. A collection of imaging techniques is available to characterize the morphology of liposomes and other nanoparticles, including atomic force microscopy, environmental scanning electron microscopy (ESEM), transmission electron microscopy (TEM) and confocal laser scanning microscopy. Evaluation of the morphology of nanomedicine is crucial for the development of nanomedicines because *in vivo* behavior of nanomedicines is heavily affected by their physical characteristics, including size, homogeneity, surface characteristics and lamellarity [211]. Because of its capacity to visualize single particles and even provide information on their inner structure, TEM represents an important method to characterize nanoparticles. Three types of TEM methods – drying, staining and cryogenic TEM (cryo-TEM) are commonly used to image nanostructures. Unlike metal particles which can be imaged directly due to their high density and stable structures, nanoparticles composed of soft materials need preservation prior to TEM [213]. Cryo-TEM is so far considered the best method to visualize the native structure of liposomes, in which an ultrathin film of specimen is quickly frozen in liquid ethane or a mixture of liquid ethane and propane to generate vitrified films to be imaged under TEM at cryogenic temperatures [214]. Figure 4.2 shows TEM images of DOX-NP® (Liposomal Encapsulated Doxorubicin) prepared with drying, negative staining and cryo-TEM methods. Because cryo-TEM requires advanced equipment and relatively complicated procedures, the faster and simpler TEM with negative staining is also a commonly used method to image liposomes [205].
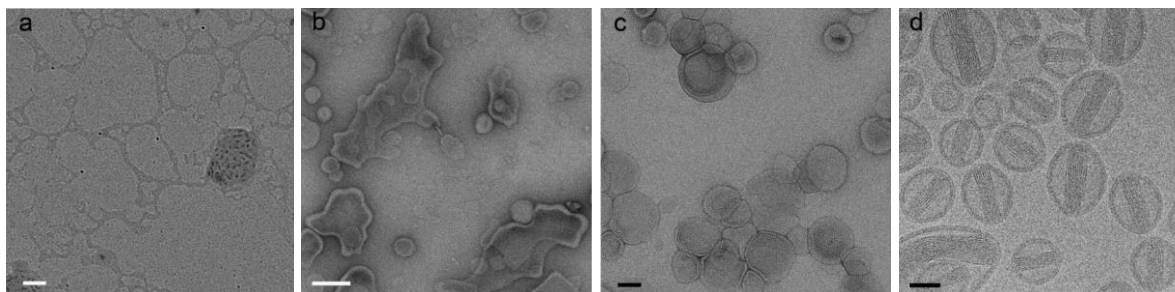
Figure 4.2. Dox-NP® imaged by commonly used TEM techniques: dried sample without staining (a), UA-stained sample after two minutes of drying (b), negative stained sample (UA) (c) and cryo-TEM (d). White scale bars represent 200 nm and black scale bars 50 nm. [205]

4.2 Materials and Methods

4.2.1 Materials. Carbon-coated copper grids (200 mesh) were purchased from Polysciences (US). Filter paper was purchased from Fisher Scientific (Hampton, NH, US). Uranyl acetate (UA) was purchased from Sigma-Aldrich (St Louis, MO, US). 2-[4-(2-hydroxyethyl)piperazin-1-yl]-ethanesulfonic acid (HEPES) and 2-(N-morpholino)ethanesulfonic acid (MES) were purchased from Fisher Scientific (Hampton, NH, US).

4.2.2 Preparation of ICL samples for TEM characterization. The morphology of ICL formulation was observed on a JEOL-JEM 1230 Electron Microscope (JEOL, Japan). Two-hundred mesh carbon-coated copper TEM grids were exposed to glow to discharge before use to increase their hydrophilicity. An aliquot (5 µL) of diluted ICL suspension (approximately 1 mM total lipids) was dripped onto the grid to wet its surface for 1 min and then blotted with a filter paper to generate a thin film. The sample film was then wetted five times with 5 µL of the negative stain (2% uranyl acetate (UA)) between blotting. The grid was dried at room temperature and then transferred into the electron microscope for imaging at an accelerating voltage of 100 kV, with the help of Dr. Fei Guo at the Electron Imaging Facility, Department of Molecular and Cellular Biology, UC Davis.

4.2.3 Preparation of ICL samples at acidic pH. To characterize the morphological changes of liposomes in response to acidic pH with TEM, the pH of ICL suspension was adjusted from 7.4 to 6.0. An aliquot (5 µL) of ICL suspension (approximately 1 mM total lipids) was dripped onto the grid and blotted with a filter paper. A small volume (5 µL) of isotonic MES buffer (pH 6.0, 10 mM MES, 140 mM NaCl) was then dripped onto the grid to cover the sample film for 5 min and then blotted prior to TEM sample staining. The TEM sample staining and imaging procedures were the same as in 4.2.2.

4.2.4 Preparation of ICL-model liposome mixtures for TEM characterization. To characterize the interaction between ICL and negatively charged model liposomes under TEM, ICL formulations were mixed with model liposomes and TEM of the mixture were taken at pH 7.4 and 6.0. An aliquot (5 µL) of ICL suspension (approximately 1 mM total lipids) and 5 µL of model liposome suspension (approximately 1 mM total lipids) were mixed and 5 µL of the mixture was dripped onto the grid and then blotted with a filter paper. For TEM of the mixture at pH 7.4, the sample on the grid was stained by 2% UA directly after the above procedures. For TEM of the mixture at pH 6.0, 5 µL of isotonic MES buffer (pH 6.0, 10 mM MES, 140 mM NaCl) was dripped onto the grid to cover the sample film for 5 min and blotted prior to negative staining. The TEM sample staining and imaging procedures were the same as in 4.2.2.

4.3 Result and Discussions.

4.3.1 Morphology of ICL at pH 7.4. As shown in Figure 4.3 (a-b), the DHI/DSPC/DPPE-PEG liposome suspension contained spherical and homogeneous particles with 80-150 nm size. The morphology of DHI liposomes at pH 6.0 (Figure 4.3 (c-d)) appears to be slightly brighter than at pH 7.4.
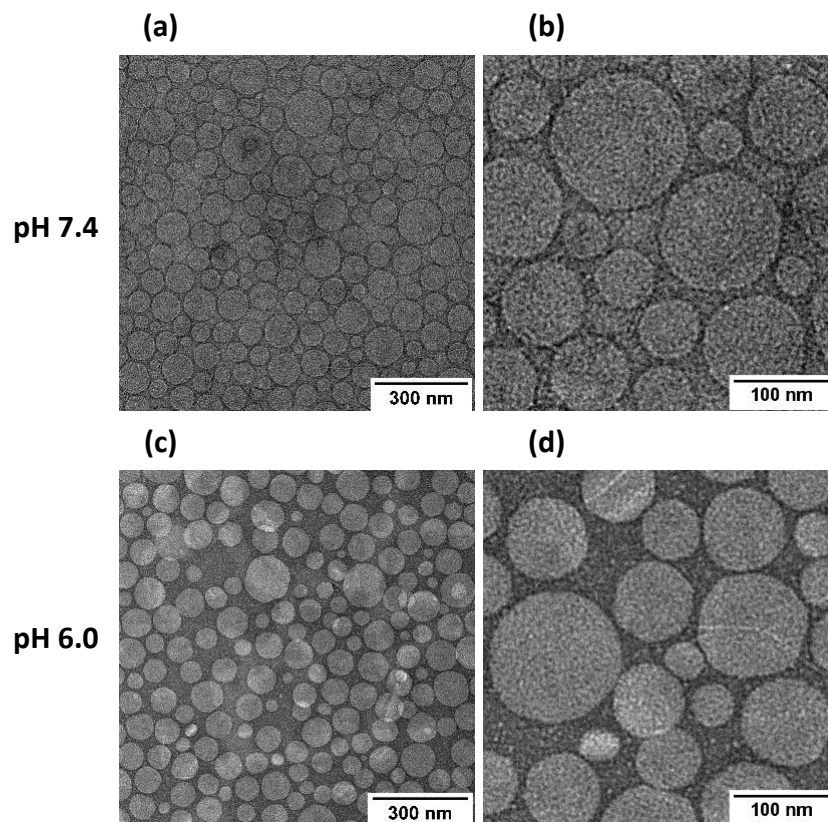
Figure 4.3. TEM images of DOX-loaded DHI/DSPC/DPPE-PEG at pH 7.4 (a-b) and 6.0 (c-d).

As can be seen in Figure 4.4 (a-b), the DHMI/DSPC/DPPE-PEG showed intact and spherical structures at pH 7.4. At pH 6.0 (Figure 4.4 (c-e)), the liposomes showed much brighter particles in the TEM images. Some collapsed, non-vesicle structures were also observed.
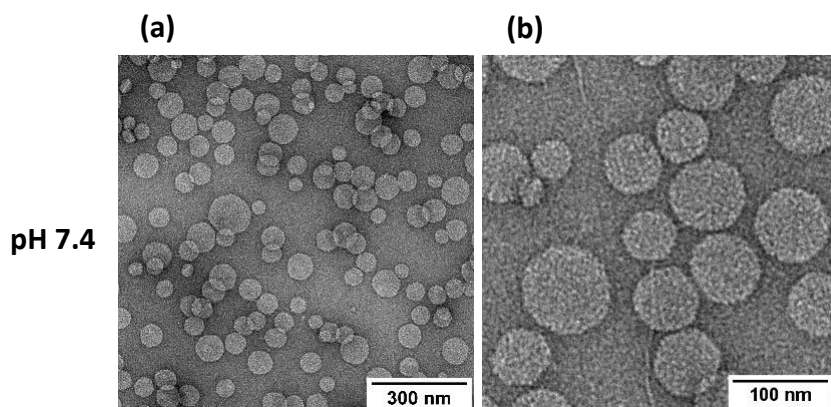
(Figure 4.4 Continued)
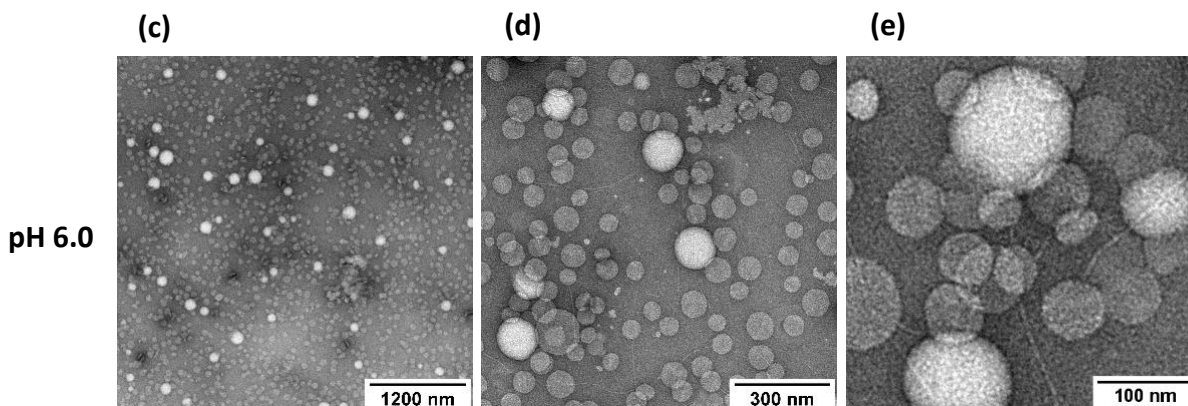
Figure 4.4. TEM images of DOX-loaded DHI/DSPC/DPPE-PEG at pH 7.4 (a-b) and 6.0 (c-e).

The darker area displayed in TEM images represent contents that are stained more by uranyl acetate, while the brighter area represents contents that are stained less with uranyl acetate. It has been known that the negative staining contrasts the specimen by staining the background and excluding the specimen, thus the stain should not bind with the specimen ideally. However, in the UA aqueous solution (pH 4.2-4.9), the uranyl species with positive charge dominate, thus negatively charged molecules stained particularly well [215]. Uranyl ions in were reported to bind specifically to phosphate groups in phospholipids, owing to both electrostatic interaction and chemical reaction [216]. In our results, the DHMI/DSPC/DPPE-PEG liposomes were inadequately contrasted at pH 7.4, but became evidently much brighter at pH 6.0, indicating that less UA stain was binding with the liposomes at pH 6.0, which is probably because the liposomes converted to cationic liposomes and became exclusive to the positively charged UA stain. This is in line with the pH-triggered acquisition of positive charges by ICL confirmed in Chapter III. Similarly, DHI/DSPC/DPPE-PEG at pH 6.0 turned slightly brighter than at pH 7.4, indicating they probably also acquired some positive charges. In addition, the images of the DHMI/DSPC/DPPE-PEG at pH 6.0 also showed some deformed and

scattered structures (Figure 4.4 (c) and (d)). These fragmented structures are probably the remains of liposomes that had burst and released drug in respond of acidic pH.

As shown in Figure 4.5 (a-b), the morphology of DHDMI/DSPC/DPPE-PEG appeared to have smaller average size compared with the corresponding DHI/DSPC/DPPE-PEG and DHMI /DSPC/DPPE-PEG liposomes. Some DHDMI/DSPC/DPPE-PEG liposomes showed two differently stained areas on the surface (Figure 4.5 (b)), which is probably due to the phase separation caused by interaction between DHDMI and DPPE-PEG. Figure 4.5 (c-e) showed evident change of morphology of DHDMI/DSPC/DPPE-PEG liposomes in that the liposomes were partially turned much brighter showed extremely sharper and clearer boundary of two differently stained phases at pH 6.0 compared with pH 7.4.
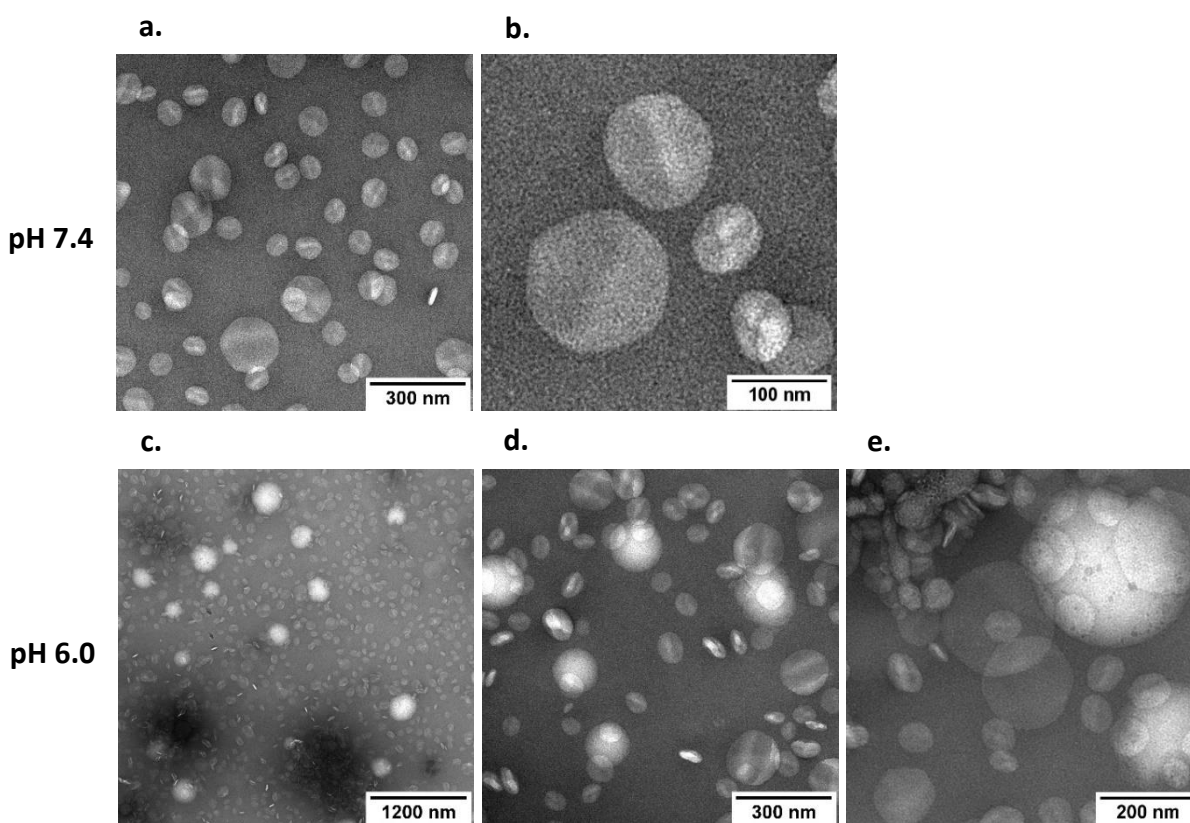
(Figure 4.5 Continued)
Figure 4.5. TEM images of DOX-loaded DHDMI/DSPC/DPPE-PEG at pH 7.4 (a-b) and 6.0 (c-e).

Similar to DHMI/PSPC/DPPE-PEG liposomes, the response of DHDMI/DSPC/DPPE-PEG liposomes to acidic pH as shown by the TEM images can also be explained by the acquisition of positive charges. The DHDMI/DSPC/DPPE-PEG converted to cationic liposomes at pH 6.0 and had less binging with the positively charged UA stain, thus appearing to be brighter compared with pH 7.4. The two differently stained phases on DHDMI/DSPC/DPPE-PEG indicated different extent of binding with UA. In response to acidic pH, the clustering of protonated DHDMI and negatively charged DPPE-PEG would cause phase separation on the liposomes. The phase without clustered DPPE-PEG would display excess positive charges than the phase with clustered DPPE-PEG, thus being stained less by UA than the phase with clustered DPPE-PEG. The sharper and clearer boundary of the two phases on DHDMI/DSPC/DPPE-PEG in Figure 4.5 (d) indicated the phase separation of liposomes was enhanced by the acidic pH 6.0.

Based on the TEM images of cholesterol ICL, the DHI/PSPC/DPPE-PEG, DHMI/PSPC/DPPE-PEG and DHDMI/PSPC/DPPE-PEG liposomes appeared to be homogeneous vesicles with size of 80-150 nm. The sizes of ICL obtained by DLS (2.3.2) (100-200 nm) were generally larger than the sizes observed under TEM, which is probably because the thickness of the hydrated PEG coating was also counted into the size measurement of ICL by DLS. It has been known that the monomer length of PEG (2 kDa) is 0.35 nm [217]. But due to the hydrophilicity of PEG, they are known to bind with water molecules to form a hydration shell that surrounds the liposome [51]. Such hydrated PEG coating was reported to have thickness of 10 nm [218], which can probably explain the gap between the sizes of ICL measured by DLS and observed under TEM.

As can be seen in Figure 4.6 (a-c), the morphology of DHI/DSPC/DPPE-PEG/Chol is not as spherical and homogenized as the cholesterol-free ICLs (such as DHI/DSPC/DPPE-PEG in Figure 4.3). The liposomes containing cholesterol Figure 4.6 (a-c) showed 80-200 nm size, and some layered structures can be seen inside of the liposomes. Figure 4.6 (d-f) showed that the liposomes containing cholesterol had some morphological change in response to acidic pH, but it didn't show the pH-triggered brighten particles and phase separation seen in images of cholesterol-free liposomes.
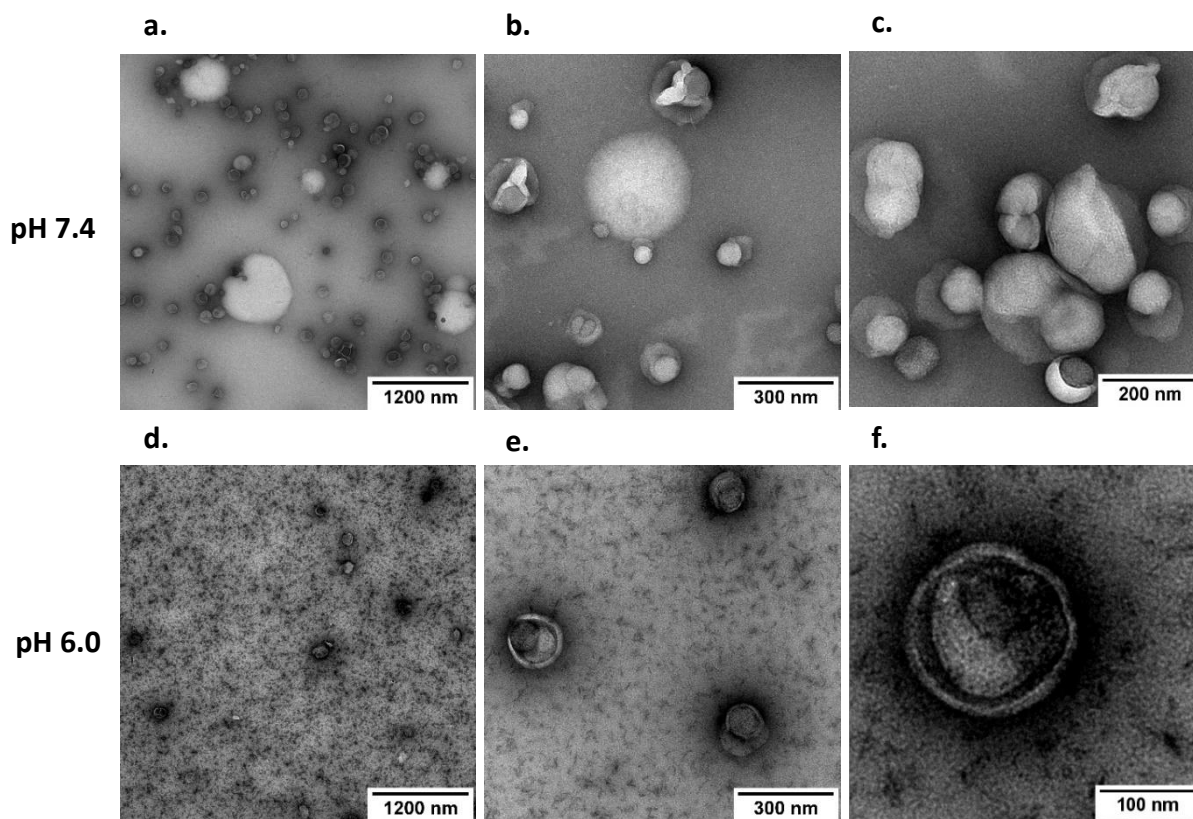
Figure 4.6. TEM images of DOX-loaded DHI/DSPC/DPPE-PEG/Chol at pH 7.4 (a-c) and 6.0 (d-f).

4.3.2 Morphology of ICL interacting with model liposomes. Compared with morphology of DHMI/DSPC/DPPE-PEG liposomes (Figure 4.7 (a)), the large membrane structures (150-300 nm) surrounded by the small liposomes in Figure 4.7 (b-c), are considered model liposomes, while the small liposomes are DHMI liposomes. At pH 6.0 (Figure 4.7 (d-f)), DHMI/DSPC/DPPE-PG liposomes appeared to assemble on the model liposomes, forming aggregation at the size of 300-600 nm. This result implied at acidic pH, the DHMI/DSPC/DPPE-PEG liposomes became positively charged to interaction with negatively charged model liposomes.
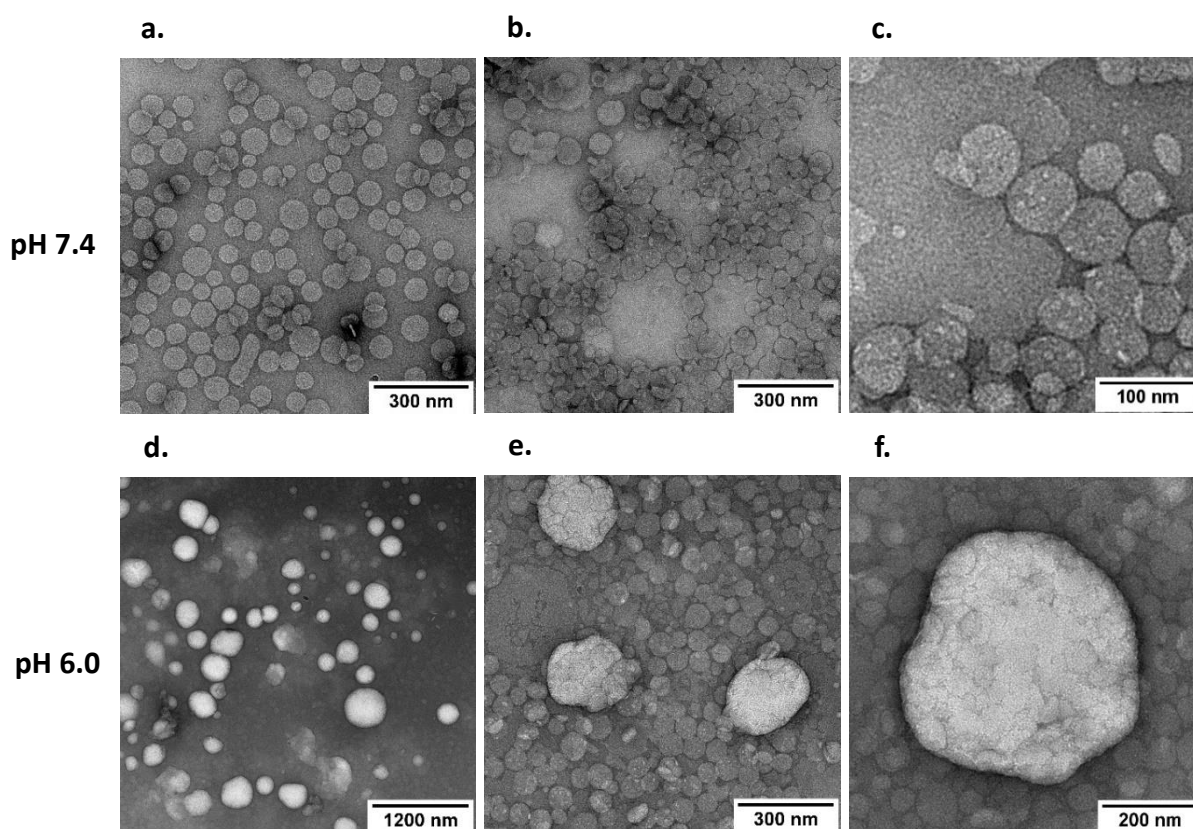
Figure 4.7. TEM images of DOX-loaded DHMI/DSPC/DPPE-PEG at pH 7.4 (a) and DOX-loaded DHDMI/DSPC/DPPE-PEG mixed with mode liposomes at pH 7.4 (b-c) and 6.0 (d-f).

4.4 Summary

The morphology of ICL formulations at physiological pH 7.4 and acidic pH 6.0 were characterized by TEM in this chapter's studies. Signified by TEM images of liposomes at pH 7.4, cholesterol-free ICL possess spherical and homogeneous morphology, while the addition of cholesterol made ICL more heterogeneous in shape (Figure 4.6 (a-c)). The morphological changes of cholesterol-free ICL in response to acidic pH suggested the acquisition of positive charges and phase separation, which was consistent with the results of elevated ζ- potentials in Chapter III (Figure 3.3) and our previous DSC thermogram report (Figure 3.2). The pH-triggered response of ICL containing DHI, DHMI and DHDMI was also in line with their pK$_a$ (DHI < DHMI < DHDMI) (Table 3.1). The DHDMI liposomes appeared to show the most evident phase separation at acidic pH but also some phase separation at pH 7.4. The DHMI liposomes showed considerable morphological response to acidic pH. The DHI liposomes showed a little change from pH 7.4 to 6.0. The bursting of ICL containing DHMI in response to acidic pH revealed in TEM images was consistent with their pH-triggered drug release (Figure 3.5 and 3.6). At acidic pH, the ICL with cholesterol did not show the interaction between the lipid components. The aggregation of ICL with negatively charged model liposomes at pH 6.0 was imaged by TEM, which further testified the positive electrification of ICL in response to acidic pH, which supported the results in Chapter III (Figure 3.4). Overall, the morphological studies by TEM significantly supported the proposed pH-sensitivity of ICL.

CHAPTER 5: EVALUATION OF ANTICANCER ACTIVITY OF DOX-LOADED IMIDAZOLE-
BASED CONVERTIBLE LIPOSOMES ON 3D MULTI-CELLULAR SPHEROIDS (MCS)

5.1 Introduction

2D monolayer cell culture has been widely utilized as *in vitro* bio-models to test the

activity of anticancer drugs, but they are not able to mimic the acidic microenvironment of solid

tumors *in vivo*. In previous studies in our group, to evaluate the pH-triggered anticancer activity

of DOX-ICL in 2D monolayer cell culture, the cells were incubated with the ICL liposomes that

were diluted in growth media whose pH was adjusted to 6.0, 6.5, 7.0 and 7.4. The pH-sensitive

ICL formulations showed increasing cytotoxicity on both HeLa and B16F10 cells as the growth

media pH was lowered from 7.4 to 6.0 at DOX concentration of 10 μg/mL (Figure 5.1). By

contrast, the cytotoxicity of NSL (DSPC/DPPE-PEG) at pH 6.0 showed no significant difference

from pH 7.4, suggesting that pH-sensitivity of ICL substantially contributed to their anticancer

activity. Among the three ICL formulations, the DHDMI liposomes, which interacted the most

with model liposomes at pH 6.0, showed the most activity, suggesting that more interaction with

cancer cells by ICL can enhance their cytotoxicity (Figure 3.4 (a)).

(a) Cell Viability on 2D B16F10

(Figure 5.1 Continued)

(b) Cell Viability on 2D HeLa Cells

pH	Untreated Cells	Free DOX	DSPC/DPPE-PEG	DHI/DSPC /DPPE-PEG	DHMI/DSPC /DPPE-PEG	DHDMI/DSPC /DPPE-PEG
7.4						
7.0		---	---			
6.5		---	---			
6.0						

Figure 5.1. Cytotoxicity of free DOX, DOX-loaded liposome and empty liposome against B16-F10 cells (a) and HeLa cells (b) after 12 hours of incubation. Data presented as mean $\pm$ SD, N = 4. [129]

As introduced in Chapter I 1.5, 3D multicellular spheroids (MCS) are more representative *in vitro* models of solid tumors than 2D monolayered cells. Therefore, MCS have been widely utilized to study tumor biology and to evaluate bioactivities of drugs. Owing to lower oxygen and nutrient distribution in their core, MCS possess a necrotic core of lower oxygen level, lower pH, and similar profile of gene expression compared to solid tumors *in vivo* [22, 146]. In contrast to 2D monolayer cells in culture, 3D MCS carries complex extracellular matrix (ECM) composed of structural proteins of great importance to cell survival, proliferation, and migration in solid tumors [150, 219]. In previous studies on ICL, the growth media of the 2D monolayer cells were extrinsically adjusted to carry low pH. By contrast, the acidic microenvironment in the core of 3D MCS is intrinsically generated, and thus is expected to trigger our pH-sensitive

ICL formulations as the acidic core of solid tumors would *in vivo* In contrast to 2D monolayer cells, the 3D MCS also impose an additional barrier for drug penetration through multiple layers of cancer cells as solid tumors *in vivo*.

The studies reported in this chapter aimed to establish 3D MCS of several commonly used cancer cells lines and to use them to evaluate the anticancer activity of ICL in comparison with NSL and free DOX. The 3D MCS of HeLa, A549, MDA-MB-231 and MDA-MB-468 cells were constructed and characterized to discover suitable conditions for the following anticancer studies. Both the cholesterol-free formulations (with pH-sensitivity) and the formulations with cholesterol (with better physicochemical characteristics) were tested on the MCS models in order to compare the impact of pH-sensitivity and physicochemical characteristics (size and EE) on the anticancer activity.

5.1.1 Necrotic cores of 3D MCS. Similar to the avascular regions of solid tumors, cells in MCS form three distinct layers, namely the outer layer composed of proliferating cells, the middle layer composed of quiescent cells, and the inner core of necrotic cells [22].

The formation of the three-layer structure is correlated to the insufficient oxygen penetration and depends closely on spheroid volume. It was reported that MCS of 500 μm or larger in diameter would assume the three-layer cell organization, which represents the cell heterogeneity in solid tumors [143, 144]. The live/dead fluorescence assay is commonly used to assess the viability of cells and distribution of the necrotic core in MCS assisted with confocal imaging [144]. The necrotic regions in HeLa, A549, MDA-MB-231 and MDA-MB-468 MCS were previously imaged using the live/dead fluorescence assay by our group (Figure 5.2) [13].
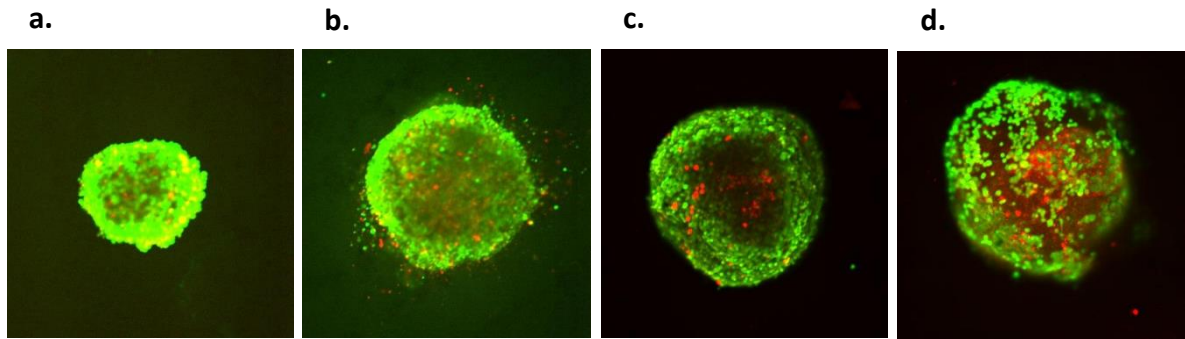
Figure 5.2. Confocal images of the distribution of live and dead cells in HeLa (a), A549 (b), MDA-MB-231 (c) and MDA-MB-468 (d) 3D MCS. Live cells display green fluoresce while dead cells red. [220, 221]

5.1.2 pH gradient of 3D MCS. In contrast to normal cells, cancer cells have higher intracellular pH (pH_i) and acidic extracellular pH (pH_e) [12]. This reversed pH gradient contributes to the accelerated growth rate, invasion and migration of cancer cells [13]. Because 3D MCS possess a hypoxic extracellular environment that is similar to solid tumor, 3D MCS also has a gradient of extracellular pH decreasing from the periphery to the core. Many confocal imaging studies have confirmed such a pH gradient inside MCS using pH-dependent fluorescent probes. The measured pH value inside MCS, although verified to be acidic, varies depending on cell lines, size, growth rate and culturing conditions. The pH in outer layer of glioma cell MCS was found to be 7.43, while the pH in the central necrotic core was 6.86, based on the ratio of SNARF-1 fluorescence at different wavelengths [222]. In a study that measured the pH at the surface of cells in MCS and in animal tumor models of HeLa, M4A4 and NM2C5 cells, the pH in the center of MCS was 6.7-6.8, while the pH in the *in vivo* tumor core was 6.1-6.4 [223]. Our previous studies [220, 221] also found the pH gradient in MDA-MB-468 MCS from 7.71 in periphery to 6.36 in center, based on the fluorescent confocal images of spheroids treated with SNARF-1. Due to the gap between the intrinsic acidity in MCS and *in vivo* tumors, pH_e of some

MCS models were further acidified by buffered media at similar pH with pH_e in solid tumor cores [224-226]. Reduced drug cellular uptake was found in this type of acidified MCS, which indicated the lowered pH_e (pH 6.0-6.4) in solid tumors was responsible to their limited drug uptake.

In this chapter's studies, the intrinsic acidic pH_e in MCS is expected to trigger ICL formulations when they penetrate to the interstitium of MCS.

5.2 Materials and Methods

5.2.1 Materials. The HeLa, A549, MDA-MB-231 and MDA-MB-468 cell lines were purchased from ATCC (Manassas, VA, US). The Dulbecco's Modification of Eagle's Medium (DMEM) media, Advanced DMEM/F12 media, Trypsin-EDTA, L-Glutamine, fetal bovine serum and collagen was purchased from Thermo-Fisher Scientific (Waltham, MA, US). The RPMI 1640 media, Penicillin-Streptomycin, 96-well Ultra-low Attachment Round-button microplates, 96-well Solid White microplates and CellTiter-Glo 3D cell viability assay were purchased from VWR (Radnor, PA, US).

5.2.2 Constructions of 3D MCS Models

5.2.2.1 Cell culture maintenance. Cervical cancer cell line HeLa, lung cancer cell line A549, and breast cancer cell lines MDA-MB-231 and MDA-MB-468 were cultured to construct MCS for the evaluation of anticancer activity. HeLa cells were maintained in DMEM media (with L-glutamine supplement) (Gibco, Carlsbad, CA, US). A549 cells were maintained in RPMI 1640 media (with L-glutamine supplement) (Corning, NY, US). The DMEM and RPMI 1640 media were supplemented with 10% fetal bovine serum (Gemimi, West Sacramento, CA) and 1% Penicillin-Streptomycin (Corning, NY, US). MDA-MB-231 and MDA-MB-468 cells were maintained in Advanced DMEM/F12 reduced serum media (Gibco, Carlsbad, CA, US)

supplemented with 5% fetal bovine serum, 1% Penicillin-Streptomycin and 1% L-glutamine

(Invitro, San Diego, CA). All cells were grown in a humidified atmosphere of 5% CO_2 in air at

37°C and passaged at 85% confluence.

5.2.2.2 Seeding and culturing of MCS. HeLa (~2000 cells/well), A549 (~5000

cells/well), MDA-MB-231 (~3000 cells/well) and MDA-MB-468 (~2000 cells/well) cells were

seeded in 96-well Ultra-low Attachment (ULA) round-bottom Microplates (Corning, NY, US) on

complete growth media containing collagen (Thermo-Fisher Scientific, Waltham, MA, US). An

aliquot (100 µL) of cell suspension was added into each well in 96-well plates, and the cell

concentrations were determined with a Handheld Automated Cell Counter (Millipore,

Burlington, MA, US). The cells were centrifuged (Table 5.1) at 7°C to aggregate in the plates.

Complete growth media (100 µL) was added into each well on the second day after seeding. The

growth media were partially changed every other day by replacing 100 µL of media in each well

with 100 µL fresh growth media to maintain a 200 µL/well total media volume. All MCS were

grown in a humidified atmosphere of 5% CO_2 in air at 37°C.

5.2.2.3 Morphology of MCS. The morphology of 3D MCS was examined on an inverted

microscope (Keyence, Osaka, Japan), and the size of MCS was measured by BZ-X Analyzer.

The spheroid volume was calculated using the following formula,

$$Spheroid\ Volume = \frac{1}{2} \times L \times S^2$$

Where L = the long axis of spheroid, S = the short axis of spheroid. The MCS reaching 500 µm

in diameter are subjected to drug treatment as a stringent and representative model.

5.2.2.4 Determination of sensitivity of MCS to anticancer drug DOX. Cell viability of

MCS treated by free DOX at incremental concentrations for 72 hours was obtained to determine

the sensitivity of MCS to DOX, and to develop cytotoxicity assays for DOX-loaded liposomes

against MCS. The MCS were treated by free DOX for 72 hours as in 4.2.2.2 and then assayed as in 4.2.2.3. IC_{50} (µM) of DOX against MCS of each cell line was then determined.

5.2.3 Cytotoxicity assays on 3D MCS treated with DOX-loaded formulations

5.2.3.1 Pretreatment of DOX-loaded liposomes. Before administration to MCS, the DOX-loaded liposomal formulations were pretreated to remove the unencapsulated DOX in the liposome suspension, which was generated by leakage during sample storage. The DOX-loaded samples stored at 4°C for over 10 days needed the pretreatment before administration to MCS. The DOX-loaded liposomes were mixed with the cation-exchange resin Dowex 50WX-4 (pretreated as in 2.2.2.2) at DOX: resin = 1:60 (w/w) and shaken on an orbital shaker (Thermo Fisher Scientific, Waltham, MA) at approximately 100 rpm for 25 min at room temperature. The resin was then removed by filtering the mixture though glass wool in a syringe. The concentration of the payload DOX of pretreated liposomes was then measured as in 2.2.4.

5.2.3.2 Treatment of 3D MCS with DOX-loaded liposomes. One hundred microleter or more growth media in each well of 96-well ULA microplate containing 200 µL media and MCS was replaced with same volume of DOX-loaded liposome or free DOX solutions in complete media at incremental concentrations. The complete media solutions of DOX were prepared by diluting water solutions of DOX with complete growth media by 6-10 folds. The final DOX concentration in each well was calculated according to the fold of dilutions. The incremental concentration set was determined referring to IC_{50} obtained in 4.2.2.4. Each treatment by DOX-loaded liposomes orfree DOX solutions were quadruplicated. The MCS were incubated in a humidified atmosphere of 5% CO_2 in air at 37°C for 72 hours.

5.2.3.3 Cell viability of 3D MCS after treatment by DOX-loaded liposomes. After 72-hour incubation, each MCS was transferred into a 96-well Solid White microplate (Corning, NY,

US) together with 100 μL media from each well and mixed with 100 μL reagent of CellTiter-Glo 3D cell viability assay (Promega, WI, US) was added to each well. The microplate was covered with foil and shaken on an orbital shaker for 5 min, then incubated for 25 min at room temperature. The luminescence of the above mixture was measured on the Synergy HT microplate reader (Biotek, Winooski, VT, US). The luminescence of MCS treated by growth media with no drug/formulation were referred as 100% cell viability.

5.3 Results and Discussion

5.3.1 Conditions to construct MCS models.
The effect of collagen and cell seeding number on the morphology of MCS was studied to explore the most suitable set of conditions to construct MCS models with different cancer cell lines.

5.3.1.1 The effect of collagen. Aiming to construct MCS with spherical structures and clear edges, collagen was mixed with cells to be seeded in ULA 96-well plates. A comparison of morphology of MDA-MB-468, A549 and HeLa MCS seeded with and without collagen are shown in Figure 5.3. The MDA-MB-468 seeded with 1% collagen, A549 seeded with 0.3% collagen and HeLa seeded with 0.1% collagen formed spherical solid structures. The MDA-MB-468 cells seeded without collagen appeared to be loose and scattered cells (Figure 5.3 (a)). The A549 cells seeded without collagen formed an irregular non-spherical aggregation (Figure 5.3 (b)), which appears denser than MDA-MB-468 without collagen. The HeLa cells seeded without collagen (Figure 5.3 (c)) formed a solid and spherical structure, but with a rougher edge than the HeLa cells seeded with collagen.
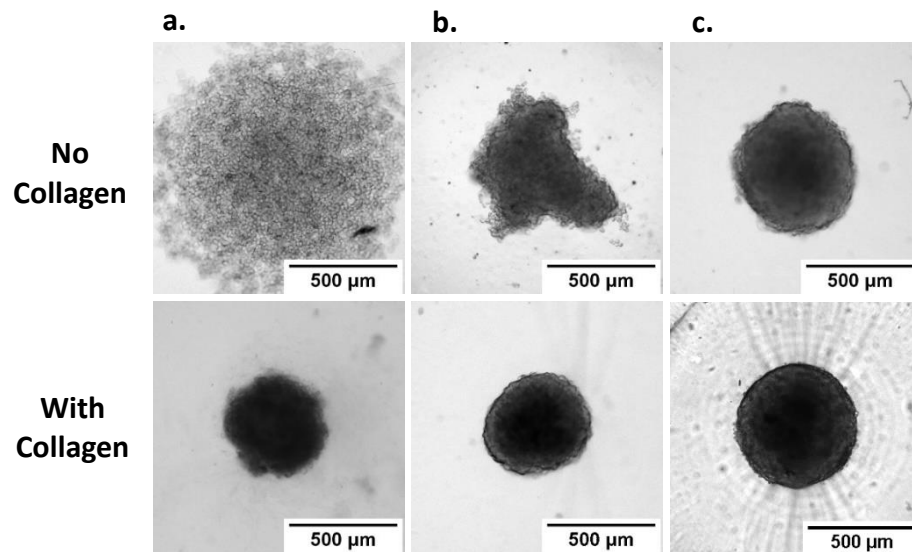
Figure 5.3. (a) Morphology of MDA-MB-468 MCS seeded with no collagen (upper, 2000 cells/well, 9 days) and 1% collagen (lower, 2000 cells/well, 9 days). (b) Morphology of A549 MCS seeded with no collagen (upper, 5000 cells/well, 9 days) and 0.3% collagen (lower, 5000 cells/well, 4 days). (c) Morphology of HeLa MCS seeded with no collagen (upper, 500 cells/well, 10 days) and 0.1% collagen (lower, 2000 cells/well, 7 days).

As a component of the extracellular matrix (ECM), collagen is the most prevalently utilized embedding material to aggregate cells for the growth of 3D spheroids [224]. The concentration of collagen needed for MCS formation changed over different cell lines, probably because it served to only complement various levels of the ECM substrates that were generated by cancer cells in culture. Our results show that, without collagen, different types of cancer cells could grow into three different types of morphologies – loose cells, irregular aggregated cells, and spheroids. HeLa cells formed spheroids without collagen and spheroids with very smooth edges with only 0.1% collagen. Similarly, the results suggested that A549 probably generate more substrates than MDA-MB-468. In comparison, A549 needed the addition of 0.3% collagen to form spheroids, while MDA-MB-468 needed 1%.

5.3.1.2 Cell seeding density. A number of different cell seeding densities were tested to find its effect on the construction of MCS. As shown in Figure 5.4, with incremental seeding

densities, the MDA-MB-468 MCS had increasing diameters. The MCS seeded at 5000 and

10000 cells/well started to have rough edges after cultured for 7-9 days, and subsequently

became more scattered over time. The MCS seeded at 2000 cells/well also showed rough edges

but after a longer period of 15 days. This result indicated as the seeding density getting higher or

spheroids growing larger, they start to lose the tight, smooth edge. The MDA-MB-468 MCS

seeded at 2000 cells/well still had a clear edge after reaching a diameter of 500 μm, which can be

the most suitable seeding and growing condition for MDA-MB-468 MCS. The scattering of cells

is also probably due to increase of aggressiveness of cancer cells after being cultured for over

time due to the hypoxia of the newly formed solid core (darker area in Figure 5.4) in the

spheroids.
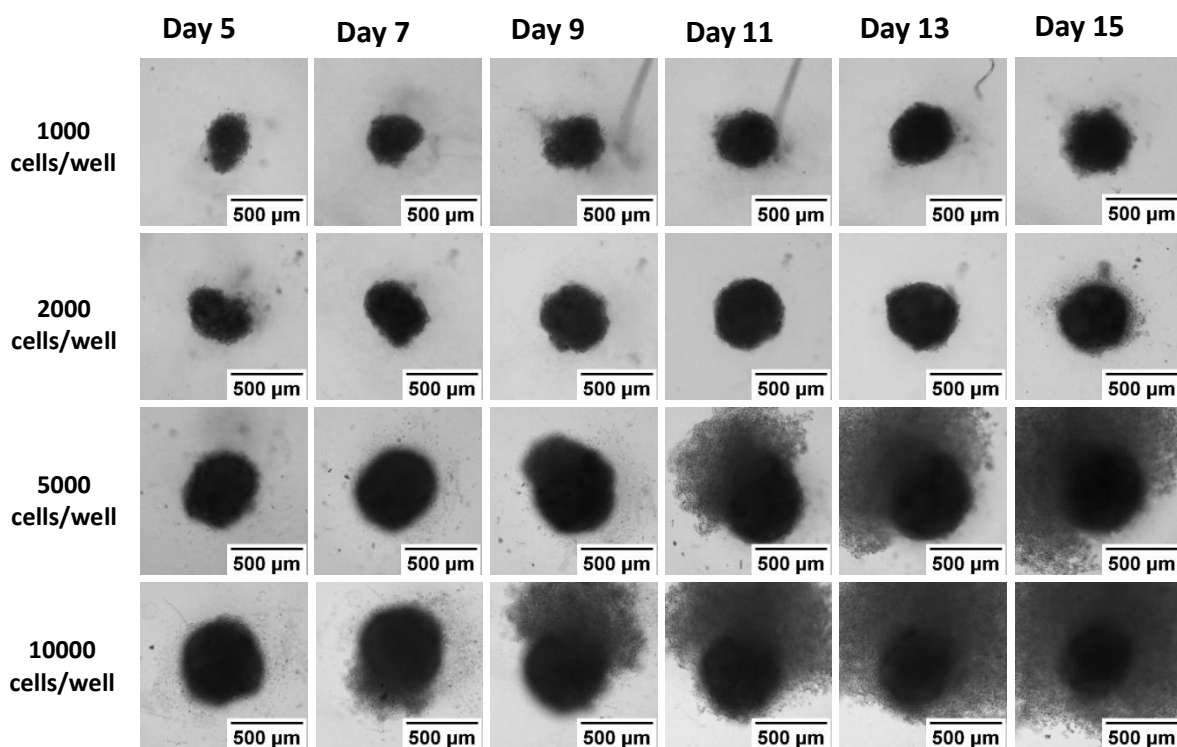
Figure 5.4. Morphology of MDA-MB-468 MCS (500, 1000, 2000, 5000, 10000 cells/well) seeded with 1% collagen after 5, 7, 9, 11, 13, 15 days in the ULA 96-well microplates.

As shown in Figure 5.5, for the HeLa cell line, which is likely to generate more ECM substrates during the growth of spheroids (Figure 5.3), the increases of seeding density did not induce scattering of cells, but induced more irregular edge of spheroids. Such deformation in response to higher seeding density was considered as a critical factor to determine the suitable seeding density of the construction of HeLa MCS.
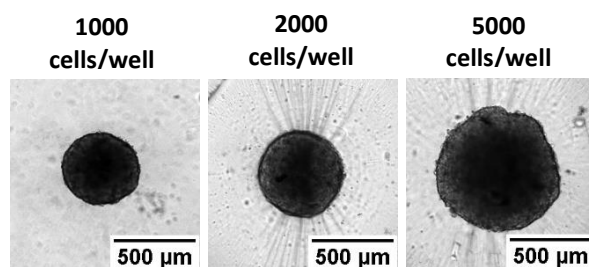
Figure 5.5. Morphology of HeLa MCS (1000, 2000, 5000 cells/well) seeded with 0.1% collagen after 6 days in the ULA 96-well microplates.

Similarly, the suitable conditions to construct MCS ofother cancer cells were selected based on the morphology of spheroids. The conditions to construct HeLa, A549, MDA-MB-231 and MDA-MB-468 3D MCS are summarized in Table 5.1. Both the collagen free (500 cells/well) and 0.1% collagen (2000 cells/well) conditions suitable to form HeLa MCS. The collagen-free HeLa MCS was later used in our cytotoxicity studies. Typical morphology of the ~500 μm HeLa, A549, MDA-MB-231 and MDA-MB-468 MCS for anticancer drug treatments are shown in Figure 5.6.

Table 5.1
Conditions to construct 3D MCS models with HeLa, A549, MDA-MB-231 and MDA-MB-468 cancer cells.

Cell Line	Hela	A549	MDA-MB-231	MDA-MB-468

(Table 5.1 Continued)

Seeding Density (cells/well)	500	2000	5000	3000	2000
Collagen (%)	0	0.1	0.3	1	1
Centrifuge Speed (g)	1000	1000	300	200	200
Centrifuge Time (min)	15	15	7	15	15
Estimated time to reach 500 μm diameter (days)	12	6	5	5	11
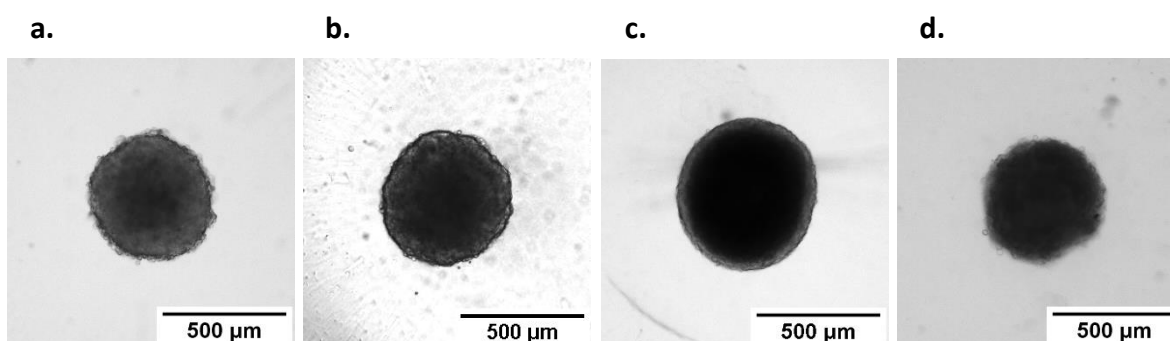
Figure 5.6. Representative morphology of MCS for anticancer drug treatment: HeLa MCS (500 cells/well, no collagen, 12 days) (a), A549 MCS (5000 cells/well, 0.3% collagen, 5 days) (b), MDA-MB-231 MCS (3000 cells/well, 1% collagen, 5 days) (c) and MDA-MB-468 MCS (2000 cells/well, 1% collagen, 11 days) (d) with diameter of 500 μm in the ULA 96-well microplates.

5.3.1 Inhibition on growth of MCS by DOX. The constructed 3D MCS models were treated with DOX at incremental concentrations to record morphology and cell viability. As can be seen in Figure 5.7, the HeLa MCS exposed to incremental DOX concentration for 72 hours showed significant changes in morphology. As the DOX concentration increased from 0 to 2 μM, the spheroid became smaller, which signified that DOX inhibited the growth of spheroids. As the DOX concentration increased from 2 to 100 μM, the spheroid showed more and more rough edges and became looser, which indicated the deformation of of the spheroids. As the DOX concentration increased from 100 to 500 μM, the spheroids showed smaller sizes besides more rough edges, which indicated remarkable loss of cells accompanying the deformation of

MCS by DOX.
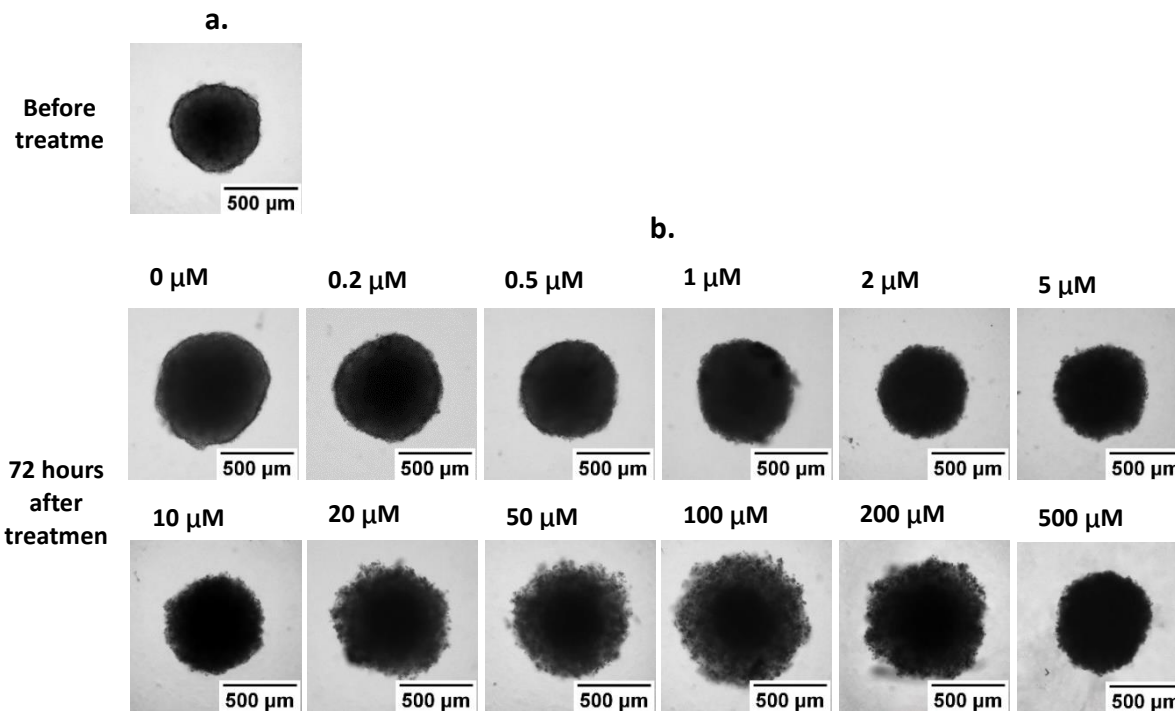
Figure 5.7. Morphology of HeLa MCS before (a) and after (b) treatment by DOX (72 hours exposure) at incremental concentrations.

The half maximal inhibitory concentration (IC_{50}) values of free DOX on HeLa, A549, MDA-MB-231 and MDA-MB-468 MCS (Table 5.2) were calculated from cell viability results in Figure 5.8 using the GraphPad Prism software. The IC50 values reported the sensitivity of each 3D MCS model to DOX, which helped determinate the suitable DOX concentration set for the cytotoxicity assay of DOX-loaded ICL. Treatment by free DOX on MCS was also carried out for comparison in the cytotoxicity assay of liposomes.
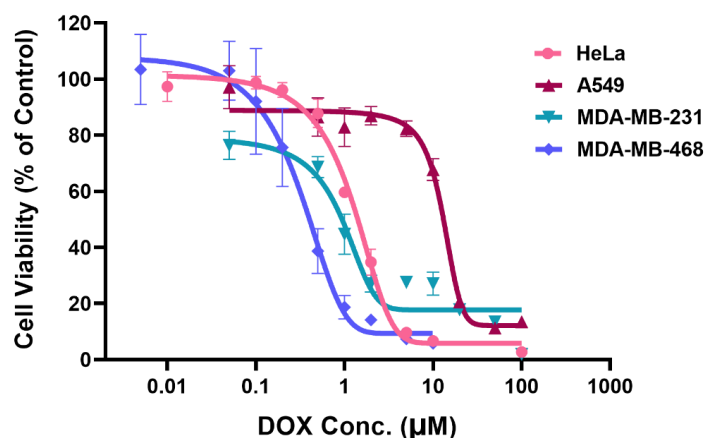
Figure 5.8. Cell viability of HeLa, A549, MDA-MB-231 and MDA-MB-468 MCS treated with free DOX for 72 hrs. Data presented as mean ± SD, N = 4.

Table 5.2

IC$_{50}$ of free DOX on HeLa, A549, MDA-MB-231 and MDA-MB-468 3D MCS.

Cell Line	Hela	A549	MDA-MB-231	MDA-MB-468
IC$_{50}$ (µM)	1.26±0.04	12.59±1.05	1.18±0.29	0.32±0.12

Note. Data presented as mean ± SD, N = 4.

5.3.2 Cytotoxicity of ICL on 3D MCS. After treatment by cholesterol-free ICL, NSL and free DOX for 72 hours, the cell viability of 3D MCS was recorded. As shown in Figure 5.9 (a), the DHI and DHMI liposomes showed better anticancer activity than NSL against HeLa MCS, while DHDMI showed similar activity to NSL. In Figure 5.9 (d), the DHI, DHMI and DHDMI liposomes showed better anticancer activity than NSL on MDA-MB-468 MCS, but the improvement is not as evident as on HeLa MCS. On both HeLa and MDA-MB-468 MCS, the DHMI liposomes expressed the best anticancer activity and was comparable to free DOX. As can be seen in Figure 5.9 (b), compared with NSL, ICL did not show better activity on A549 MCS except for DHI at the highest DOX concentration of 100 µM. In Figure 5.9 (c), ICL showed similar inhibition trend with NSL.

(a) Cell Viability on Hela MCS

(b) Cell Viability on A549 MCS

(c) Cell Viability on MDA-MB-231 MCS

(d) Cell Viability on MDA-MB-468 MCS
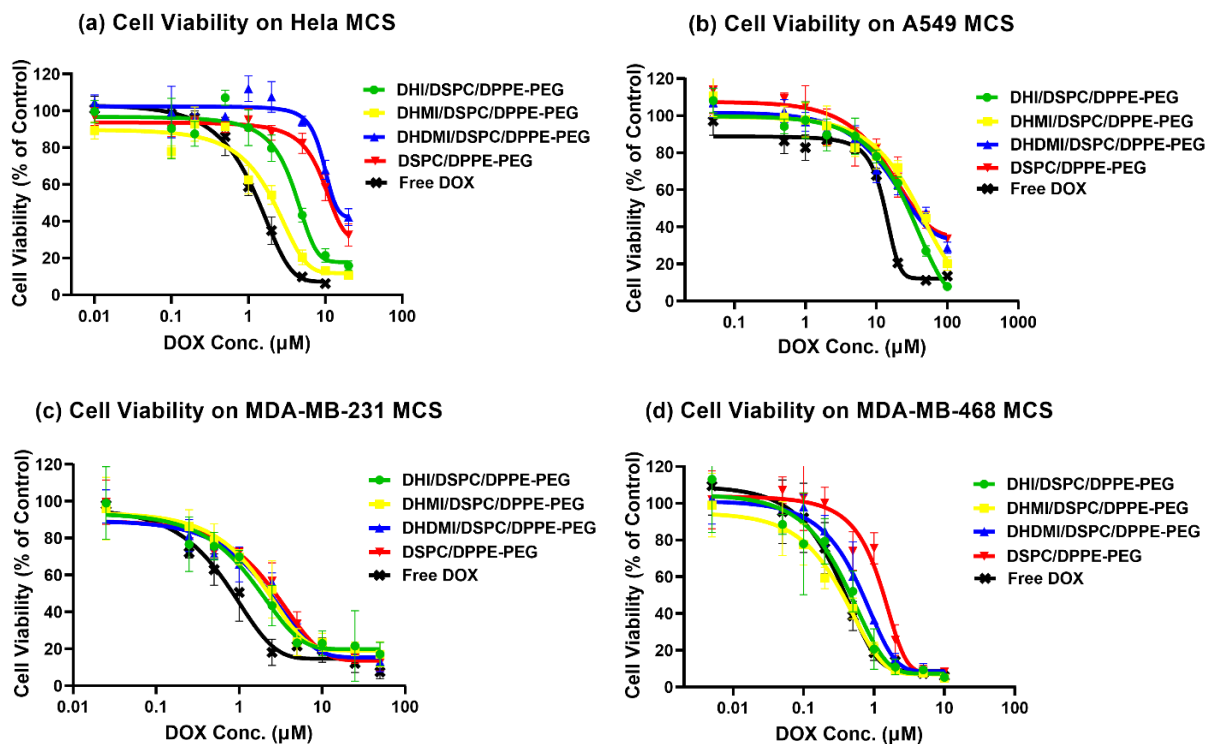
Figure 5.9. Cell viability of Hela (a), A549 (b), MDA-MB-231 (c), MDA-MB-468 (d) MCS treated with cholesterol-free ICL, NSL and free DOX for 72 hours. Data presented as mean ± SD, N = 4.

Figure 5.10 showed the results of cytotoxicity of free DOX, ICL and NSL containing 25% cholesterol on 3D MCS. All the ICL formulations showed similar anticancer activity with NSL against HeLa, A549 and MDA-MB-231 MCS.

(a) Cell Viability on Hela MCS

(b) Cell Viability on A549 MCS

(Figure 5.10 Continued)
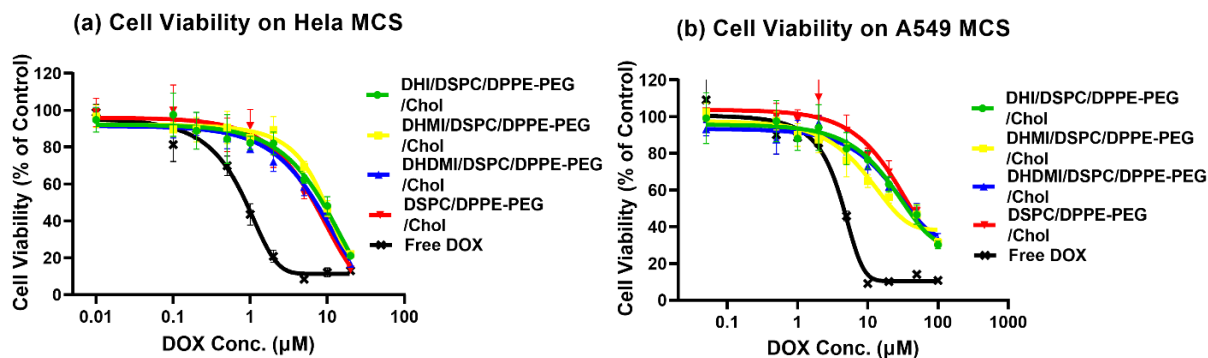
(c) Cell Viability on MDA-MB-231 MCS
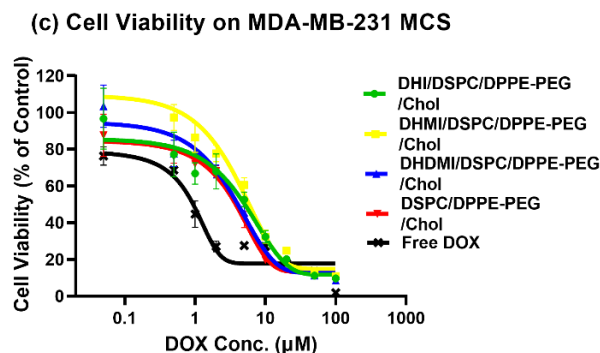
Figure 5.10. Cell viability of Hela, A549, MDA-MB-231 MCS treated with cholesterol-containing ICL (25 mol%), cholesterol-containing NSL (25 mol%) and free DOX for 72 hours. Data presented as mean ± SD, N = 4.

According to the pH-sensitivity studies (Chapter III), the cholesterol free ICL showed pH-sensitivity in terms of displaying positive surface charges and drug release, while the ICL containing cholesterol did not show pH-sensitivity. Our cytotoxicity studies were carried out on MCS models, which were confirmed to provide an acidic extracellular microenvironment. The MCS cytotoxicity studies showed that ICL containing cholesterol exerted similar anticancer activity with NSL, in contrast to the cholesterol-free ICL, which showed evidently higher anticancer activity than NSL on two MCS models. The cytotoxicity results were consistent with the pH-sensitivity, which suggested that the cholesterol-containing ICL lost their anticancer activities because the addition of cholesterol suppressed the liposomal pH-sensitivity from the imidazole-based lipids. On the HeLa and MDA-MB-468 MCS, the cholesterol-free ICL with DHMI showed the most anticancer activity among the formulations and was comparable with free DOX. The other cholesterol-free ICL containing DHI and DHDMI, even though showed upgraded activity compared with NSL, they expressed lower activity compared with free DOX. The lower activity of ICL compared with free DOX is probably due to the limited penetration of liposomes compared with small molecule drugs. Based on the cell viability results in Figure 5.9

and 5.10, the IC50 values of cholesterol-free ICL, ICL containing cholesterol and free DOX on

MCS were calculated and are summarized in Table 5.3, which shows noticeable increase of IC_{50}

of ICL with cholesterol compared with the cholesterol-free ICL.

Table 5.3
IC_{50} values of DOX-loaded liposomes and free DOX on HeLa, A549, MDA-MB-231 and MDA-MB-468 3D MCS.

IC_{50} (µM)	Lipid Mol Ratio	Hela	A549	MDA-MB-231	MDA-MB-468
DHI/DSPC/DPPE-PEG	25/70/5	3.82±1.13***	~30	1.38±1.31	0.38±0.21**
DHMI/DSPC/DPPE-PEG	25/70/5	2.07±1.13***	~40	1.77±1.21	0.31±0.15***
DHDMI/DSPC/DPPE-PEG	25/70/5	9.51±1.15	~35	1.86±1.24	0.63±0.10**
DSPC/DPPE-PEG	95/5	11.41±1.28	~35	2.37±1.29	1.24±0.13
DHI/DSPC/DPPE-PEG/Chol	25/45/5/25	~10	~30	5.13±1.46	-
DHMI/DSPC/DPPE-PEG/Chol	25/45/5/25	10.38±1.33	29.07±2.73	3.62±1.17	-
DHDMI/DSPC/DPPE-PEG/Chol	25/45/5/25	~10	24.06±1.40	3.26±1.18	-
DSPC/DPPE-PEG/Chol	70/5/25	~10	33.88±1.62	3.98±1.10	-
Free DOX	-	1.26±0.04	12.59±1.05	1.18±0.29	0.32±0.12

Note. Data presented as mean ± SD, N = 4. ** p < 0.01, *** p < 0.001 (to the IC_{50} of DSPC/DPPE-PEG)

Among these three ICL that do not contain cholesterol, the ranking of anticancer activity

against 3D MCS was DHMI > DHI > DHDMI. According to the pH-sensitivity studies, the

ranking of acidic pH-triggered cationic conversion is DHDMI > DHMI > DHI, while the ranking

of acidic pH-triggered drug release is DHMI > DHI > DHDMI. Ranking of their activity on 2D

monolayered cells, as reported in our previous cytotoxicity studies (Figure 5.1), was precisely in

line with their pH-triggered cationic conversion. However, their activity on 3D MCS appeared

to be more consistent with their pH-triggered drug release. In 2D cell culture at acidic pH, the ICL would convert to cationic liposomes and have better interaction with cancer cells, thus significantly improved the local concentration of drug on cells. In 3D MCS models, ICL would be triggered by acidic pH after penetrating into the acidic interstitium of MCS, where the enhanced local concentration of drug induced by improved liposome-cell interaction might take less effect. In the meantime, the cellular uptake of DOX inside MCS would be more affected by the drug release at the acidic interstitial space inside MCS.

5.4 Summary

3D MCS models of HeLa, A549, MDA-MB-231 and MDA-MB-468 cell lines were successfully constructed under optimized conditions. The anticancer activity of DOX-loaded ICL in comparison with DOX-loaded NSL and free DOX was evaluated with cytotoxicity on MCS models. Based on the IC_{50} values, the cholesterol-free ICL, especially the DHMI liposomes, showed upgraded anticancer activity against MCS compared with NSL. The addition of cholesterol resulted in lower activity of ICL and caused ICL to show similar inhibition trend with NSL, which was consistent with the previously reported suppression of ICL pH-sensitivity by the addition of cholesterol (Chapter III). The cholesterol-free ICL were studied in comparison with ICL containing cholesterol because the pH-sensitivity of cholesterol-free ICL and the better physicochemical characteristics (size and EE) of ICL containing cholesterol were both expected to improve the anticancer activity of liposomes on MCS. Our cytotoxicity studies indicated that the anticancer activity of the ICL is mostly enhanced by their pH-sensitivity.

CHAPTER 6: SUMMARY

As the second leading cause of death globally, cancer is a major concern for human health. Most cancers form malignant solid tumors, which possess different biological features from healthy tissues, including fenestrated vascular walls, hypoxia, necrosis, acidic microenvironment, and unique extracellular matrix (ECM). These abnormal features pose challenges as well as opportunities for anticancer treatment. Poorly developed vasculature in tumor compared to normal vasculature present unique advantages for nanomedicines over small molecule drugs against cancer. Nanomedicines more easily move from the porous tumor blood vessel into tumor interstitium and then accumulate there due to the lack of tumoral lymphatic drainage, a phenomenon known as the enhanced permeability and retention (EPR) effect. Moreover, the acidic pH in tumor interstitium (pH 6.0-7.0) represents a promising stimulus to trigger nanomedicines to promote cellular uptake of the cargo drugs.

Liposomes are capable nanocarriers of both hydrophilic and hydrophobic agents due to the amphiphilicity of their lipid components. Liposomes are the most commonly used nanocarriers and have yielded multiple nanomedicine products in the market by now. The previously reported stealth liposomes coated with PEG have shown enhanced accumulation in tumors owing to their prolonged circulation time. However, the PEG coating also hinders their interaction with cancer cells. In order to improve the anticancer activity of stealth liposomes by improving their interaction with cancer cells, but without removing their long circulation (stealth) property, three novel, synthetic imidazole-based lipids were introduced to the liposome composition to develop the pH-sensitive, imidazole-based convertible liposomes (ICL). At acidic pH, the imidazole-based lipids would protonate to acquire positive charges, thus clustering with the negatively charged PEGylated lipids. Such lipid-lipid electrostatic interaction would

induce phase separation of the bilayer to generate a PEG-free domain, which displays excess positive charges and have enhanced interaction with negatively charged cancer cells. The pH-sensitivity introduced by the imidazole-based lipids is expected to improve the anticancer activity of stealth liposomes.

The ICL formulations were successfully prepared, characterized, and optimized to have small particle sizes (< 200 nm) and sufficient EE (> 40%). After synthesizing the imidazole-based lipids DHI, DHMI and DHDMI, ICL were prepared using film hydration, freeze-anneal-thawing, and extrusion methods. Doxorubicin (DOX) was chosen as the cargo drug to be loaded in ICL using the remote loading method with manganese sulfate gradient. A collection of methods was used to improve the physicochemical characteristics of ICL, including reducing loading time, incorporating cholesterol, mixing with resin at $T \geq T_m$, filtration, and reducing the input DOX concentration. Incorporating cholesterol and reducing the input DOX were found to be the most feasible methods to improve the physicochemical properties of ICL by maintaining both small size and high EE.

The ICL formulations were tested on their pH-sensitivity. ζ- potential change, interaction with model liposomes, and drug release of ICL in response to the change of pH (6.0-7.0) were assayed to test the pH-sensitivity of ICL with and without cholesterol. In response to the drop of pH, the cholesterol-free ICL raised their ζ- potentials and aggregated with negatively charged model liposomes. The drop of pH also enhanced the drug release from cholesterol-free ICL. Among the three ICL formulations, the DHDMI/DSPC/DPPE-PEG showed the most substantial pH-triggered conversion to cationic liposomes, while the DHMI/DSPC/DPPE-PEG showed the most significant pH-triggered drug release. However, ICL with cholesterol didn't show any of such changes at lowered pH.

Transmission electron microscopy (TEM) was used to study the morphology of ICL and their interaction with model liposomes at physiological pH 7.4 and acidic pH 6.0. At pH 7.4, the cholesterol-free ICL samples showed intact, spherical, and homogeneous vesicles, while the ICL with cholesterol showed more heterogeneous in shape. At pH 6.0, the surface of cholesterol-free ICL, especially DHDMI/DSPC/DPPE-PEG, showed evident phase separation. In contrast, the ICL with cholesterol did not show phase separation. TEM also showed that the cholesterol-free ICL aggregated with negatively charged model liposomes at pH 6.0 but had no interactions with model liposomes at pH 7.4, which demonstrated their pH-triggered conversion into cationic liposomes.

The anticancer activities of ICL formulations were evaluated in MCS in comparison with non-sensitive stealth liposomes (NSL). 3D multicellular spheroids (MCS) were chosen to assess the anticancer activities of liposomes, because they more closely resemble the biological features of solid tumors than 2D cell cultures, including the acidic microenvironment. The 3D MCS of HeLa, A549, MDA-MB-231 and MDA-MB-468 cell lines were successfully constructed by exploring the suitable seeding and culturing conditions. Cytotoxicity assays on 3D MCS were carried out to evaluate the anticancer activity of ICL formulations. According to the IC_{50} values, the cholesterol-free ICL, especially DHMI/DSPC/DPPE-PEG, showed considerably enhanced activity on MCS compared to NSL. However, ICL with cholesterol showed anticancer activities that were similar to NSL but lower than cholesterol-free ICL.

In summary, it was found that pH-sensitivity is successfully introduced to PEGylated, stealth liposomes by the incorporation of imidazole-based lipids, and the pH-sensitivity correlated with the enhanced anticancer activity of the resultant ICL liposomes. In the pH-sensitivity studies, cholesterol-free ICL showed both pH-triggered conversion into cationic

liposomes and pH-triggered drug release. Under TEM, the phase separation and bursting of ICL appeared to be consistent with their pH-sensitivity. The IC_{50} values of ICL formulations against 3D MCS confirmed that liposomes with the pH-sensitivity from the imidazole-based lipids showed improved anticancer activity than the non-sensitive stealth liposomes. Among the three ICL formulations, DHDMI/DSPC/DPPE-PEG showed the most pH-sensitivity in conversion, and the best activity against 2D cancer cells (previous studies); DHMI/DSPC/DPPE-PEG showed the most pH-sensitivity in drug release as well as the best activity against 3D MCS. It appears that in 3D MCS, which are more like solid tumors *in vivo* than 2D cells, the triggered release of liposomal delivery systems probably plays a more critical role than the enhanced interaction with cancer cells. Moreover, although the incorporation of cholesterol can improve the physicochemical characteristics of ICL, it would also suppress the pH-sensitivity of ICL. Against 3D MCS, unlike the cholesterol-free ICL, the ICL with cholesterol showed similar anticancer activity with the non-sensitive stealth liposomes, indicating that removing the pH-sensitivity of liposomes would decrease the anticancer activity. The pH-sensitivity of ICL played a more critical role for activities against MCS than good physicochemical characteristics. In conclusion, the pH-sensitivity introduced by the imidazole-based lipids can enhance the anti-cancer activity of stealth liposomes.

REFERENCES

1. Organization, W.H. *Cancer*. 2018 [cited 2018 September 12]; Available from: https://www.who.int/health-topics/cancer#tab=tab_1.

2. Siegel, R.L., K.D. Miller, and A. Jemal, *Cancer statistics, 2018.* CA Cancer J Clin, 2018. **68**(1): p. 7-30.

3. Anand, P., et al., *Cancer is a preventable disease that requires major lifestyle changes.* Pharm Res, 2008. **25**(9): p. 2097-116.

4. Society, A.C. *How is cancer diagnosed?* 2013 [cited 2013 January 29]; Available from: https://www.cancer.org/treatment/understanding-your-diagnosis/tests/testing-biopsy-and-cytology-specimens-for-cancer/how-is-cancer-diagnosed.html.

5. Brown, J.M. and A.J. Giaccia, *The unique physiology of solid tumors: opportunities (and problems) for cancer therapy.* Cancer Res, 1998. **58**(7): p. 1408-16.

6. Hockel, M. and P. Vaupel, *Tumor hypoxia: definitions and current clinical, biologic, and molecular aspects.* J Natl Cancer Inst, 2001. **93**(4): p. 266-76.

7. Giaccia, A.J., *Hypoxic Stress Proteins: Survival of the Fittest.* Semin Radiat Oncol, 1996. **6**(1): p. 46-58.

8. Hockel, M., et al., *Hypoxic cervical cancers with low apoptotic index are highly aggressive.* Cancer Res, 1999. **59**(18): p. 4525-8.

9. Grau, C. and J. Overgaard, *Effect of cancer chemotherapy on the hypoxic fraction of a solid tumor measured using a local tumor control assay.* Radiother Oncol, 1988. **13**(4): p. 301-9.

10. Rotin, D., B. Robinson, and I.F. Tannock, *Influence of hypoxia and an acidic environment on the metabolism and viability of cultured cells: potential implications for cell death in tumors.* Cancer Res, 1986. **46**(6): p. 2821-6.

11. Tannock, I.F., *Oxygen diffusion and the distribution of cellular radiosensitivity in tumours.* Br J Radiol, 1972. **45**(535): p. 515-24.

12. Reshetnyak, Y.K., *Imaging Tumor Acidity: pH-Low Insertion Peptide Probe for Optoacoustic Tomography.* Clin Cancer Res, 2015. **21**(20): p. 4502-4.

13. Zagaynova, E.V., et al., *Imaging of Intracellular pH in Tumor Spheroids Using Genetically Encoded Sensor SypHer2.* Adv Exp Med Biol, 2017. **1035**: p. 105-119.

14. Tannock, I.F. and D. Rotin, *Acid pH in tumors and its potential for therapeutic exploitation.* Cancer Res, 1989. **49**(16): p. 4373-84.

15. Hellstrand, P., *Role of the sarcoplasmic reticulum in smooth muscle.* Bioessays, 2002. **24**(5): p. 483-4.

16. Warburg, O., F. Wind, and E. Negelein, *The Metabolism of Tumors in the Body.* J Gen Physiol, 1927. **8**(6): p. 519-30.

17. Sattler, U.G., et al., *Glycolytic metabolism and tumour response to fractionated irradiation.* Radiother Oncol, 2010. **94**(1): p. 102-9.

18. Kato, Y., et al., *Acidic extracellular microenvironment and cancer.* Cancer Cell Int, 2013. **13**(1): p. 89.

19. Nallanthighal, S., J.P. Heiserman, and D.J. Cheon, *The Role of the Extracellular Matrix in Cancer Stemness.* Front Cell Dev Biol, 2019. **7**: p. 86.

20. Frantz, C., K.M. Stewart, and V.M. Weaver, *The extracellular matrix at a glance.* J Cell Sci, 2010. **123**(Pt 24): p. 4195-200.

21. Chang, Q., et al., *Biodistribution of cisplatin revealed by imaging mass cytometry identifies extensive collagen binding in tumor and normal tissues.* Sci Rep, 2016. **6**: p. 36641.

22. Millard, M., et al., *Drug delivery to solid tumors: the predictive value of the multicellular tumor spheroid model for nanomedicine screening.* Int J Nanomedicine, 2017. **12**: p. 7993-8007.

23. Karanth, H. and R.S. Murthy, *pH-sensitive liposomes--principle and application in cancer therapy.* J Pharm Pharmacol, 2007. **59**(4): p. 469-83.

24. Hallahan, D.E., et al., *Spatial and temporal control of gene therapy using ionizing radiation.* Nat Med, 1995. **1**(8): p. 786-91.

25. Lemmon, M.J., et al., *Anaerobic bacteria as a gene delivery system that is controlled by the tumor microenvironment.* Gene Ther, 1997. **4**(8): p. 791-6.

26. Malhotra, V. and M.C. Perry, *Classical chemotherapy: mechanisms, toxicities and the therapeutic window.* Cancer Biol Ther, 2003. **2**(4 Suppl 1): p. S2-4.

27. Cannon, J.G., *Goodman and Gilman's The Pharmacological Basis of Therapeutics. 11th Edition Edited by Laurence Brunton, John Lazo, and Keith Parker. McGraw Hill, New York. 2005. xxiii + 2021 pp. 21 × 26 cm. ISBN 0-07-142280-3. $149.95.* Journal of Medicinal Chemistry, 2006. **49**(3): p. 1222-1222.

28. Zhang, J., P.L. Yang, and N.S. Gray, *Targeting cancer with small molecule kinase inhibitors.* Nat Rev Cancer, 2009. **9**(1): p. 28-39.

29. Hanahan, D. and R.A. Weinberg, *The hallmarks of cancer.* Cell, 2000. **100**(1): p. 57-70.

30. Johnstone, R.W., A.A. Ruefli, and S.W. Lowe, *Apoptosis: a link between cancer genetics and chemotherapy.* Cell, 2002. **108**(2): p. 153-64.

31. Emil Frei, I.I.I.E., Joseph Paul, *Combination Chemotherapy*. 2003.

32. Allen, T.M., *Ligand-targeted therapeutics in anticancer therapy.* Nat Rev Cancer, 2002. **2**(10): p. 750-63.

33. Partridge, A.H., H.J. Burstein, and E.P. Winer, *Side effects of chemotherapy and combined chemohormonal therapy in women with early-stage breast cancer.* J Natl Cancer Inst Monogr, 2001(30): p. 135-42.

34. Yao, X., et al., *Cisplatin nephrotoxicity: a review.* Am J Med Sci, 2007. **334**(2): p. 115-24.

35. Chatterjee, K., et al., *Doxorubicin Cardiomyopathy.* Cardiology, 2010. **115**(2): p. 155-162.

36. Goldman, B., *Multidrug resistance: can new drugs help chemotherapy score against cancer?* J Natl Cancer Inst, 2003. **95**(4): p. 255-7.

37. Crowley, E., C.A. McDevitt, and R. Callaghan, *Generating inhibitors of P-glycoprotein: where to, now?* Methods Mol Biol, 2010. **596**: p. 405-32.

38. Luqmani, Y.A., *Mechanisms of drug resistance in cancer chemotherapy.* Med Princ Pract, 2005. **14 Suppl 1**: p. 35-48.

39. Gottesman, M.M., T. Fojo, and S.E. Bates, *Multidrug resistance in cancer: role of ATP-dependent transporters.* Nat Rev Cancer, 2002. **2**(1): p. 48-58.

40. Miller, C.R., et al., *Liposome-cell interactions in vitro: effect of liposome surface charge on the binding and endocytosis of conventional and sterically stabilized liposomes.* Biochemistry, 1998. **37**(37): p. 12875-83.

41. Muller, R.H. and C.M. Keck, *Challenges and solutions for the delivery of biotech drugs – a review of drug nanocrystal technology and lipid nanoparticles.* Journal of Biotechnology, 2004. **113**(1): p. 151-170.

42.   Torchilin, V.P., *Passive and active drug targeting: drug delivery to tumors as an example.* Handb Exp Pharmacol, 2010(197): p. 3-53.

43.   Attia, M.F., et al., *An overview of active and passive targeting strategies to improve the nanocarriers efficiency to tumour sites.* J Pharm Pharmacol, 2019. **71**(8): p. 1185-1198.

44.   de Jonge, M.J.A. and J. Verweij, *Renal Toxicities of Chemotherapy.* Seminars in Oncology, 2006. **33**(1): p. 68-73.

45.   Matsumura, Y. and H. Maeda, *A new concept for macromolecular therapeutics in cancer chemotherapy: mechanism of tumoritropic accumulation of proteins and the antitumor agent smancs.* Cancer Res, 1986. **46**(12 Pt 1): p. 6387-92.

46.   Scherphof, G.L., et al., *Uptake and intracellular processing of targeted and nontargeted liposomes by rat Kupffer cells in vivo and in vitro.* Ann N Y Acad Sci, 1985. **446**: p. 368-84.

47.   Maeda, H., *Toward a full understanding of the EPR effect in primary and metastatic tumors as well as issues related to its heterogeneity.* Adv Drug Deliv Rev, 2015. **91**: p. 3-6.

48.   Nagamitsu, A., K. Greish, and H. Maeda, *Elevating blood pressure as a strategy to increase tumor-targeted delivery of macromolecular drug SMANCS: cases of advanced solid tumors.* Jpn J Clin Oncol, 2009. **39**(11): p. 756-66.

49.   Yuan, F., et al., *Microvascular permeability and interstitial penetration of sterically stabilized (stealth) liposomes in a human tumor xenograft.* Cancer Res, 1994. **54**(13): p. 3352-6.

50.   Yokoi, K., et al., *Capillary-wall collagen as a biophysical marker of nanotherapeutic permeability into the tumor microenvironment.* Cancer Res, 2014. **74**(16): p. 4239-46.

51.   van Vlerken, L.E., T.K. Vyas, and M.M. Amiji, *Poly(ethylene glycol)-modified nanocarriers for tumor-targeted and intracellular delivery.* Pharm Res, 2007. **24**(8): p. 1405-14.

52.   Bazak, R., et al., *Cancer active targeting by nanoparticles: a comprehensive review of literature.* J Cancer Res Clin Oncol, 2015. **141**(5): p. 769-84.

53.   Danhier, F., O. Feron, and V. Preat, *To exploit the tumor microenvironment: Passive and active tumor targeting of nanocarriers for anti-cancer drug delivery.* J Control Release, 2010. **148**(2): p. 135-46.

54.   Srinivasan, R., *Nanotechnology for cancer therapy*. 2008: Cyber Tech Publications.

55.   Peer, D., et al., *Nanocarriers as an emerging platform for cancer therapy.* Nat Nanotechnol, 2007. **2**(12): p. 751-60.

56.   Bae, Y.H. and K. Park, *Targeted drug delivery to tumors: myths, reality and possibility.* J Control Release, 2011. **153**(3): p. 198-205.

57.   Galvin, P., et al., *Nanoparticle-based drug delivery: case studies for cancer and cardiovascular applications.* Cell Mol Life Sci, 2012. **69**(3): p. 389-404.

58.   Lentacker, I., et al., *New strategies for nucleic acid delivery to conquer cellular and nuclear membranes*. J Control Release, 2008. **132**(3): p. 279-88.

59.   Huang, X., et al., *pH-sensitive micelles self-assembled from polymer brush (PAE-g-cholesterol)-b-PEG-b-(PAE-g-cholesterol) for anticancer drug delivery and controlled release.* Int J Nanomedicine, 2017. **12**: p. 2215-2226.

60.   Noyhouzer, T., et al., *Ferrocene-Modified Phospholipid: An Innovative Precursor for Redox-Triggered Drug Delivery Vesicles Selective to Cancer Cells.* Langmuir, 2016. **32**(17): p. 4169-4178.

61. Elersic, K., et al., *Electric-field controlled liposome formation with embedded superparamagnetic iron oxide nanoparticles.* Chem Phys Lipids, 2012. **165**(1): p. 120-4.

62. Garcia-Jimeno, S., et al., *Reversible and irreversible aggregation of magnetic liposomes.* Nanoscale, 2017. **9**(39): p. 15131-15143.

63. Huang, S.L. and R.C. MacDonald, *Acoustically active liposomes for drug encapsulation and ultrasound-triggered release.* Biochim Biophys Acta, 2004. **1665**(1-2): p. 134-41.

64. Luo, D., et al., *Doxorubicin encapsulated in stealth liposomes conferred with light-triggered drug release.* Biomaterials, 2016. **75**: p. 193-202.

65. Walsh, M.D., et al., *Pharmacokinetics and antitumor efficacy of XMT-1001, a novel, polymeric topoisomerase I inhibitor, in mice bearing HT-29 human colon carcinoma xenografts.* Clin Cancer Res, 2012. **18**(9): p. 2591-602.

66. Yingchoncharoen, P., D.S. Kalinowski, and D.R. Richardson, *Lipid-Based Drug Delivery Systems in Cancer Therapy: What Is Available and What Is Yet to Come.* Pharmacol Rev, 2016. **68**(3): p. 701-87.

67. Martin, J.D., et al., *Improving cancer immunotherapy using nanomedicines: progress, opportunities and challenges.* Nat Rev Clin Oncol, 2020. **17**(4): p. 251-266.

68. Casals, E., et al., *Cancer resistance to treatment and antiresistance tools offered by multimodal multifunctional nanoparticles.* Cancer Nanotechnol, 2017. **8**(1): p. 7.

69. Nagy, Z.K., et al., *Comparison of electrospun and extruded Soluplus(R)-based solid dosage forms of improved dissolution.* J Pharm Sci, 2012. **101**(1): p. 322-32.

70. Din, F.U., et al., *Effective use of nanocarriers as drug delivery systems for the treatment of selected tumors.* Int J Nanomedicine, 2017. **12**: p. 7291-7309.

71. Zimmer, A. and J. Kreuter, *Microspheres and nanoparticles used in ocular delivery systems.* Advanced Drug Delivery Reviews, 1995. **16**(1): p. 61-73.

72. Choi, Y.H. and H.K. Han, *Nanomedicines: current status and future perspectives in aspect of drug delivery and pharmacokinetics.* J Pharm Investig, 2018. **48**(1): p. 43-60.

73. De Jong, W.H. and P.J. Borm, *Drug delivery and nanoparticles:applications and hazards.* Int J Nanomedicine, 2008. **3**(2): p. 133-49.

74. Minchin, R., *Nanomedicine: sizing up targets with nanoparticles.* Nat Nanotechnol, 2008. **3**(1): p. 12-3.

75. Jain, R.K. and T. Stylianopoulos, *Delivering nanomedicine to solid tumors.* Nat Rev Clin Oncol, 2010. **7**(11): p. 653-64.

76. Weiss, R.B., *The anthracyclines: will we ever find a better doxorubicin?* Semin Oncol, 1992. **19**(6): p. 670-86.

77. Gordon, A.N., et al., *Phase II study of liposomal doxorubicin in platinum- and paclitaxel-refractory epithelial ovarian cancer.* J Clin Oncol, 2000. **18**(17): p. 3093-100.

78. Bulbake, U., et al., *Liposomal Formulations in Clinical Use: An Updated Review.* Pharmaceutics, 2017. **9**(2).

79. Beltrán-Gracia, E., et al., *Nanomedicine review: clinical developments in liposomal applications.* Cancer Nanotechnology, 2019. **10**(1): p. 11.

80. Wang, R., P.S. Billone, and W.M. Mullett, *Nanomedicine in Action: An Overview of Cancer Nanomedicine on the Market and in Clinical Trials.* Journal of Nanomaterials, 2013. **2013**: p. 629681.

81. Gabizon, A.A., *Pegylated liposomal doxorubicin: metamorphosis of an old drug into a new form of chemotherapy.* Cancer Invest, 2001. **19**(4): p. 424-36.

82. Gabizon, A., H. Shmeeda, and Y. Barenholz, *Pharmacokinetics of pegylated liposomal*

Doxorubicin: review of animal and human studies. Clin Pharmacokinet, 2003. **42**(5): p. 419-36.

83. Immordino, M.L., F. Dosio, and L. Cattel, *Stealth liposomes: review of the basic science, rationale, and clinical applications, existing and potential.* Int J Nanomedicine, 2006. **1**(3): p. 297-315.

84. Cevc, G., *Rational design of new product candidates: the next generation of highly deformable bilayer vesicles for noninvasive, targeted therapy.* J Control Release, 2012. **160**(2): p. 135-46.

85. Samad, A., Y. Sultana, and M. Aqil, *Liposomal drug delivery systems: an update review.* Curr Drug Deliv, 2007. **4**(4): p. 297-305.

86. Xia, Y., et al., *Liposome-based probes for molecular imaging: from basic research to the bedside.* Nanoscale, 2019. **11**(13): p. 5822-5838.

87. Bangham, A.D., M.M. Standish, and J.C. Watkins, *Diffusion of univalent ions across the lamellae of swollen phospholipids.* J Mol Biol, 1965. **13**(1): p. 238-52.

88. Sabin, J., et al., *Size and stability of liposomes: a possible role of hydration and osmotic forces.* Eur Phys J E Soft Matter, 2006. **20**(4): p. 401-8.

89. Ventola, C.L., *Progress in Nanomedicine: Approved and Investigational Nanodrugs.* P T, 2017. **42**(12): p. 742-755.

90. Elbayoumi, T.A. and V.P. Torchilin, *Current trends in liposome research.* Methods Mol Biol, 2010. **605**: p. 1-27.

91. Chatin, B., et al., *Liposome-based Formulation for Intracellular Delivery of Functional Proteins.* Mol Ther Nucleic Acids, 2015. **4**: p. e244.

92. Lee, Y.W., et al., *Protein Delivery into the Cell Cytosol using Non-Viral Nanocarriers.* Theranostics, 2019. **9**(11): p. 3280-3292.

93. Fang, Y., et al., *Lipid-Coated, pH-Sensitive Magnesium Phosphate Particles for Intracellular Protein Delivery.* Pharm Res, 2019. **36**(6): p. 81.

94. Sun, Q., et al., *A Collaborative Assembly Strategy for Tumor-Targeted siRNA Delivery.* Journal of the American Chemical Society, 2015. **137**(18): p. 6000-6010.

95. Khaw, B.A., et al., *Intracytoplasmic gene delivery for in vitro transfection with cytoskeleton-specific immunoliposomes.* J Control Release, 2001. **75**(1-2): p. 199-210.

96. Bruun, K. and C. Hille, *Study on intracellular delivery of liposome encapsulated quantum dots using advanced fluorescence microscopy.* Scientific Reports, 2019. **9**(1): p. 10504.

97. Daraee, H., et al., *Application of liposomes in medicine and drug delivery.* Artificial Cells, Nanomedicine, and Biotechnology, 2016. **44**(1): p. 381-391.

98. Zylberberg, C. and S. Matosevic, *Pharmaceutical liposomal drug delivery: a review of new delivery systems and a look at the regulatory landscape.* Drug Deliv, 2016. **23**(9): p. 3319-3329.

99. Le, N.T.T., et al., *Soy Lecithin-Derived Liposomal Delivery Systems: Surface Modification and Current Applications.* Int J Mol Sci, 2019. **20**(19).

100. Akbarzadeh, A., et al., *Liposome: classification, preparation, and applications.* Nanoscale Res Lett, 2013. **8**(1): p. 102.

101. Agrawal, A.K. and C.M. Gupta, *Tuftsin-bearing liposomes in treatment of macrophage-based infections.* Adv Drug Deliv Rev, 2000. **41**(2): p. 135-46.

102. Senior, J. and G. Gregoriadis, *Is half-life of circulating liposomes determined by changes in their permeability?* FEBS Lett, 1982. **145**(1): p. 109-14.

103. McIntosh, T.J., *The effect of cholesterol on the structure of phosphatidylcholine bilayers.*

Biochim Biophys Acta, 1978. **513**(1): p. 43-58.

104. Needham, D., T.J. McIntosh, and D.D. Lasic, *Repulsive interactions and mechanical stability of polymer-grafted lipid membranes.* Biochim Biophys Acta, 1992. **1108**(1): p. 40-8.

105. Van Slooten, M.L., et al., *Liposomes as sustained release system for human interferon-gamma: biopharmaceutical aspects.* Biochim Biophys Acta, 2001. **1530**(2-3): p. 134-45.

106. Yamaoka, T., Y. Tabata, and Y. Ikada, *Distribution and tissue uptake of poly(ethylene glycol) with different molecular weights after intravenous administration to mice.* J Pharm Sci, 1994. **83**(4): p. 601-6.

107. Kawano, K. and Y. Maitani, *Effects of polyethylene glycol spacer length and ligand density on folate receptor targeting of liposomal Doxorubicin in vitro.* J Drug Deliv, 2011. **2011**: p. 160967.

108. Nag, O.K. and V. Awasthi, *Surface engineering of liposomes for stealth behavior.* Pharmaceutics, 2013. **5**(4): p. 542-69.

109. Lamichhane, N., et al., *Liposomes: Clinical Applications and Potential for Image-Guided Drug Delivery.* Molecules, 2018. **23**(2).

110. Senapati, S., et al., *Controlled drug delivery vehicles for cancer treatment and their performance.* Signal Transduction and Targeted Therapy, 2018. **3**(1): p. 7.

111. Parr, M.J., et al., *Accumulation of liposomal lipid and encapsulated doxorubicin in murine Lewis lung carcinoma: the lack of beneficial effects by coating liposomes with poly(ethylene glycol).* J Pharmacol Exp Ther, 1997. **280**(3): p. 1319-27.

112. Gabizon, A., et al., *Long-circulating liposomes for drug delivery in cancer therapy: a review of biodistribution studies in tumor-bearing animals.* Advanced Drug Delivery Reviews, 1997. **24**(2): p. 337-344.

113. Waterhouse, D.N., et al., *A comparison of liposomal formulations of doxorubicin with drug administered in free form: changing toxicity profiles.* Drug Saf, 2001. **24**(12): p. 903-20.

114. Paliwal, S.R., R. Paliwal, and S.P. Vyas, *A review of mechanistic insight and application of pH-sensitive liposomes in drug delivery.* Drug Deliv, 2015. **22**(3): p. 231-42.

115. Chatzipanteli, K., et al., *Importance of posttraumatic hypothermia and hyperthermia on the inflammatory response after fluid percussion brain injury: biochemical and immunocytochemical studies.* J Cereb Blood Flow Metab, 2000. **20**(3): p. 531-42.

116. Kong, G., et al., *Efficacy of liposomes and hyperthermia in a human tumor xenograft model: importance of triggered drug release.* Cancer Res, 2000. **60**(24): p. 6950-7.

117. Amstad, E., et al., *Triggered release from liposomes through magnetic actuation of iron oxide nanoparticle containing membranes.* Nano Lett, 2011. **11**(4): p. 1664-70.

118. Huang, S.L., D.D. McPherson, and R.C. Macdonald, *A method to co-encapsulate gas and drugs in liposomes for ultrasound-controlled drug delivery.* Ultrasound Med Biol, 2008. **34**(8): p. 1272-80.

119. Koziolek, M., et al., *Investigation of pH and Temperature Profiles in the GI Tract of Fasted Human Subjects Using the Intellicap((R)) System.* J Pharm Sci, 2015. **104**(9): p. 2855-63.

120. Liu, L., et al., *pH-Responsive carriers for oral drug delivery: challenges and opportunities of current platforms.* Drug Deliv, 2017. **24**(1): p. 569-581.

121. Gilabert-Oriol, R., et al., *Liposomal Formulations to Modulate the Tumour Microenvironment and Antitumour Immune Response.* Int J Mol Sci, 2018. **19**(10).

122. Somiya, M., *Where does the cargo go?: Solutions to provide experimental support for the "extracellular vesicle cargo transfer hypothesis".* J Cell Commun Signal, 2020. **14**(2): p. 135-146.

123. Zheng, Y., et al., *Fliposomes: trans-2-aminocyclohexanol-based amphiphiles as pH-sensitive conformational switches of liposome membrane - a structure-activity relationship study.* Chem Phys Lipids, 2018. **210**: p. 129-141.

124. Drummond, D.C., M. Zignani, and J. Leroux, *Current status of pH-sensitive liposomes in drug delivery.* Prog Lipid Res, 2000. **39**(5): p. 409-60.

125. Needham, D. and M.W. Dewhirst, *The development and testing of a new temperature-sensitive drug delivery system for the treatment of solid tumors.* Adv Drug Deliv Rev, 2001. **53**(3): p. 285-305.

126. Romberg, B., W.E. Hennink, and G. Storm, *Sheddable coatings for long-circulating nanoparticles.* Pharm Res, 2008. **25**(1): p. 55-71.

127. Karve, S., et al., *The use of pH-triggered leaky heterogeneities on rigid lipid bilayers to improve intracellular trafficking and therapeutic potential of targeted liposomal immunochemotherapy.* Biomaterials, 2009. **30**(30): p. 6055-64.

128. Levin, M., et al., *Steroid-responsive nephrotic syndrome: a generalised disorder of membrane negative charge.* Lancet, 1985. **2**(8449): p. 239-42.

129. Gyanani, V., *Turning stealth liposomes into cationic liposomes for anticancer drug delivery*. 2013, University of the Pacific: Ann Arbor. p. 144.

130. Pampaloni, F., E.G. Reynaud, and E.H.K. Stelzer, *The third dimension bridges the gap between cell culture and live tissue.* Nature Reviews Molecular Cell Biology, 2007. **8**(10): p. 839-845.

131. Souza, G.R., et al., *Three-dimensional tissue culture based on magnetic cell levitation.* Nature Nanotechnology, 2010. **5**(4): p. 291-296.

132. Baillargeon, P., et al., *Automating a Magnetic 3D Spheroid Model Technology for High-Throughput Screening.* SLAS Technol, 2019. **24**(4): p. 420-428.

133. Fang, Y. and R.M. Eglen, *Three-Dimensional Cell Cultures in Drug Discovery and Development.* SLAS Discov, 2017. **22**(5): p. 456-472.

134. Fey, S.J. and K. Wrzesinski, *Determination of drug toxicity using 3D spheroids constructed from an immortal human hepatocyte cell line.* Toxicol Sci, 2012. **127**(2): p. 403-11.

135. Inch, W.R., J.A. McCredie, and R.M. Sutherland, *Growth of nodular carcinomas in rodents compared with multi-cell spheroids in tissue culture.* Growth, 1970. **34**(3): p. 271-82.

136. Mapanao, A.K. and V. Voliani, *Three-dimensional tumor models: Promoting breakthroughs in nanotheranostics translational research.* Applied Materials Today, 2020. **19**: p. 100552.

137. Cui, X., Y. Hartanto, and H. Zhang, *Advances in multicellular spheroids formation.* Journal of The Royal Society Interface, 2017. **14**(127): p. 20160877.

138. Gong, X., et al., *Generation of Multicellular Tumor Spheroids with Microwell-Based Agarose Scaffolds for Drug Testing.* PLoS One, 2015. **10**(6): p. e0130348.

139. Sant, S. and P.A. Johnston, *The production of 3D tumor spheroids for cancer drug discovery.* Drug Discov Today Technol, 2017. **23**: p. 27-36.

140. Buffa, F.M., et al., *Radiation response and cure rate of human colon adenocarcinoma spheroids of different size: the significance of hypoxia on tumor control modelling.* Int J

Radiat Oncol Biol Phys, 2001. **49**(4): p. 1109-18.

141. Gorlach, A. and H. Acker, *pO2- and pH-gradients in multicellular spheroids and their relationship to cellular metabolism and radiation sensitivity of malignant human tumor cells.* Biochim Biophys Acta, 1994. **1227**(3): p. 105-12.

142. Jamieson, L.E., D.J. Harrison, and C.J. Campbell, *Chemical analysis of multicellular tumour spheroids.* Analyst, 2015. **140**(12): p. 3910-3920.

143. Cox, M.C., et al., *Toward the Broad Adoption of 3D Tumor Models in the Cancer Drug Pipeline.* ACS Biomaterials Science & Engineering, 2015. **1**(10): p. 877-894.

144. Huang, Y., et al., *Optical Coherence Tomography Detects Necrotic Regions and Volumetrically Quantifies Multicellular Tumor Spheroids.* Cancer Res, 2017. **77**(21): p. 6011-6020.

145. Langan, L.M., et al., *Direct Measurements of Oxygen Gradients in Spheroid Culture System Using Electron Parametric Resonance Oximetry.* PLoS One, 2016. **11**(2): p. e0149492.

146. Daster, S., et al., *Induction of hypoxia and necrosis in multicellular tumor spheroids is associated with resistance to chemotherapy treatment.* Oncotarget, 2017. **8**(1): p. 1725-1736.

147. Baker, B.M. and C.S. Chen, *Deconstructing the third dimension: how 3D culture microenvironments alter cellular cues.* J Cell Sci, 2012. **125**(Pt 13): p. 3015-24.

148. Kim, S.A., E.K. Lee, and H.J. Kuh, *Co-culture of 3D tumor spheroids with fibroblasts as a model for epithelial-mesenchymal transition in vitro.* Exp Cell Res, 2015. **335**(2): p. 187-96.

149. Lazzari, G., P. Couvreur, and S. Mura, *Multicellular tumor spheroids: a relevant 3D model for the in vitro preclinical investigation of polymer nanomedicines.* Polymer Chemistry, 2017. **8**(34): p. 4947-4969.

150. Asghar, W., et al., *Engineering cancer microenvironments for in vitro 3-D tumor models.* Materials Today, 2015. **18**(10): p. 539-553.

151. Alghuwainem, A., A.T. Alshareeda, and B. Alsowayan, *Scaffold-Free 3-D Cell Sheet Technique Bridges the Gap between 2-D Cell Culture and Animal Models.* Int J Mol Sci, 2019. **20**(19).

152. Hamilton, G., *Multicellular spheroids as an in vitro tumor model.* Cancer Letters, 1998. **131**(1): p. 29-34.

153. Lazzari, G., et al., *Multicellular spheroid based on a triple co-culture: A novel 3D model to mimic pancreatic tumor complexity.* Acta Biomaterialia, 2018. **78**: p. 296-307.

154. Phillips, R.M., *Targeting the hypoxic fraction of tumours using hypoxia-activated prodrugs.* Cancer Chemother Pharmacol, 2016. **77**(3): p. 441-57.

155. Voissiere, A., et al., *Development and characterization of a human three-dimensional chondrosarcoma culture for in vitro drug testing.* PLoS One, 2017. **12**(7): p. e0181340.

156. Grist, S.M., et al., *Long-term monitoring in a microfluidic system to study tumour spheroid response to chronic and cycling hypoxia.* Scientific Reports, 2019. **9**(1): p. 17782.

157. Agarwal, R., et al., *Effect of shape, size, and aspect ratio on nanoparticle penetration and distribution inside solid tissues using 3D spheroid models.* Adv Healthc Mater, 2015. **4**(15): p. 2269-80.

158. Dias, D.R., A.F. Moreira, and I.J. Correia, *The effect of the shape of gold core-mesoporous silica shell nanoparticles on the cellular behavior and tumor spheroid*

penetration. J Mater Chem B, 2016. **4**(47): p. 7630-7640.

159.   Jaganathan, H., et al., *Three-Dimensional In Vitro Co-Culture Model of Breast Tumor using Magnetic Levitation.* Scientific Reports, 2014. **4**(1): p. 6468.

160.   Geckil, H., et al., *Engineering hydrogels as extracellular matrix mimics.* Nanomedicine (Lond), 2010. **5**(3): p. 469-84.

161.   Dhandayuthapani, B., et al., *Polymeric Scaffolds in Tissue Engineering Application: A Review.* International Journal of Polymer Science, 2011. **2011**: p. 290602.

162.   Tatsumi, K. and T. Okano, *Hepatocyte Transplantation: Cell Sheet Technology for Liver Cell Transplantation.* Curr Transplant Rep, 2017. **4**(3): p. 184-192.

163.   Ikada, Y., *Challenges in tissue engineering.* J R Soc Interface, 2006. **3**(10): p. 589-601.

164.   Breslin, S. and L. O'Driscoll, *Three-dimensional cell culture: the missing link in drug discovery.* Drug Discovery Today, 2013. **18**(5): p. 240-249.

165.   Ovsianikov, A., A. Khademhosseini, and V. Mironov, *The Synergy of Scaffold-Based and Scaffold-Free Tissue Engineering Strategies.* Trends Biotechnol, 2018. **36**(4): p. 348-357.

166.   Tevis, K.M., Y.L. Colson, and M.W. Grinstaff, *Embedded Spheroids as Models of the Cancer Microenvironment.* Adv Biosyst, 2017. **1**(10).

167.   Yamada, N., et al., *Thermo-responsive polymeric surfaces; control of attachment and detachment of cultured cells.* Die Makromolekulare Chemie, Rapid Communications, 1990. **11**(11): p. 571-576.

168.   Matsuura, K., et al., *Cell sheet approach for tissue engineering and regenerative medicine.* J Control Release, 2014. **190**: p. 228-39.

169.   Lee, D. and C. Cha, *The Combined Effects of Co-Culture and Substrate Mechanics on 3D Tumor Spheroid Formation within Microgels Prepared via Flow-Focusing Microfluidic Fabrication.* Pharmaceutics, 2018. **10**(4).

170.   Yuan, T., et al., *Co-culture of tumor spheroids and monocytes in a collagen matrix-embedded microfluidic device to study the migration of breast cancer cells.* Chinese Chemical Letters, 2019. **30**(2): p. 331-336.

171.   Huwyler, J., J. Drewe, and S. Krahenbuhl, *Tumor targeting using liposomal antineoplastic drugs.* Int J Nanomedicine, 2008. **3**(1): p. 21-9.

172.   Gabizon, A.A., *Stealth liposomes and tumor targeting: one step further in the quest for the magic bullet.* Clin Cancer Res, 2001. **7**(2): p. 223-5.

173.   Homan, R. and H.J. Pownall, *Transbilayer diffusion of phospholipids: dependence on headgroup structure and acyl chain length.* Biochim Biophys Acta, 1988. **938**(2): p. 155-66.

174.   Avanti Polar Lipids, I. *What Is The Transition Temperature Of The Lipid?* 2018; Available from: https://avantilipids.com/tech-support/faqs/transition-temperature.

175.   Rawicz, W., et al., *Effect of chain length and unsaturation on elasticity of lipid bilayers.* Biophys J, 2000. **79**(1): p. 328-39.

176.   Avanti Polar Lipids, I. *Phase Transition Temperatures for Glycerophospholipids.* Available from: https://avantilipids.com/tech-support/physical-properties/phase-transition-temps.

177.   Anderson, M. and A. Omri, *The effect of different lipid components on the in vitro stability and release kinetics of liposome formulations.* Drug Deliv, 2004. **11**(1): p. 33-9.

178.   Pantusa, M., et al., *Shifts in chain-melting transition temperature of liposomal membranes by polymer-grafted lipids.* Biochimica et Biophysica Acta (BBA) - Biomembranes, 2003. **1614**(2): p. 165-170.

179.   Amselem, S., A. Gabizon, and Y. Barenholz, *Optimization and upscaling of doxorubicin-containing liposomes for clinical use.* J Pharm Sci, 1990. **79**(12): p. 1045-52.

180.   Bertrand, N. and J.C. Leroux, *The journey of a drug-carrier in the body: an anatomo-physiological perspective.* J Control Release, 2012. **161**(2): p. 152-63.

181.   Fonseca, M.J., E.C.A. van Winden, and D.J.A. Crommelin, *Doxorubicin induces aggregation of small negatively charged liposomes.* European Journal of Pharmaceutics and Biopharmaceutics, 1997. **43**(1): p. 9-17.

182.   Cheung, B.C., et al., *Loading of doxorubicin into liposomes by forming Mn2+-drug complexes.* Biochim Biophys Acta, 1998. **1414**(1-2): p. 205-16.

183.   Ladbrooke, B.D., R.M. Williams, and D. Chapman, *Studies on lecithin-cholesterol-water interactions by differential scanning calorimetry and X-ray diffraction.* Biochim Biophys Acta, 1968. **150**(3): p. 333-40.

184.   Lu, T., et al., *Influence of polymer size, liposomal composition, surface charge, and temperature on the permeability of pH-sensitive liposomes containing lipid-anchored poly(2-ethylacrylic acid).* Int J Nanomedicine, 2012. **7**: p. 4917-26.

185.   Needham, D. and R.S. Nunn, *Elastic deformation and failure of lipid bilayer membranes containing cholesterol.* Biophys J, 1990. **58**(4): p. 997-1009.

186.   Corvera, E., et al., *The permeability and the effect of acyl-chain length for phospholipid bilayers containing cholesterol: theory and experiment.* Biochimica et Biophysica Acta (BBA) - Biomembranes, 1992. **1107**(2): p. 261-270.

187.   Bhattacharya, S. and S. Haldar, *Interactions between cholesterol and lipids in bilayer membranes. Role of lipid headgroup and hydrocarbon chain-backbone linkage.* Biochim Biophys Acta, 2000. **1467**(1): p. 39-53.

188.   Rubenstein, J.L., B.A. Smith, and H.M. McConnell, *Lateral diffusion in binary mixtures of cholesterol and phosphatidylcholines.* Proc Natl Acad Sci U S A, 1979. **76**(1): p. 15-8.

189.   Folmsbee, M. and M. Moussourakis, *Sterilizing filtration of liposome and related lipid-containing solutions: enhancing successful filter qualification.* PDA J Pharm Sci Technol, 2012. **66**(2): p. 161-7.

190.   Singh, B., et al., *Benchmarking of Sterilizing-Grade Filter Membranes with Liposome Filtration.* PDA J Pharm Sci Technol, 2018. **72**(3): p. 223-235.

191.   Zimmer, A., et al., *Synthesis of cholesterol modified cationic lipids for liposomal drug delivery of antisense oligonucleotides.* Eur J Pharm Biopharm, 1999. **47**(2): p. 175-8.

192.   Heberle, F.A. and G.W. Feigenson, *Phase separation in lipid membranes.* Cold Spring Harb Perspect Biol, 2011. **3**(4).

193.   O'neill, E.S.W.J., *Differential microcalorimeter*. 1962: U.S.

194.   Koyama, T., et al., *Characterizing the Gel to Liquid Crystal Transition in Lipid-Bilayer Model Systems.* 1999. **4**: p. 12-15.

195.   Carneiro-da-Cunha, M.G., et al., *Influence of concentration, ionic strength and pH on zeta potential and mean hydrodynamic diameter of edible polysaccharide solutions envisaged for multinanolayered films production.* 2011. **85**: p. 522-528.

196.   Bergstrand, N., et al., *Interactions between pH-sensitive liposomes and model membranes.* Biophys Chem, 2003. **104**(1): p. 361-79.

197.   Chen, H., et al., *Unsaturated cationic ortho esters for endosome permeation in gene delivery.* J Med Chem, 2007. **50**(18): p. 4269-78.

198.   Huang, J., *Exploration of molecular interactions in cholesterol superlattices: effect of multibody interactions.* Biophys J, 2002. **83**(2): p. 1014-25.

199. Magarkar, A., et al., *Cholesterol level affects surface charge of lipid membranes in saline solution.* Scientific Reports, 2014. **4**(1): p. 5005.
200. Gregoriadis, G., *Drug entrapment in liposomes.* FEBS Lett, 1973. **36**(3): p. 292-6.
201. Lindblom, G. and G. Orädd, *Lipid lateral diffusion and membrane heterogeneity.* Biochimica et biophysica acta, 2009. **1788**(1): p. 234-244.
202. Kheirolomoom, A. and K.W. Ferrara, *Cholesterol transport from liposomal delivery vehicles.* Biomaterials, 2007. **28**(29): p. 4311-20.
203. de Broglie, L., *The reinterpretation of wave mechanics.* Foundations of Physics, 1970. **1**(1): p. 5-15.
204. Cheville, N.F. and J. Stasko, *Techniques in electron microscopy of animal tissue.* Vet Pathol, 2014. **51**(1): p. 28-41.
205. Baxa, U., *Imaging of Liposomes by Transmission Electron Microscopy.* Methods Mol Biol, 2018. **1682**: p. 73-88.
206. Amzallag, A., et al., *3D reconstruction and comparison of shapes of DNA minicircles observed by cryo-electron microscopy.* Nucleic Acids Res, 2006. **34**(18): p. e125.
207. Bravman, J.C., R.M. Anderson, and M.L. McDonald, *Specimen Preparation for Transmission Electron Microscopy of Materials (Materials Research Society Proceedings. Volume 115).* 1988, MATERIALS RESEARCH SOCIETY PITTSBURGH PA.
208. Yashroy, R.J.J.o.B., *Lamellar dispersion and phase separation of chloroplast membrane lipids by negative staining electron microscopy.* 1990. **15**(2): p. 93-98.
209. Scarff, C.A., et al., *Variations on Negative Stain Electron Microscopy Methods: Tools for Tackling Challenging Systems.* J Vis Exp, 2018(132).
210. Serwer, P., *Flattening and shrinkage of bacteriophage T7 after preparation for electron microscopy by negative staining.* Journal of Ultrastructure Research, 1977. **58**(3): p. 235-243.
211. Robson, A.-L., et al., *Advantages and Limitations of Current Imaging Techniques for Characterizing Liposome Morphology.* 2018. **9**(80).
212. Ruozi, B., et al., *AFM, ESEM, TEM, and CLSM in liposomal characterization: a comparative study.* Int J Nanomedicine, 2011. **6**: p. 557-63.
213. Franken, L.E., E.J. Boekema, and M.C.A. Stuart, *Transmission Electron Microscopy as a Tool for the Characterization of Soft Materials: Application and Interpretation.* Adv Sci (Weinh), 2017. **4**(5): p. 1600476.
214. Tivol, W.F., A. Briegel, and G.J. Jensen, *An improved cryogen for plunge freezing.* Microsc Microanal, 2008. **14**(5): p. 375-9.
215. Microsystems, L. *Brief Introduction to Contrasting for EM Sample Preparation.* 2013 [cited 2013 October 2]; Available from: https://www.leica-microsystems.com/science-lab/brief-introduction-to-contrasting-for-em-sample-preparation/.
216. Ting-Beall, H.P., *Interactions of uranyl ions with lipid bilayer membranes.* J Microsc, 1980. **118**(2): p. 221-7.
217. Cruje, C. and D.B.J.J.o.N.R. Chithrani, *Polyethylene Glycol Density and Length Affects Nanoparticle Uptake by Cancer Cells.* 2014. **1**.
218. Upadhyayula, S., et al., *Coatings of Polyethylene Glycol for Suppressing Adhesion between Solid Microspheres and Flat Surfaces.* Langmuir, 2012. **28**(11): p. 5059-5069.
219. Priwitaningrum, D.L., et al., *Tumor stroma-containing 3D spheroid arrays: A tool to study nanoparticle penetration.* J Control Release, 2016. **244**(Pt B): p. 257-268.

220. Lu, Y., *Fliposomes with a pH-Sensitive Conformational Switch for Anticancer Drug Delivery against Triple Negative Breast Cancer*. 2019, University of the Pacific: Ann Arbor. p. 137.

221. Zhao, S., *Design and <i>in vitro</i> Characterization of Lipids with a pH-Sensitive Conformational Switch and Their Liposomes for Anticancer Drug Delivery*. 2018, University of the Pacific: Ann Arbor. p. 129.

222. Cody, S.H., et al., *Intracellular pH mapping with SNARF-1 and confocal microscopy. I: A quantitative technique for living tissue and isolated cells.* Micron, 1993. **24**(6): p. 573-580.

223. Anderson, M., et al., *Probe for the measurement of cell surface pH in vivo and ex vivo.* Proc Natl Acad Sci U S A, 2016. **113**(29): p. 8177-81.

224. Hofschroer, V., et al., *Extracellular protonation modulates cell-cell interaction mechanics and tissue invasion in human melanoma cells.* Sci Rep, 2017. **7**: p. 42369.

225. Hulikova, A., R.D. Vaughan-Jones, and P. Swietach, *Dual role of CO2/HCO3(-) buffer in the regulation of intracellular pH of three-dimensional tumor growths.* J Biol Chem, 2011. **286**(16): p. 13815-26.

226. Swietach, P., et al., *Importance of intracellular pH in determining the uptake and efficacy of the weakly basic chemotherapeutic drug, doxorubicin.* PLoS One, 2012. **7**(4): p. e35949.